POLITECNICO DI TORINO

Energy Department

Master Degree in Energy and Nuclear Engineering

DESIGN OF A TECHNOLOGY DEMONSTRATOR OF A THERMOCHEMICAL HEAT STORAGE EXPLOITING WATER ADSORPTION IN MICROPOROUS MEDIA

Thesis advisors:

Prof. Eng. Eliodoro Chiavazzo

Eng. Alessandro Scattina

Eng. Nicolò Zampieri

Candidate:

Giulio Zaniboni

October 24, 2019

I

Abstract

Thermal energy storage (TES) has attracted an increasing importance in the past few years, thanks to the progressive shift of energy production towards renewables and the recent introduction of energy efficiency policies. A TES system is able to collect and store heat in various forms, maintaining it for a later use. Among TES, thermochemical energy storage is an interesting technology thanks to its high energy density and the nearly-zero thermal losses. This work focuses on the thermal and structural design of a small-scale thermochemical energy storage based on (although not limited to) the adsorption reaction of water and zeolite 13X. The device must be able to store (charge phase) at least $100 \, Wh$ of thermal energy and release it (discharge phase) in form of a heat flux at a minimum temperature of $35°C$. This heat flux can be exploited, for example, in a floor heating system. The water adsorption has been studied by using a numerical model based on the Langmuir isotherm formulation. Then, a theoretical model that exploits the analogy between the working principle of a phase changing material and the water vapour adsorption is developed. Finally, all the components of the device are designed in order to obtain the desired operating conditions.

Acknowledgements

I would like to express my deep and sincere gratitude to my advisor, Prof. Eng. Eliodoro Chiavazzo, and to my co-advisors, Eng. Scattina and Eng. Zampieri, for giving me the opportunity to do this work and to provide me with the knowledge and guidance necessary to complete it.

I am extremely grateful to my parents, Anna and Stefano, for their love, patience and sacrifices, for educating and preparing me for my future.

At last, I want to thank my sister Miriam, my grandparents, my cousins, uncles, aunts and the friends of "Palazzo Beaumont", for their precious help and constant support. They all kept me going, and this work would not have been possible without them.

Index

List of Figures

VIII

List of Tables

Glossary

3-D Three-Dimensional.

AC Absorption chiller.

ACS Adsorption Chiller Storage.

AHP Adsorption Heat Pump.

AHT Absorption Heat Transformers.

ASME American Society of Mechanical Engineers.

BPVC Boiler & Pressure Vessel Code.

CAD Computer Aided Design.

CAES Compressed Air Energy Storage.

COP Coefficient Of Performance.

CSP Concentrated Solar Power.

DEC Dehumidification and Evaporative Cooling.

DHW Domestic Hot Water.

EC Electrochemical Capacitors.

FC Fuel Cell.

FEM Finite Element Analysis.

GHG Green House Gas.

LHS Latent Heat Storage.

MEPA E-Market of the Public Administration

MOF Metal Organic Framework.

PCM Phase Change Material.

PHES Pumped Hydroelectric Storage.

RFB Redox Flow Batteries

SCP Specific Cooling Power.

SMES Superconductive Magnetic Energy Storage.

SWS Selective Water Sorbent.

TCS Thermochemical Storage.

TPES Total Primary Energy Supply.

1 Introduction

In the past years energy consumption and requirements have considerably increased. The main reasons are the economic growth of the developing countries, and the continuous increase in world population [1]. The biggest part of energy production still comes from traditional sources like crude oil, coal and natural gas, whose emissions cause serious repercussions on the environment, like global warming and air pollution. Moreover, traditional energy sources are progressively and inevitably going to deplete. To overcome these issues many countries have adopted new policies to help the implementation of a continuously increasing fraction of renewables in the energy fields. The three post-2015 agendas for action, the Paris Agreement, the 2030 Agenda for Sustainable Development and the Sendai Framework for Disaster Risk Reduction are great examples. The primary goal of the Paris Agreement is to keep the average rise in global temperature below 2°C, and as close as possible to 1.5°C, above pre-industrial levels, as shown in Figure 1 [2].
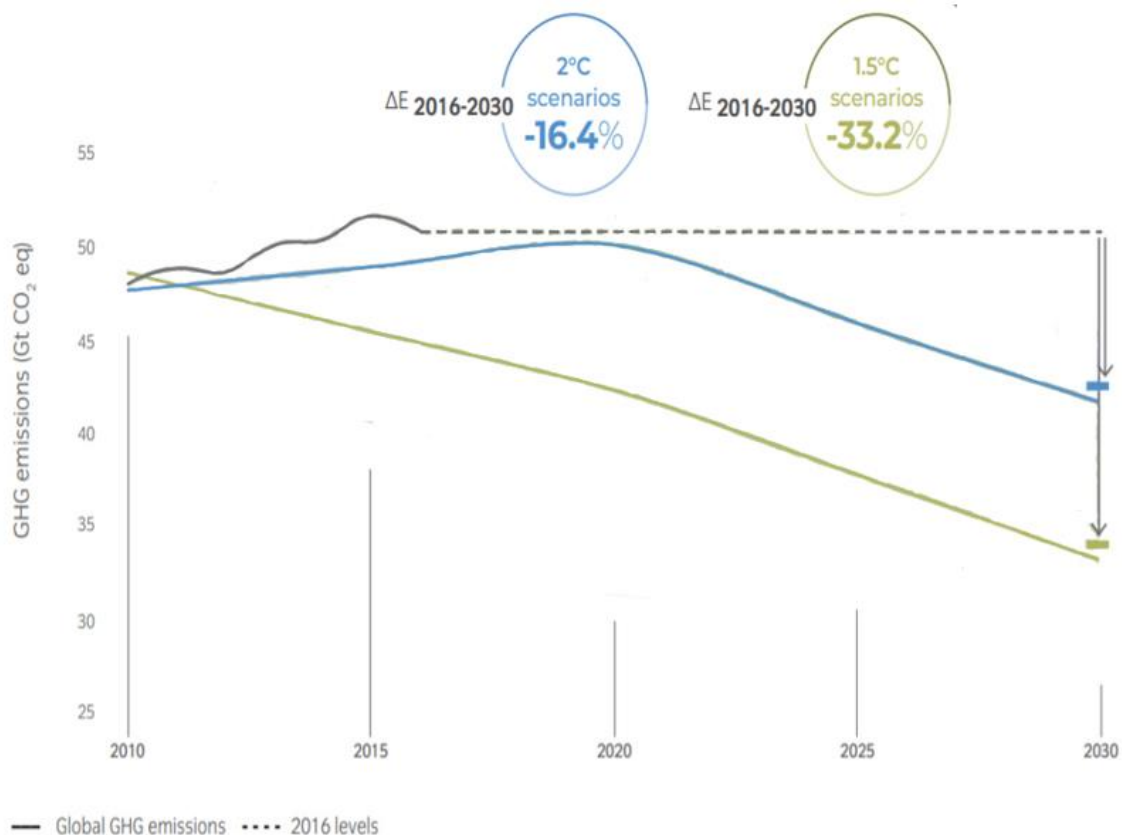
Figure 1 GHG emissions and Paris Agreement Scenarios [2]

Global energy demand grew by 2% in 2017 after two years of low growth. However, demand would be much higher if not for progress on energy efficiency, which could provide more than 40% of the abatement required by 2040 to be in line with the Paris agreement. Energy efficiency, combined with renewable energy and other measures, is therefore indispensable to achieve global climate targets [3]. One way to improve energy efficiency is to recover waste heat fluxes from power plants and industries. There are many possibilities to do this, e.g. in furnace, it is possible to use thermal energy from high temperature exhaust. The most commonly used waste heat recovery methods are preheating combustion air, steam generation and water heating. Another approach is to use waste heat to drive a sorption chiller, when a cooling load is needed. Renewable energy sources include solar, wind, hydrothermal, biomass, biofuel and geothermal energy. In 2016, world Total Primary Energy Supply (TPES) was 13671 Mtoe, of which 13.7% was produced from renewable energy sources, as shown in Figure 2 [4].
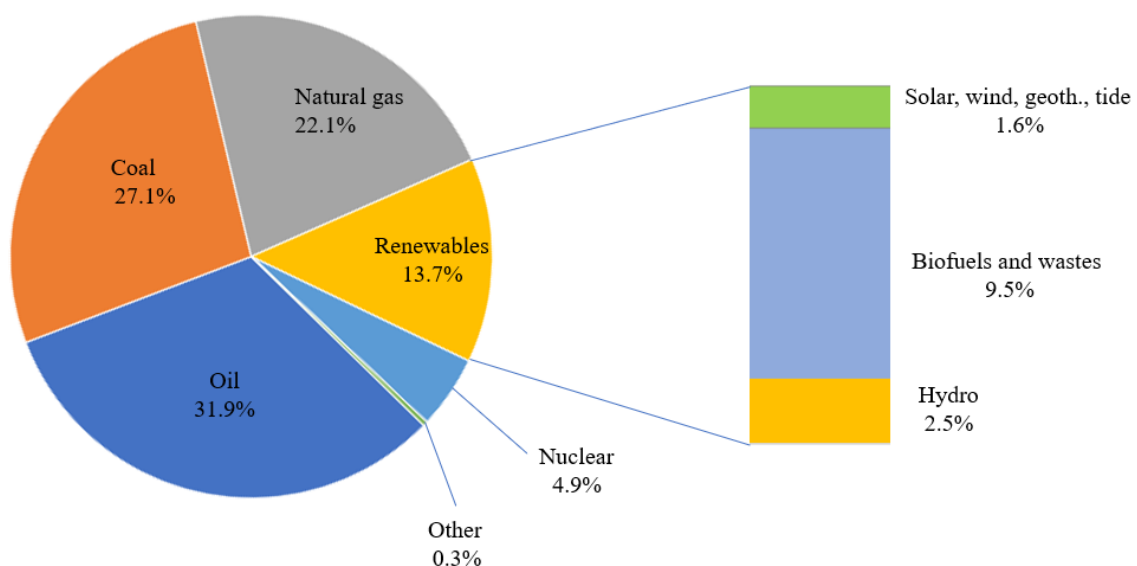
Figure 2 Total primary energy supply percentages [4]

Exploiting waste fluxes and renewables, especially wind and solar, has a huge drawback. They can produce a large amount of energy, but they are intermittent sources and they often cannot match the request of users. Energy storage has become a relevant topic of research because it provides flexibility both for thermal and electric power plants, decoupling production and demand.

A storage system can absorb the production peak coming for instance from intermittent renewable sources and ensures its availability for the moment it is requested by the user. For example, photovoltaic plant electricity stored in batteries is disposable at any given time.

1.1   Energy storage

Energy can be stored in several forms, such as chemical, kinetic or potential, and then converted into electricity if needed. This section is a review of the main types of storage systems.

1.1.1   Mechanical energy storage

One of the oldest forms to store energy, flywheels have been used to achieve smooth operation of machines. Nowadays they are sophisticated devices, where mechanical energy is transferred to and from the flywheel by an electric engine [5]. Advantages of these systems include high power density, long lifespan and environmentally friendly operation. To achieve higher efficiency, they work in vacuum chambers in order to reduce the aerodynamic drag losses [6]. Flywheels are used especially in aerospace and automotive applications where large power is required in short times, for example regenerative braking, as well as for wind power and smart grid energy storage [7]. Another widely adopted electricity storage technology is pumped hydroelectric storage (PHES). PHES is an established, mature and commercially available solution for electricity storage. It is used to stabilize the electricity grid through peak shaving, load balancing and frequency regulation [8]. PHES stores energy in the form of potential energy of water that is pumped from a low reservoir to a high reservoir. In this type of system, low cost electric power is used for pumping water from the lower reservoir to the upper one. When the power demand is high, the stored water is released through hydro turbines to produce electric power [9]. Another interesting example of mechanical storage is Compressed Air Energy Storage (CAES), in which off-peak electricity is used for storing compressed air in an underground cavern. This air is then heated and expanded in a gas turbine to produce electricity during peak demand hours. As it derives from gas turbine technology, CAES technology is readily available and reliable. In this respect, we note the following two plants: one constructed in Germany and the other in the USA of 390 MW and 110 MW turbine capacities, respectively [10].

1.1.2 Electrochemical storage

Systems for electrochemical energy storage and conversion include batteries and electrochemical capacitors (ECs) [11]. Battery storage technologies include lead-acid, lithium-ion, sodium-based batteries and redox flow batteries (RFBs). These technologies provide a potential solution to large-scale energy storage and to reduce the mismatch between intermittent electricity production and customer requirements for the instant delivery of electric power [12]. Batteries release and recharge energy very slowly, i.e. they have low power density, therefore for rapid power delivery and recharging electrochemical capacitors known as supercapacitors might be an option [13]. The battery is composed of three main components: the anode and the cathode, made of different chemicals, and the electrolyte, which separates them. When the battery is connected to an electric device, a chemical reaction takes place on the electrodes and an electric current is generated. Supercapacitors or ultracapacitors have recently attracted considerable attention due to theirs high power density, high charge/discharge rates and long life-cycle performance. A supercapacitor is composed by two electrodes typically coated with active carbon, an electrolyte and a separator. They are considered as one of the most promising electrochemical energy storage devices, having the potential to complement the batteries for energy storage applications, i.e., those for portable and wearable electronic, electrical and hybrid vehicles [14]. Currently the major drawback of supercapacitors is the low energy density (generally about 5 Wh/kg) [15], compared to commercialized lithium-ion batteries (about 100 Wh/kg) [16].

1.1.3 Superconductive Magnetic Energy Storage

A superconducting magnetic energy storage (SMES) is an energy storage device that stores electrical energy in a magnetic field. In SMES, a superconductive coil allows a direct electrical current to flow through it with no resistive loss, due to the operating cryogenic temperature [17]. These devices have high power density and high efficiency, so they are used where fast changing loads are involved.

1.2 Thermal energy storage

Energy demands in the commercial, industrial, and utility sectors vary on daily, weekly, and seasonal bases. These demands can be matched with the help of thermal energy storage (TES) systems. The use of TES for applications such as space and water heating, cooling, air-conditioning, and so on has recently received much attention. These systems have an enormous potential to make the use of thermal energy more effective and for facilitating large-scale energy transition from fossil fuel to renewable using plants [16]. Figure 3 shows the schematic concept of a thermal energy storage.
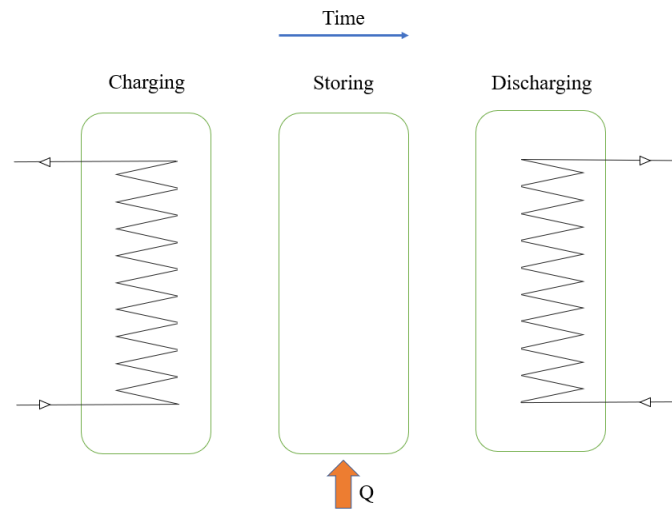
Figure 3 Heat storage working principles [16]

Typically, in the scientific literature, authors are used to distinguish among three different categories of TES: sensible heat storage, latent heat storage and thermochemical heat storage. The first two systems are more common (and technologically mature) as they present a lower level of complexity and have been investigated for longer time. The third one is still under development.

1.3 Sensible thermal energy storage

The most popular approach to heat storage involves preserving energy in the form of sensible heat, usually by raising the temperature of water, rocks, soil and other materials. In most of the applications at low temperature, water is being used as the storage medium [18]. The amount of energy input to a sensible TES is related to the mass of storage material and its heat capacity as well as the temperature difference of the storage medium, between its initial and final states. This stored heat Q can thus be expressed as:

$$Q = mc_p\Delta T \tag{1.1}$$

Where m and c_p denote the mass and the specific heat of the storage material respectively, and ΔT is the temperature difference before and after the storage operation [19]. Those systems can achieve relatively small energy density, thus typically implying high volumes of storage material to cope with usual heat demands. One additional drawback is that sensible storage systems have significant heat losses towards the environment, caused by the temperature difference between them. For these reasons it is not a viable option for long term storage applications [20].

1.4 Latent thermal energy storage

Latent heat storage (LHS) makes use of the heat absorbed or released by the storage material during its (solid-liquid or liquid-gas) phase-change. The storage capacity of an LHS system with phase change materials is given by:

$$Q = m\int_{T_l}^{T_m} c_{ps}\, dT + m\Delta H_m + m\int_{T_m}^{T_H} c_{pl} dT \tag{1.2}$$

where T_m is the melting point of the phase changing material (PCM), ΔH_m is the phase change enthalpy, c_{ps} and c_{pl} are the specific heat of the PCM in solid and liquid state respectively [21]. LHS systems may be cost-effective and convenient because latent heat is usually much higher than the sensible heat exchange for a given medium, which is related to its specific heat. Furthermore, latent TES system operate over a small temperature range, since the heat

interaction occurs at constant temperature [22]. There are also a few drawbacks that researchers are still studying solutions for. One issue has to do with the fact that PCMs have typically very low thermal conductivity. Hence, one possible option is to encapsulate them in high-conductive structures to enhance the heat transfer. Another possible option is the addition of high-conductivity particles in the PCM, such as carbon based (graphite) and metallic nanoparticles. The application of finned pipes and tubes has been introduced as one more efficient way to improve the thermal conductivity of PCMs [23]. On a system level, this technology has the same disadvantages as the sensible heat storage: thermal losses due to temperature gradient with the environment and relatively small energy density. Another issue is that these materials do not have long term stability, therefore they must be substituted generally after 10 years. Current applications make use of PCMs embedded in wallboards, walls, floors and ceilings. Since the phase change occurs at constant temperature, embedding PCMs in the structural components of buildings may prevent excessive room temperature fluctuations, thus reducing the cooling and the heating requirements [24].

1.5   Thermochemical heat storage

Thermochemical energy storage is a promising new technology because it provides near-zero thermal losses and high energy density. This is due to the fact that energy is stored in the form of chemical potential by a reversible chemical reaction such as redox reaction or chemi-physi-sorption reaction. The research on this system is still at an early stage therefore there are no commercially available thermochemical energy storage systems.

1.5.1   Redox reactions

Recently, there has been a growing effort in the study of thermochemical heat storage based on reduction-oxidation reactions, particularly with multivalent metal oxides. These processes are interesting because they can work in an open system in which air is used both as a heat transfer fluid and a reactant, thus avoiding the need of reactant gas.

Storage plants based on redox reactions store and release heat through the following reactions [25]:

$$\text{Charge/reduction} \quad MO_x + \Delta H \rightarrow MO_{x-y} + \frac{y}{2}O_2(g)$$

$$\text{Discharge/oxidation} \quad MO_{x-y} + \frac{y}{2}O_2(g) \rightarrow MO_x + \Delta H$$
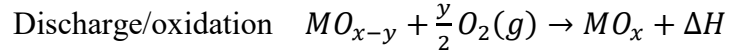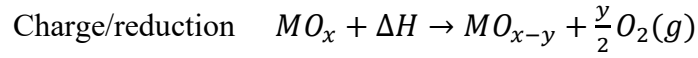
The high energy storage density and the possibility of working at higher temperature ranges (600-1000°) make reduction-oxidation cycles of metal oxides a promising concept for energy storage, especially with plants that uses solar concentrators, often referred to as Concentrated Solar Power (CSP) [26]. Several oxides have been analysed as possible candidates for this application: BaO_2, Co_3O_4, and Mn_2O_3 redox reactions are thermodynamically advantageous at temperatures in the $700 - 1000°C$ range. Among them, Co_3O_4 showed the best reversibility behaviour [27].

1.5.2   Sorption energy storage

Sorption is a reversible physical or chemical process in which one substance, called sorbate, establishes reversible bonds with another substance, called sorbent. During this process (sorption), heat is released, while during the reverse process (desorption), an external heat source is needed to separate the two substances. In other words, this technology exploits a heat source, e.g. solar thermal, and stores it in the form of chemical potential. Heat transformation based on adsorption/desorption in microporous adsorbents has been considered in a number of applications such as adsorption chiller (ACS), adsorption heat pump (AHP) or thermochemical storage (TCS) since the 1980s. Before that, most of the adsorbents like zeolites were used only for gas separation or catalysis processes, therefore they were not optimized to be used for adsorption reactions. Within the last decade, intensive research on adsorbents led to steadily improvement of the existing sorbent materials and the development of new ones with an enhanced adsorption capacity [28].

1.6 Thesis motivations

The aim of this work is the design of a lab-scale, thermochemical storage device which works with adsorption of water into solid sorbent materials. Although not limited to, for the sake of simplicity, we here consider zeolite 13X as this is a common and well characterized sorbent. In the near future, the object of this thesis will be possibly used as a technology demonstrator in the laboratory of Politecnico di Torino. After the initial presentation of the state of the art of TES technologies, the thesis will explain the design process of the whole system. Initially, using two software programs developed at the Department of Energy of Politecnico di Torino, the adsorption cycle points were established. The main design target is to obtain a system capable of storing a minimum amount of energy in the order of 100 Wh (charge phase), with a discharge phase occurring at a temperature of at least $35°C$ (temperature level that could be useful for instance for a floor heating system). A maximum desorption temperature of $90°C$ is considered. After the working cycle is defined, the thesis proceeds with the geometric design of the two vessels, one for the sorption reaction and the other for the sorbate evaporation/condensation (water). Both vessels are expected to operate under evacuated conditions (established by a proper vacuum pump) with a minimum absolute pressure in the order of $12,2\ mbar$ (corresponding to the water vapour pressure at $10°C$). The structural design of pressurized vessels is consistent with the ASME Boiler & Pressure Vessels Code (BPVC), Section VIII, Division I and the material properties are taken from Section II, Part D. This code provides also the rules for the design of the lids necessary to seal the vessels. The geometry designed on the software Solidworks is then imported into the software Hypermesh, in order to perform an FEM analysis on the vessels and ensure they are not subject to permanent deformations. Inside both vessels is placed a heat exchanger which is a copper tube coil. Three configurations of the heat exchanger inside the reactor vessel have been designed, and all have been considered as potentially viable. The designed parts are reported in this work, as well as all of their executive CAD drawings, which will be used to build them. Finally, a theoretical model for the adsorption reaction is developed considering the water as a phase change material (PCM).

2 Sorption storage systems

Sensible and latent heat storage devices store heat together with its corresponding amount of entropy. In these so-called "direct" heat storage media, heat – i.e. energy – is transferred directly to the storage medium. The achievable energy density is limited by the entropy storage capacity of the material. Otherwise the adsorption process is a reversible physico-chemical reaction suitable to store heat in an indirect way [29]. The conceptual scheme of a direct storage system is shown in Figure 4.
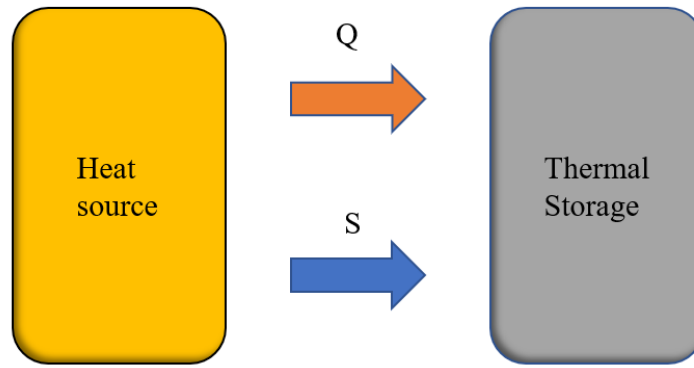
Figure 4 Direct thermal storage concept

The term Q is the heat released by the source to the storage in $J\ kg^{-1}$, and S, in $J\ kg^{-1}\ K^{-1}$, is the entropy associated to Q by the relationship:

$$dS = \frac{\delta Q}{T} \qquad (2.1)$$

Modifying the equation above:

$$\frac{Q}{m} = \bar{T}\frac{\Delta S}{m} \qquad (2.2)$$

where m is the mass of the material, ΔS is the entropy variation during the heat transfer phase and $\bar{T}$ is the average operating temperature.

The left part of the equation is the energy density, the right part is the entropy density multiplied by the mean temperature. This equation explains that the quantity of energy that can be accumulated is dependent on the variation of entropy that can be induced in the storage material, if we consider the temperature constant. Unfortunately, there is a physical limitation to the quantity of entropy a material can withstand. This issue in conjunction with the thermal losses due to the temperature gradient with the environment, are the main reasons direct systems are not very efficient. Operating with an indirect system solves both issues, because the energy flux is separated from the entropy flux and the system is isothermal with the environment. Figure 5 shows the working principle of indirect storage systems.
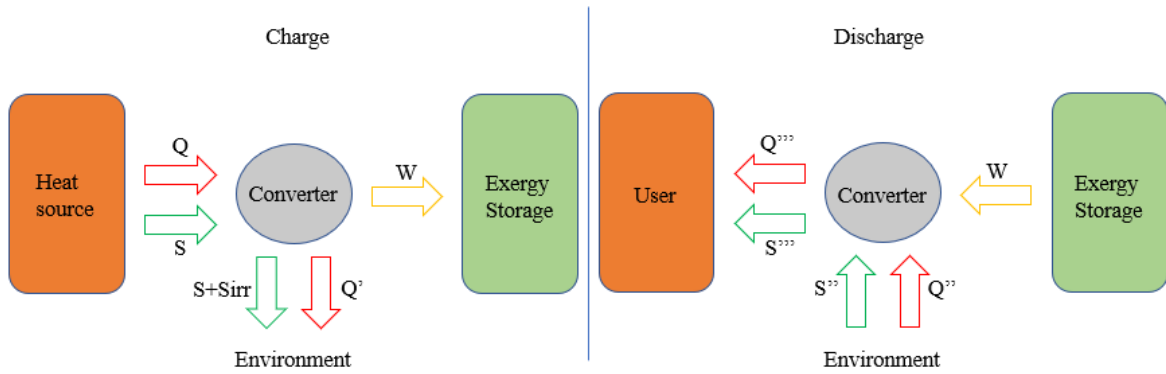
Figure 5 Indirect thermal storage concept

Entropy and energy fluxes, S and Q, enter a converter which releases a portion of heat Q' and the entropy $S + S_{irr}$ towards the environment (S_{irr} caused by irreversibilities in the converter), while only the exergy flux W charges the storage. During the discharge phase, the exergy stored W is sent to the converter, together with the heat Q'' and its associated entropy flux S'' taken from the ambient. In return the converter gives back the heat flux Q''' together with its entropy flux S''' to the user. Sorption storage systems perform a reversible chemical reaction, which is endothermic in one direction, and exothermic in the other direction. Having A and B reactants, during the storage discharging phase the following reaction occurs:

$$A + B \rightarrow AB + heat$$
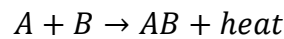
During the charging phase the inverse reaction occurs:

$$AB + heat \rightarrow A + B$$
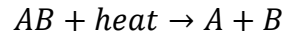
After this process A and B are kept in separate reservoirs, ready to be mixed again if heat is needed. The general sorption reaction is:

$$A + B \leftrightarrow AB + heat$$
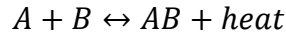
The heat needed for the charging reaction, and consequently the storable heat, depends greatly on the types of bonds between the reactants A and B. There are two categories of sorption reactions: chemisorption and physisorption. The first one involves strong ionic or covalent bonds between adsorbent and adsorbate; the second one implies weaker bonds, like Van der Waals or hydrogen bonds. Stronger chemical bonds imply that the necessary heat to charge/discharge the system is much higher for the chemisorption systems, about 40-400 $kJ\ mol^{-1}$, with respect to physisorption, which is about 20-70 $kJ\ mol^{-1}$. Let us consider the variation of the Gibbs free energy of the above reaction (at constant temperature T):

$$\Delta G = \Delta H - T\Delta S \tag{2.3}$$

where ΔH and ΔS are the enthalpy and entropy variation of the reaction respectively. If products and reactants are in equilibrium $\Delta G = 0$, if $\Delta G > 0$ the direct reaction is not spontaneous and if $\Delta G < 0$ the direct reaction happens spontaneously. In other words, a spontaneous direct reaction happens at environmental condition without the need of an energy source, thus it has $\Delta G < 0$. If the sorption reaction is at equilibrium, $\Delta G = 0$ therefore we can define the temperature of equilibrium as:

$$T^* = \frac{\Delta H}{\Delta S} \tag{2.4}$$

Any deviation from this temperature will cause the system to react accordingly, shifting the equilibrium towards the reactants or the products. To invert the sorption reaction and recharge the storage, it is necessary to use a heat source at a temperature higher than the equilibrium one, e.g. $T > T^*$. Otherwise, the sorption reaction is spontaneous, so it only needs the reactants to

be in contact. Sorption TES can have two main configurations: open loop and closed loop. Open loop configuration exchanges mass with the environment: the ambient air is sent by a fan into the absorbent bed, which absorbs air humidity and releases heat. The same heat increases the temperature of the dry air, which is then sent to the users as a heat source. This system can only work with water as sorbate, since it uses ambient air, and must operate with environmentally friendly sorbents. Furthermore, the humidity content in the air may not be sufficient to perform an efficient sorption reaction, therefore a humidifier is sometimes required. For these reasons usually the heat produced by the sorption reaction is not enough for DHW purposes or space heating, so the system needs a heat recovery unit as backup. The main advantage of this system is simplicity of application and operation, because its working principle is very similar to a well-studied technology, e.g. desiccant cooling (DEC) which is used in air conditioning systems. DEC combines sorption dehumidification, heat recovery, heating and evaporation, as it takes air from the ambient and dehumidifies it thanks to a liquid or solid desiccant (SiO_2 (silica gel), ClLi (lithium chloride), Al_2O_3 (activated alumina), LiBr (lithium bromide) or zeolite). The dry air is then evaporatively cooled by a heat exchanger and it is ready to refrigerate and dehumidify buildings [30], while the wet absorbent must be regenerated by heat. Closed loop systems have a wider range of applications because they can use every absorbent-sorbate couple, since they do not exchange mass with the environment. For this reason, sorbate and adsorbent need two separate vessels, one where the sorption and desorption reactions occurs, the other where the sorbate is evaporated/condensed. Thus, these systems are more complicated than open loop ones. Furthermore, typical sorbates require vacuum pumps to reach the appropriate working conditions, therefore these systems are also referred to as "evacuated". Finally, both vessels require an internal heat exchanger in order to enhance the evaporation of the sorbate, thus making the overall design more complex. The vapour is transferred from one vessel to the other owing to a pressure difference. Thermochemical energy storage systems can be classified also by the predominant type of reaction that occurs during the sorption process: liquid absorption, solid adsorption and chemical reaction (shown in Figure 6) [31].
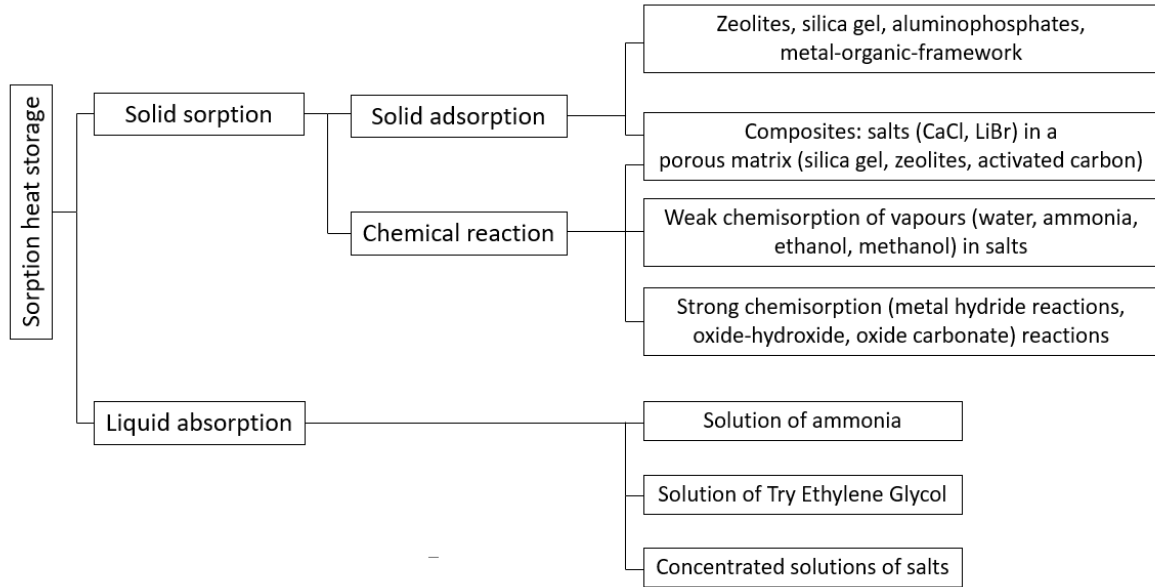
Figure 6 Sorption heat storage technologies [31]

2.1 Physisorption based systems

This technology is mainly used in sorption chillers and low-temperature heat storage. Their working cycle is the same, but the useful effect is located at different stages of the process. The cycle is composed of a charging, a conservation, and a discharge phase. Figure 7 describes how it works, the black lines representing the sorbent, and the blue lines representing the sorbate. In point 1, the system is completely discharged, and the sorbate is absorbed onto the sorbent in the reactor. The recharge phase, from state 1 to 3, is composed of an isosteric heating (state 1-2) and an isobaric heating (state 2-3). During the first step, the energy spent in the reactor (adsorber) is not sufficient for the desorption, until the temperature reaches the desorption temperature T_{des}. At that point (state 2) the sorbate starts desorbing from the sorbent and it can move to the condenser if the throttling valve is open. In state 3 the desorption is interrupted, the working pair is fully (or partially) separated, and the storage is charged. When energy is requested by the user, the water is evaporated (state E-1) and sent to the reactor where the adsorption reaction occurs, releasing the useful heating effect (state 4-1).
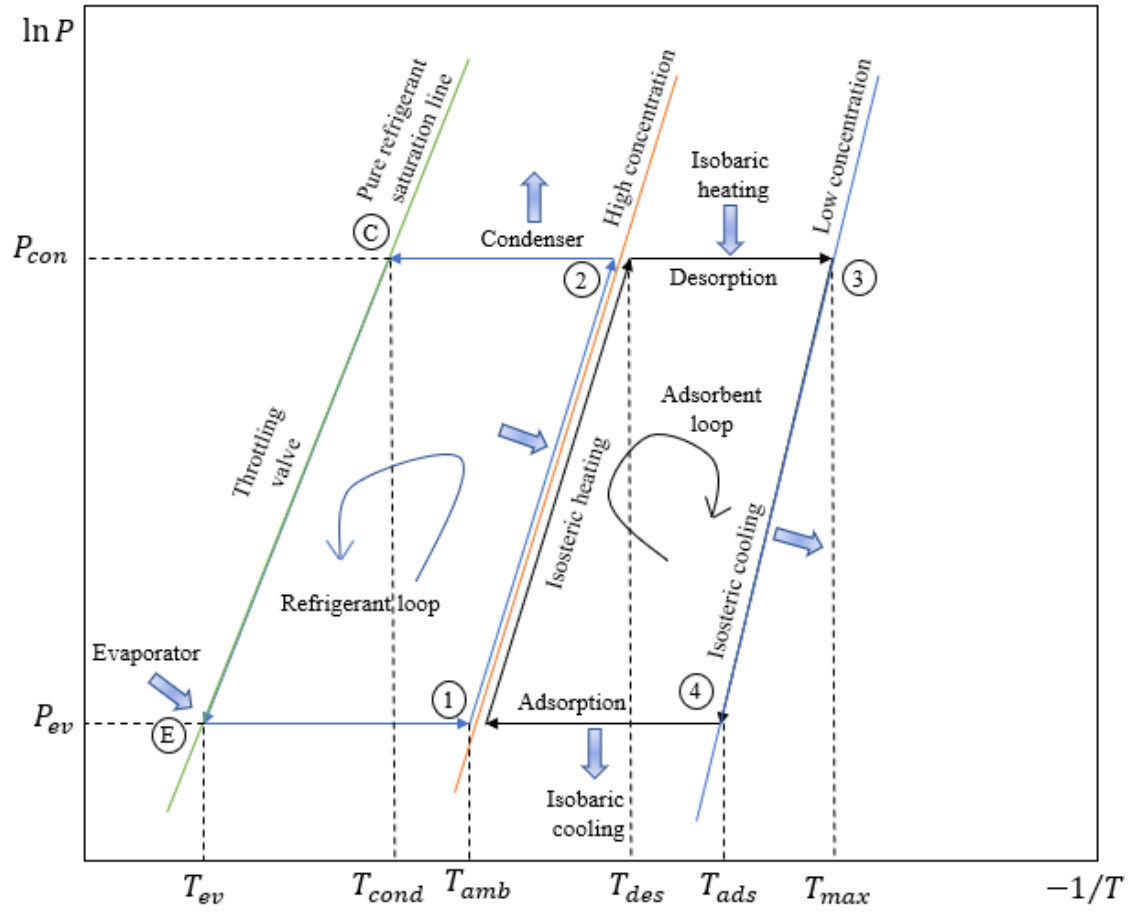
Figure 7 Clapeyron diagram of the basic adsorption cycle [32]

Figure 8 shows the functioning scheme of a basic adsorption cycle implementing the above process.

Charging phase from state 3 to state 1

Heat input from solar energy

Adsorbate vapour flow

Heat released into the environment

Reactor

Evaporator/condenser

Discharging phase from state 4 to state 1

Heat output for end user

Adsorbate vapour flow

Cold output for space cooling

Reactor

Evaporator/condenser
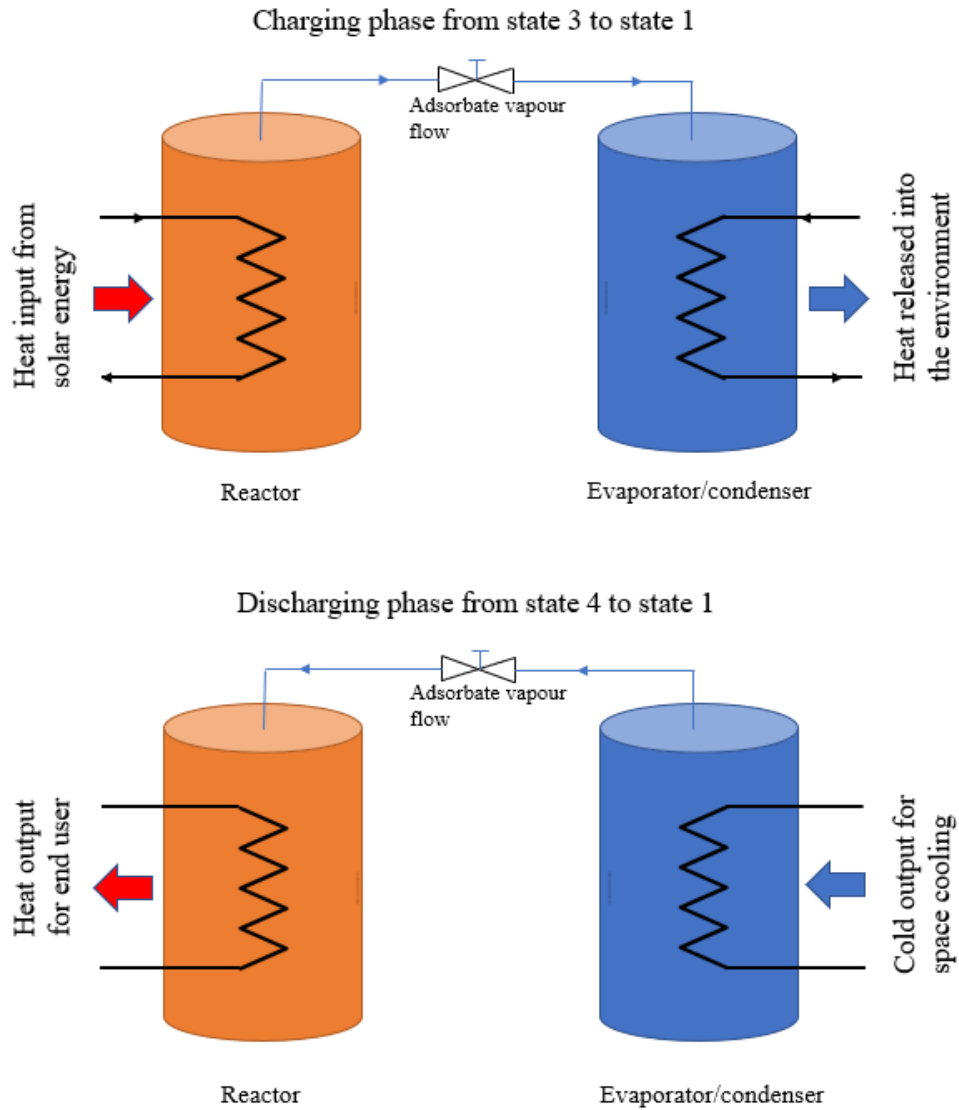
Figure 8 Adsorption system scheme

2.1.1 Liquid absorption systems

Liquid absorption is a well-established technology used for space heating and cooling exploiting heat at temperatures under 100°C, which would otherwise be wasted to the environment. Instead, it drives the thermodynamic cycle of absorption heat pumps (AHP), absorption chillers (AC), and absorption heat transformers (AHT) [33]. Absorption chillers are thermally driven, therefore they do not require an electric power input. Hence, where power is

expensive or unavailable, absorption machines may provide reliable and quiet cooling. Various types of refrigerant–absorbent pairs are used but the most common ones are LiBr–water and ammonia–water [34]. Until now, no absorption storage system has reached the commercial stage, because further research efforts are needed to find optimal working pairs for this technology. The vast majority of the prototypes under development focus on long-term, inter-seasonal storage [35].

2.1.2 Solid adsorption systems

Adsorption technologies have been used extensively for separation and purification of gases for the past few decades but their exploitation for refrigeration and heating purposes is rather recent [36]. Adsorption is a surface phenomenon occurring at the interface of two phases, in which cohesive forces including Van der Waals forces and hydrogen bonding, keep the fluid molecules confined within the pores of a solid [37]. Figure 9 illustrates the various steps of the reaction: at the first stage the molecules are absorbed at low pressure in the best sites of the surface (smaller pores), where the bonding potential of the atoms of the sorbent is higher; as the vapor pressure increases, the coverage on the adsorbent surface forms a single layer (stage 2); multi-layer coverage starts to appear thanks to further increase of the pressure (stage 3); the adsorption stops when all the available sites are filled and the maximum coverage is reached (stage 4) [38].

Increasing gas pressure
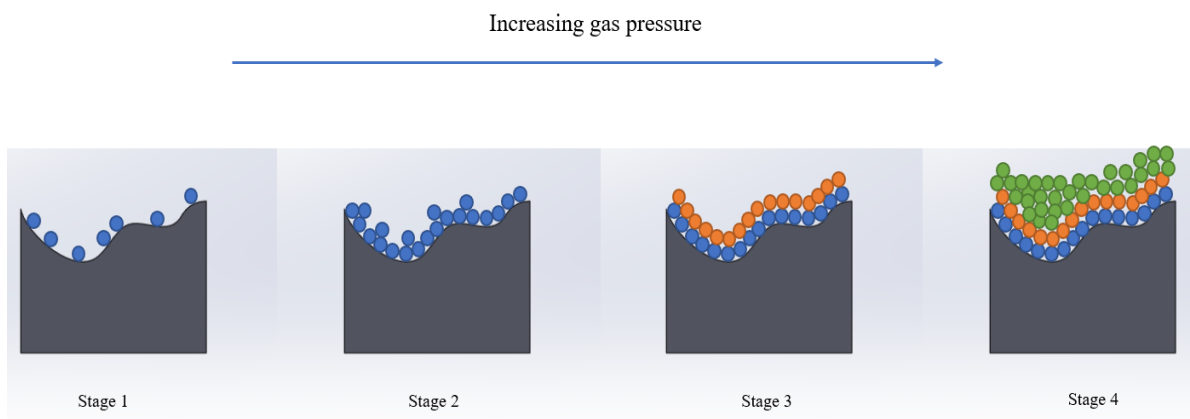
Figure 9 Adsorption reaction phases

17

The process can be described with an adsorption isotherm on a pressure-uptake plane, the form of which depends on the type of adsorbent material used, as shown in Figure 10 [39].
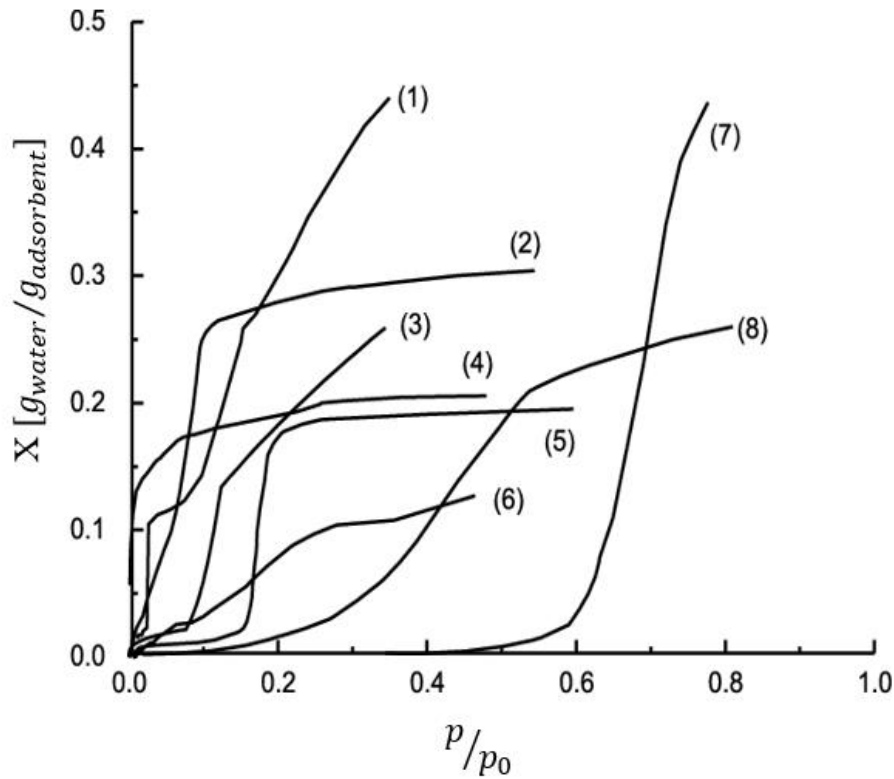
Figure 10 Water adsorption isotherms: (1) SWS-1L; (2) FAM- Z02; (3) SWS-5L; (4) zeolite 13X; (5) FAM-Z01; (6) silica Fuji Silys RD; (7) carbon aerogel a-CA-54; (8) pitch-based ACF P5 [39]

Researcher interest in adsorption technologies for residential and commercial buildings is driven by many advantages such as [40]:

- Possible exploitation of waste heat, solar, geothermal energy with low thermal value
- long life cycle
- low maintenance costs
- low noises and vibration
- zero-emissions operation
- non-hazardous, non-pollutant materials

Systems using water as a sorbate may be a good option to satisfy all the above requirements. In this context, zeolites are showing great potential for heat storage applications. Zeolites can be

easily synthesized with a precise chemical composition and structure of the micropores, therefore zeolite crystals present both large heat of adsorption and significant water adsorption capabilities, without noticeable structural degradation [41]. Since this technology is rather recent, studies have not reached sufficient maturity to overcome many of the current technological barriers such as low coefficient of performance (COP) values, complex structural design and intermittent working principle. At present, many of the research efforts are focused on the development of new materials, in order to improve the efficiency of the adsorption/desorption cycle [42].

2.2 Chemisorption based systems

Reversible chemical reactions of inorganic salts with water or other fluid reaction couples for the purpose of thermal energy storage have been studied for decades. Numerous reversible reactions can be used to store heat: oxide hydration or carbonation, hydration of hygroscopic salts and metal hydration [43]. Salt hydrates are the most used materials in chemical sorption storage systems. The general reversible hydration reaction of a salt can be written as follows:

$$Salt \cdot nH_2O + energy \leftrightarrow Salt + nH_2O$$
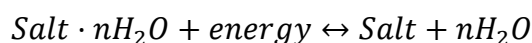
A key factor for a successful development of a chemisorption machine for a specific application is the choice of the sorbent salt. Different salts undergo different reactions, where the uptake may vary from a few grams to more than $1\ kg$ of refrigerant per kg of salt. Furthermore, the equilibrium pressure of one reaction can be several times higher than the equilibrium pressure of other reactions, at the same temperature. Thus, sorption machines designed to effectively use low-grade waste heat, or solar energy even during low insolation days, should contain salts that can desorb at temperatures as low as 60–70 °C. Moreover, the salts should have high adsorption capacity per unit mass of salt to ensure relatively high specific cooling capacity and COP [44]. Table 1 shows the promising materials for this technology.

Table 1 Common chemisorption reactions [45]

Material name	Reaction			Energy storage density	Desorption temperature
	$A+$	B	$\leftrightarrow C$	GJ/m^3	$°C$
Magnesium sulphate	$MgSO_4$	H_2O	$MgSO_4 \cdot 7H_2O$	2.8	122
Iron carbonate	FeO	CO_2	$FeCO_3$	2.6	180
Iron hydroxide	FeO	H_2O	$Fe(OH)_2$	2.2	150
Calcium sulphate	$CaSO_4$	H_2O	$CaSO_4 \cdot 2H_2O$	1.4	89

2.3 Materials key characteristics for adsorption heat storage

The key characteristics that reactants should have are [46] [47]:

- high energy storage density (Wh/kg or kWh/m³)
- low charging temperature
- high uptake of sorbate
- high chemical and high thermodynamic stability (high number of operation cycles without losing the material properties)
- high thermal conductivity
- low corrosivity
- low toxicity, low environmental impact and low costs

No material currently available can satisfy all the above characteristics, therefore the material selection should be screened and optimized to match the application requirements. Different working pairs or materials considered mainly employ water as sorbate, due to its environmentally friendly properties, high evaporation heat and low cost [47]. The way materials interact with water largely depends on the structure of the micropores and on its composition, and they can be divided in two categories: hydrophilic and hydrophobic. A hydrophilic material tends to attract water molecules at very low vapour pressure, while a hydrophobic material

necessitates higher pressures. Porous materials are most frequently characterized in terms of pore sizes derived from gas sorption data, and IUPAC conventions have been proposed for classifying pore sizes and gas sorption isotherms that reflect the relationship between porosity and sorption (see Figure 11) [48].
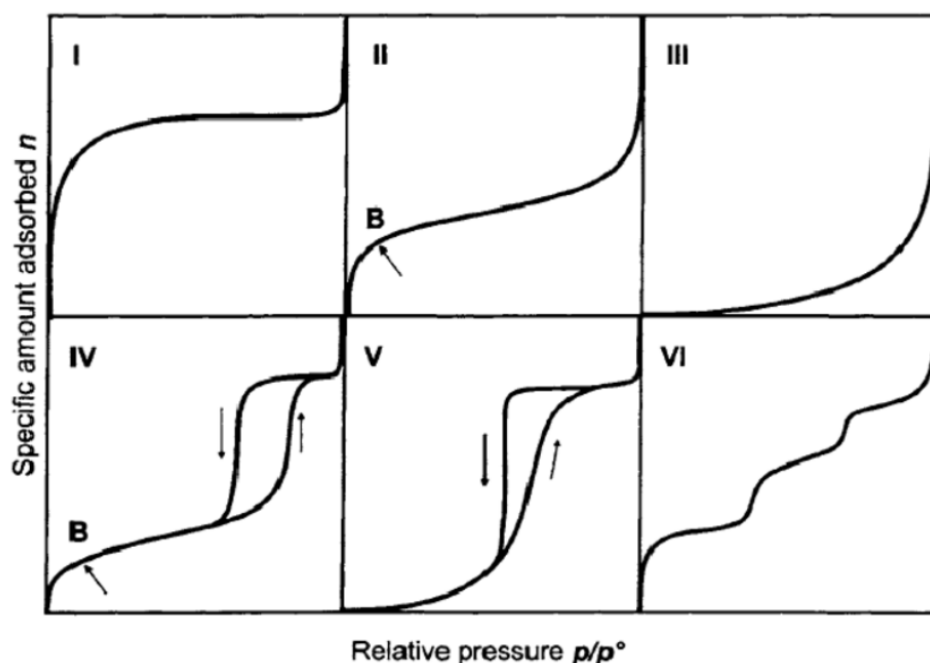
Figure 11 Physisorption isotherm types according to the IUPAC classification [49]

These curves describe the amount of vapour adsorbed with respect to the variation of the relative pressure at constant temperature. Type I isotherms are typical of microporous solids and the steep increase of vapour absorbed at low relative pressure indicates that the material is strongly hydrophilic. The Langmuir isotherm belongs to the Type I isotherm, which approaches a limiting value as p/p_0 tends to 1 [50]. Type II and type III describe adsorption on macroporous adsorbents with strong and weak adsorbate-adsorbent interaction respectively [51]. Type IV isotherm shows a hysteresis loop, attributed to the filling/vacating of mesopores by capillary condensation. The lower branch represents sorption, while the upper branch represents desorption. Type V isotherm has a characteristic S-curve and hysteresis loop. This isotherm is witnessed for the adsorption of water onto various types of zeolites. The Type VI isotherm exhibits multilayer adsorption on a uniform non-porous surface. In this type the adsorption happens in steps [52].

Figure 12 shows how the pores are distributed inside the material. Pore sizes below $2\ nm$ are denoted micropores, those in the range of $2\ nm$ to $50\ nm$ are called mesopores, and those above $50\ nm$ are macropores.
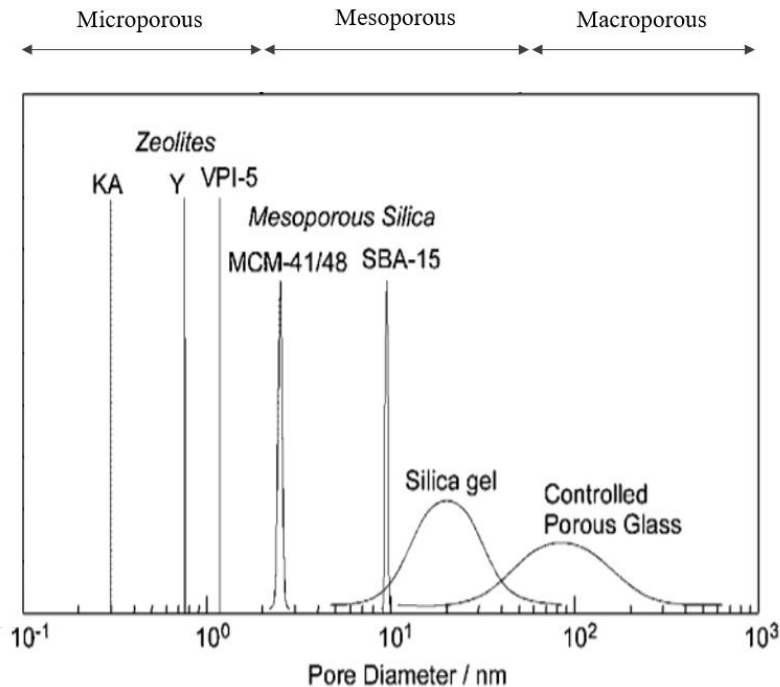
Figure 12 Classification of porous materials according to their pore diameters [53]

Figure 13 shows the different shapes pores can assume: through pores are open at two or more sides, blind pores are open at only one side, and closed pores does not have any opening. Every pore can be isolated, but more frequently they are connected forming a pore network.
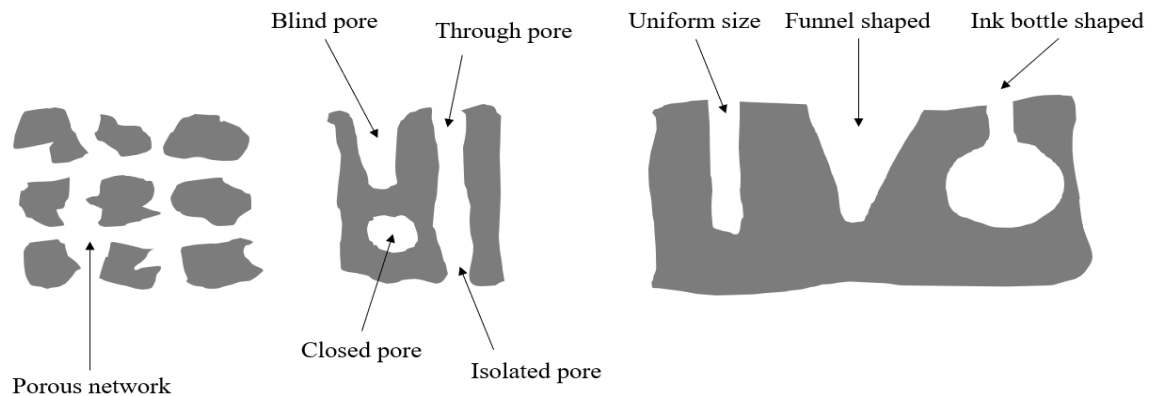
Figure 13 Different pore shapes [54]

2.4 Common materials for adsorption heat storage

The most studied materials employed in sorption plants are presented in this section.

2.4.1 Silica gel

Silica gel is an incompletely dehydrated polymeric structure of colloidal salicylic acid with the formula $SiO_2 \cdot nH_2O$. This amorphous material consists of spherical particles of 2-20 nm in size, sticking together to form the adsorbent silica gel [55]. The porous structure may change between open and closed systems. In a closed system the sorption reaction happens at partial pressures in the range of $0.1 - 0.3$ therefore the silica gel needs a microporous structure in order to exchange a sufficient amount of water. In opened systems the partial pressure is higher therefore it is enough to use a mesoporous silica gel. The low regeneration temperature, in the range of 50-90°C, makes it particularly suitable for industrial and residential applications where all heat fluxes below 100°C are generally wasted into the environment. Other advantages are the relatively low cost and the fact that it is environmentally friendly. Only three types of silica gel are commercially available: Type-RD, Type A and Type 3A [56]. The key shortcoming with silica gel is the low water exchange within a typical cycle, especially for closed systems, which therefore requires large volumes of adsorbent. Another disadvantage is the low temperature increase during the adsorption process. For these reasons, silica gel has low cooling capacity, low specific cooling capacity and low COP [57]. It remains a possible option if employed for long term storage because costs are the main issue.

2.4.2 Zeolites

Zeolites are crystalline alumino-silicates, characterized by a high specific surface area (about $700 \ m^2/g$) and wide microporous volumes, which make these materials perfectly suitable for water vapor adsorption. Thanks to their porous structure, zeolites are usually highly hydrophilic, which allow them to obtain high adsorption capacities even at low partial pressures. This high affinity for water, of course, causes strong bonding that requires high desorption temperatures (more than $150°C$). Zeolites A, 13X and Y are the most common synthetic zeolite types employed for adsorption heat storage [58]. These materials are used generally in open systems in industrial facilities because they require higher regeneration

23

temperatures than silica gel and air is the most efficient heat transfer medium. Thanks to their crystalline structure they guarantee higher thermal stability over high frequency cycles than silica gel. The general chemical formula of zeolites is:

$$M_{x/n}\left[(AlO_2)_x(SiO_2)_y\right] \cdot zH_2O$$

where n is the valency of the metal cation M, which balance the negative charges in the aluminosilicate framework. Type 13X is one of the best performing zeolites for heat storage purposes due to high water uptake and fast reaction kinetics. In an open system configuration experiments on zeolite 13X, a maximum sorption temperature of 80°C was achieved with a water vapor pressure of 20 mbar and a hydration temperature of 35°C [59]. Table 2 shows the classification of the zeolites based on their framework.

Table 2 Different zeolite types [60]

Zeolite types	Si/Al	Types of zeolite
Low silica	1-1.5	A, X, LSX, sodalite
Intermediate silica	2-5	Y, L, mordenite, erionite
High silica	10-4000	Dealuminated Y, ZSM-5
All silica	∞	silicalite

2.4.3 Zeo-like materials

Recently, new types of microporous sorbent materials have been proposed. They are called zeo-like materials because their crystalline structure is similar to that of zeolites. The two categories which showed the best reaction performances are Aluminophospates (AIPOs) and Silica-Aluminophospates (SAPOs). The adsorption isotherms of these materials show a S-shape curve, which indicates a good applicability to heat transformation [61]. Indeed, they combine high capacity of water adsorption with moderate hydrophilicity, therefore they can be regenerated at low temperatures in the range of 60-100°C maintaining high performance [62]. A recent study [40] tested a commercial SAPO-34 known as AQSOA Z02, both by means of a

thermogravimetric analysis and by atomistic simulations. The isotherms measured with the thermogravimetric analysis presented an S-shaped curve (e.g. Type V), with an average adsorption heat equal to $61.8\ kJ/mol$. This feature makes SAPO-34 interesting for sorption applications, since a significant quantity of refrigerant (e.g. water) can be exchanged in a narrow temperature/pressure range. The cost of these material is higher than zeolites because the synthesis process to produce them is more expensive and an industrial production is still not existent [62].

2.4.4 Active carbons

Active carbons are characterized by high specific surfaces and high micropore volume. They are used mainly with ammonia and alcohols, thanks to their affinity with them. Active carbons are commercially available and cheap therefore they are promising for TES applications, but they can be applied only on closed systems because they have poor water sorption capabilities. Similarly to silica gels, they are mainly studied to be employed as substrate or matrix for composites sorbent or to enhance the thermo-dynamical properties of other sorbent materials.

2.4.5 Metal organic frameworks

Metal organic frameworks (MOFs) are made by connecting inorganic and organic units through reticular synthesis, which forms highly strong bonds. Organic units are usually carboxylates or other similar negatively charged molecules which, connected with the metal-containing unit, build robust crystalline structures with high porosities, e.g. 50% on volume. For this reason, MOFs can reach extremely high specific surface areas, in the range of $1000 - 10000\ m^2/g$, significantly higher than zeolites, silica gel or activated carbon [63]. MOFs have a great potential to be employed for energy storage and other sorption transformations because their reticular synthesis process can tune the porosity, the pore structure and the crystalline structure. In the past decade, 20'000 types of metal organic framework were created, in order to better understand how to combine the inorganic and organic units to obtain specific properties of the final material synthesized. As of today, MIL-101(Cr), MIL-100(Cr), MIL-100(Al) and MIL-100(Fe) showed good cyclic water adsorption/desorption performances and good hydrothermal stabilities and they were recommended as promising adsorbents in dry regions at medium or high humidity conditions [64]. This class of materials is still far from being commercially

available because the costs of production are still too high and their properties as sorption material are still to be explored.

2.4.6 Composite materials

Composite materials are compounds made by impregnating an adsorbent material matrix (silica gel, vermiculite) with a hygroscopic salt like calcium-chloride ($CaCl_2$). The initial aim was to enhance the water uptake of the sorbent in order to increase the COP and the specific cooling power (SCP) of adsorption chillers. In fact, the first composite materials were called Selective Water Sorbents (SWS) and were formed by a silica gel, porous carbon, zeolite matrix and salts ($CaCl_2$, LiBr etc.) [65]. Today the research is trying to develop new composite materials to overcome the main disadvantages they have: poor thermochemical stability of the salt during the sorption cycle and poor heat transfer properties [43]. The interest in these materials is justified by the fact that combinations of the salt and the porous matrix allows to tune the characteristics of the adsorption material in order to meet the needs of the application.

3 Theoretical model

In this chapter, the assumed design constraints will be explained. The design of the demonstrator has four main objectives:

- it must be able to store at least $100\ Wh$ of thermal energy
- during the discharge phase, heat must be delivered at a temperature of at least $35°C$ (having floor heating as a reference for a possible final use)
- it must be able to operate exploiting a heat source at ambient temperature in both summer and winter
- it must use water as sorbate

The design includes six components: two cylindrical pressure vessels, one acting as an evaporator/condenser for the sorbate and the other is the reactor where the adsorption reaction takes place. One heat exchanger is held within the pressure vessels and it is made of a copper pipe. Both vessels are closed by a cylindrical lid tightened with bolts, which compresses an O-ring that guarantees a vacuum tight seal. The design of the whole device consists of two parts. The first develops a theoretical model and design of the adsorption reaction cycle. The second deals with the structural design of all the components and the production of the engineering drawings.

3.1 Sorption reaction

Every sorption reaction produces a determined quantity of thermal energy, which is called heat of adsorption. The general adsorption reaction is:

$$A + B \rightarrow AB + heat$$

where A is the adsorbent, B is the adsorbate and the thermal energy released during the sorption of one mole of adsorbate is called isosteric heat. In general, the heat of adsorption is generated by the release of the kinetic energy as the molecules of the sorbate are trapped into the adsorption sites on the sorbent surface. In other terms, it is the molar enthalpy difference between gas phase and adsorbed phase of the sorbate material [66].

A widely used formula for computing the isosteric heat is based on the Clausius-Clapeyron equation, assuming the sorbate vapour as an ideal gas:

$$q_{st} = RT^2 \left(\frac{\partial \ln p}{\partial T} \right)_X \qquad (3.1)$$

Where R is the universal constant of gases and x is the adsorbate uptake measured in $[\frac{g_{sorbate}}{g_{sorbent}}]$. The isosteric heat of adsorption q_{st} can be obtained from calorimetric experiments or from the analysis of the adsorption isotherms at different temperatures. The equation (3.1) can be written as:

$$\frac{q_{st}}{R} = \left(\frac{\partial \ln p}{\partial - 1/T} \right)_X \qquad (3.2)$$

Equation (3.2) demonstrates that isosteres transformation in the thermodynamic Clapeyron chart ($\ln p \div - \frac{1}{T}$) are characterized by a slope equals to $\frac{q_{st}}{R}$.

3.2 Adsorption isotherms

Adsorption isotherms are curves that express the variation of the gas uptake by the adsorbent as a function of the (relative) pressure, at constant temperature. Depending on the type of material and on the dimension and distribution of micropores, different models are used to predict his behaviour during the adsorption reaction. The first important scientific contributions to the field and popular examples of isotherm formulation are due the work of Freundlich and Langmuir about 100 years ago. Strictly speaking, the latter formulations are limited to the monolayer adsorption of an ideal gas, which is an accurate assumption only at low pressures for a homogeneous material [67].

3.2.1 Langmuir isotherm

In 1916, the chemist and physician Irvin Langmuir formulated an adsorption isotherm based on four hypotheses:

- only one layers of sorbate forms onto the surface of the solid adsorbent
- the sorbent sites are all energetically equivalent
- the reaction is reversible
- the interactions between sorbate molecules are negligible as compared to the sorbate-sorbent interactions

The ratio between the number of sites occupied by the sorbate molecules n_s and the total number of sites in the sorbent volume n_{tot} is called coverage and it is indicated with the symbol θ:

$$\theta = \frac{n_s}{n_{tot}} \tag{3.3}$$

Langmuir isotherm expresses the dependence of the coverage from the pressure and the temperature:

$$\theta(p,T) = \frac{H(T) \cdot p}{1 + H(T) \cdot p} \tag{3.4}$$

where p is the pressure and $H(T)$ is the Henry's constant which depends on the temperature T. At low pressures this equation reduces to Henry's law, thus it is thermodynamically consistent.

3.2.2 Toth isotherm

Toth isotherms are a correction to the Langmuir formulation that uses fitting parameters to better match experimental results. Toth isotherm is calculated with the following equation:

$$\theta(T) = \frac{p}{\left(\frac{1}{H(T)} + p^\tau\right)^{\frac{1}{\tau}}} \tag{3.5}$$

Where the parameter τ represents the system heterogeneity. If it deviates away from unity, the system becomes less homogeneous [68].

3.2.3   Isosteric heat at low coverage

In cases of low coverage, the equations of the Langmuir model can be written this way:

$$q_{st} = RT^2 \left(\frac{\partial \ln p}{\partial T}\right)_X = -RT^2 \left(\frac{\partial \ln H}{\partial T}\right)_X \tag{3.6}$$

At this point an assumption must be made on the potential energy of adsorption of the sites, which is called ε. Considering a rectangular potential for simplicity, it can be proven that:

$$H(T) = \frac{\bar{C}}{T} e^{\frac{\varepsilon}{RT}} \tag{3.7}$$

These two equations connect the isosteric heat with the adsorption potential of the sites, and the result can be written as:

$$q_{st,x\to0} = \varepsilon + RT \tag{3.8}$$

Other formulations of the potential energy of adsorption, like an armonic potential, can be considered, and in that case the isosteric heat is:

$$q_{st,x\to0} = \varepsilon - \frac{RT}{2} \tag{3.9}$$

In this work, the maximum cycle temperature is equal to $363.15\ K$, therefore the term RT is equal to $3.02\ \frac{kJ}{kg}$. The values of the isosteric heat for zeolite 13X is about $60\ \frac{kJ}{kg}$ [69], therefore the temperature contribution in equations (3.8) and (3.9) is considered negligible. It follows that:

$$q_{st,x\to0} \approx \varepsilon \tag{3.10}$$

3.2.4   Heat of adsorption

According to a study by Smith, Henry's constant can be written as [70]:

$$H(T) = \frac{1}{p_0} e^{\frac{\Delta S_0}{R}} \cdot e^{\frac{\varepsilon}{RT}} \tag{3.11}$$

where p_0 is the reference pressure and ΔS_0 is the entropic variation. The heat released/adsorbed during the adsorption/desorption reaction is:

$$dQ = \pm q_{st} dn_s \tag{3.12}$$

where q_{st} is the isosteric heat and dn_s is the variation in number of moles. During adsorption the heat is released from the reaction therefore it is considered negative, while during desorption heat is stored into the material therefore it is assigned a positive sign. In the Langmuir model, at the evaporation pressure, the heat released during the storage cycle is:

$$Q_{ads} = n_{tot} \int_{\theta_{min}}^{\theta_{max}} q_{st}[\theta, T(\theta), p = p_e] d\theta \tag{3.13}$$

Changing variable to express the dependence on the temperature and considering low coverage the integral in equation (3.13) becomes:

$$Q_{ads} = n_{tot} \int_{T(\theta_{min})}^{T(\theta_{max})} \frac{d\theta}{dT} q_{st}(T) dT \approx n_{tot} \int_{T(\theta_{min})}^{T(\theta_{max})} \varepsilon d\theta = n_{tot} \varepsilon \Delta\theta \tag{3.14}$$

This equation shows that Q_{ads} depends on the physico-chemical characteristics of the material:

$$Q_{ads} = Q(\varepsilon, \Delta S_0) \tag{3.15}$$

Finally, the quantities of zeolite and water necessary to produce the target energy power $Q_{target} = 100 \, Wh$ has been found, considering that zeolite maximum water uptake x_max is equal to $0.3 \, kg_{H_2O}/kg_{zeo}$ [71]:

$$m_{zeo} = \frac{Q_{target}\overline{M_{H_2O}}}{x\_max \frac{Q_{ads}}{3.61}} \tag{3.16}$$

31

$$m_{H_2O} = \frac{Q_{target} \overline{M_{H_2O}}}{\frac{Q_{ads}}{3.61}}$$ (3.17)

where the factor 3.61 converts from Wh to kJ.

3.3 Entropic parameter

The entropic parameter is the difference in entropy between the water vapour surrounding the zeolite and the condensed phase inside its micropores. In order to have an estimate of the latter value, we can calculate it as an average between two known conditions. The first condition considers the water inside the zeolite volume as ice, therefore calculates the entropic parameter as [72]:

$$\Delta S_0 = s_{site}^s - s_0^g \approx s_0^{ice} - s_0^{vapour} = (41 \cdot 10^{-3} - 188,84 \cdot 10^{-3}) \frac{kJ}{mol \cdot K}$$
$$= -147,84 \frac{J}{mol \cdot K}$$ (3.17)

where s_0^{ice} is the standard molar entropy of frozen water and s_0^{vapour} is the standard molar entropy of water vapour. Dividing the value found by the universal gas constant R, it is calculated:

$$\frac{\Delta S_0}{R} \approx \frac{-147,84}{8,314} \approx -17,7$$ (3.18)

The second condition considers the adsorbed water as in liquid state:

$$\Delta S_0 = s_{site}^s - s_0^g \approx s_0^{liquid} - s_0^{vapour} = 69,95 \cdot 10^{-3} - 188,84 \cdot 10^{-3} \frac{kJ}{mol \cdot K}$$
$$= -118,89 \frac{J}{mol \cdot K}$$ (3.19)

Dividing the value found by the universal gas constant R, it is calculated:

$$\frac{\Delta S_0}{R} \approx \frac{-118{,}89}{8{,}314} \approx -14{,}3 \tag{3.20}$$

The mean value between those found in equations (3.17) and (3.19) is:

$$\frac{\Delta S_0}{R} \approx -16 \tag{3.21}$$

and is the value considered in the model used for the design of the adsorption cycle.

3.4 Assumptions

The zeolite 13X is microporous and can be considered homogeneous, therefore if we consider the water vapour as an ideal gas the Langmuir isotherm can be used for the theoretical calculations. It is assumed that the desorption reaction reaches a maximum temperature of 90°C. The adsorption device must vaporize the water at 10°C (during winter) and at 30°C (during summer). In order to evaporate the water at such low temperatures, the adsorber must be evacuated down to the saturation pressure of water at the above temperatures. The relation between saturation pressure and temperature of a chemically pure liquid in equilibrium with its vapour is given by the Antoine's equation:

$$\log P = A - \frac{B}{C + T} \tag{3.22}$$

where P is the pressure in $mmHg$, T is the temperature in $°C$ and A, B, and C are the so-called Antoine coefficients, that depend on substance type and on temperature range. In table 3 are referenced the values of the three Antoine's coefficients:

Table 3 Antoine equation parameters for water between 1-100 °C [73]

Antoine coefficients		
A	B	C
8.07131	1730.63	233.426

4 Results

The pressures calculated by the Antoine's equation are 12.2 $mbar$ and 42.3 $mbar$ respectively. These pressures are in the range of medium-vacuum and can be reached using a diaphragm vacuum pump, usually employed for laboratory experiments. Since a good vacuum tightness of the whole device is difficult to achieve, a diaphragm vacuum pump Laboport N810.3 FT.18G, which is able to ensure an absolute pressure of 8 $mbar$, has been chosen. This pump presents high compatibility with water vapour and a pumping flow rate of 10 L/min at atmospheric pressure. This device is shown in Figure 14.

Figure 14 Diaphragm vacuum pump Laboport N810.3 FT.18G [74]

A vacuum control unit model VC-900 will monitor the pressure inside the reactor vessel, shown in Figure 15. This device presents a resolution of 1 $mbar$, therefore it is suitable for the operating conditions considered. The VC-900 can be connected to a computer through a USB connection, therefore the pressure can be monitored by a dedicated software.

Figure 15 Vacuum control unit VC-900 [75]

The pressure inside the evaporator/condenser vessel is calculated with the Antoine's equation, using the value of temperature measured by a thermocouple inserted in the tank by means of a thermowell. The reactor vessel temperature is also monitored with three thermocouples inserted in the same way specified above. The thermowells are constituted of a stainless steel 316 housing (with length $50\ mm$), suitable to work with a probe diameter of $3\ mm$. The flow of water vapour between the evaporator/condenser and the reactor vessel is controlled by a two-way brass ball-valve, suitable both for high and for low pressure applications. The mass flow of water inside the heat exchangers will be monitored directly by a variable area flowmeter, installed on the inlet pipe. This device is able to measure a mass flow range of $5 \div 46\ L/min$. On the evaporator/condenser side, the water sent to the heat exchanger is taken from the water mains, while on the reactor side the water flowing inside the heat exchanger is circulated by means of a recirculation pump.

4.1 Numerical results

Figure 16 shows the relation between saturation pressure of water vapour and water temperature calculated with the Antoine equation in a temperature range of $-10 \div 40\ °C$.
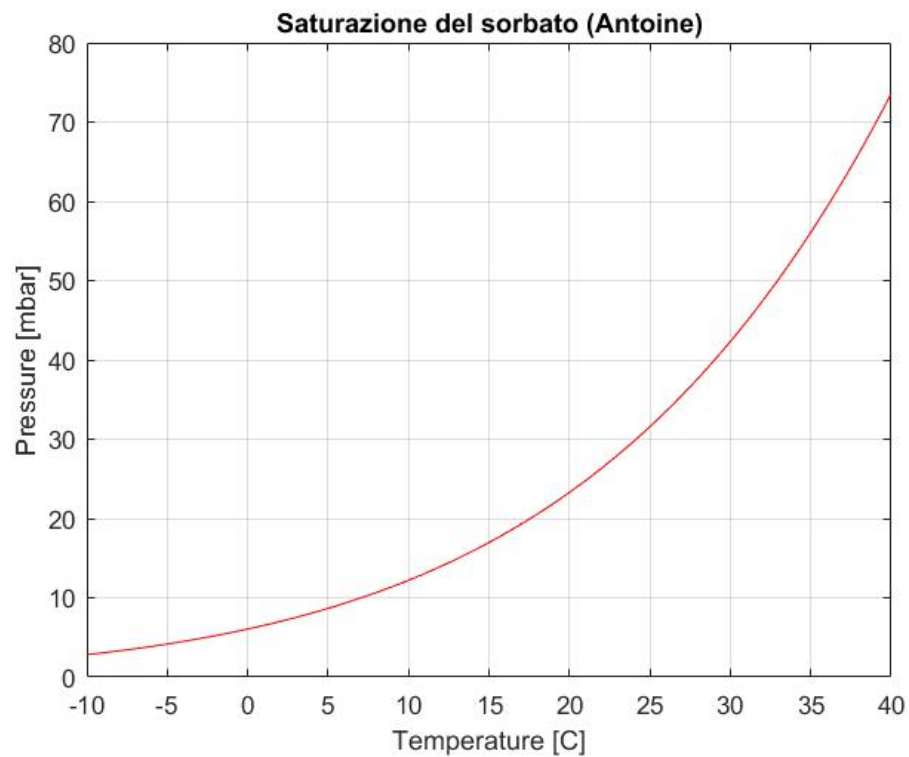
Figure 16 Saturation pressure of water vapour according to Antoine's equation

The calculation performed on MATLAB using the theoretical model gave the plot of the adsorption cycle on a pressure-coverage chart, shown in Figure 17. A molar heat of adsorption of 16.98 kJ/mol was found while the variation in the coverage is 0.283.
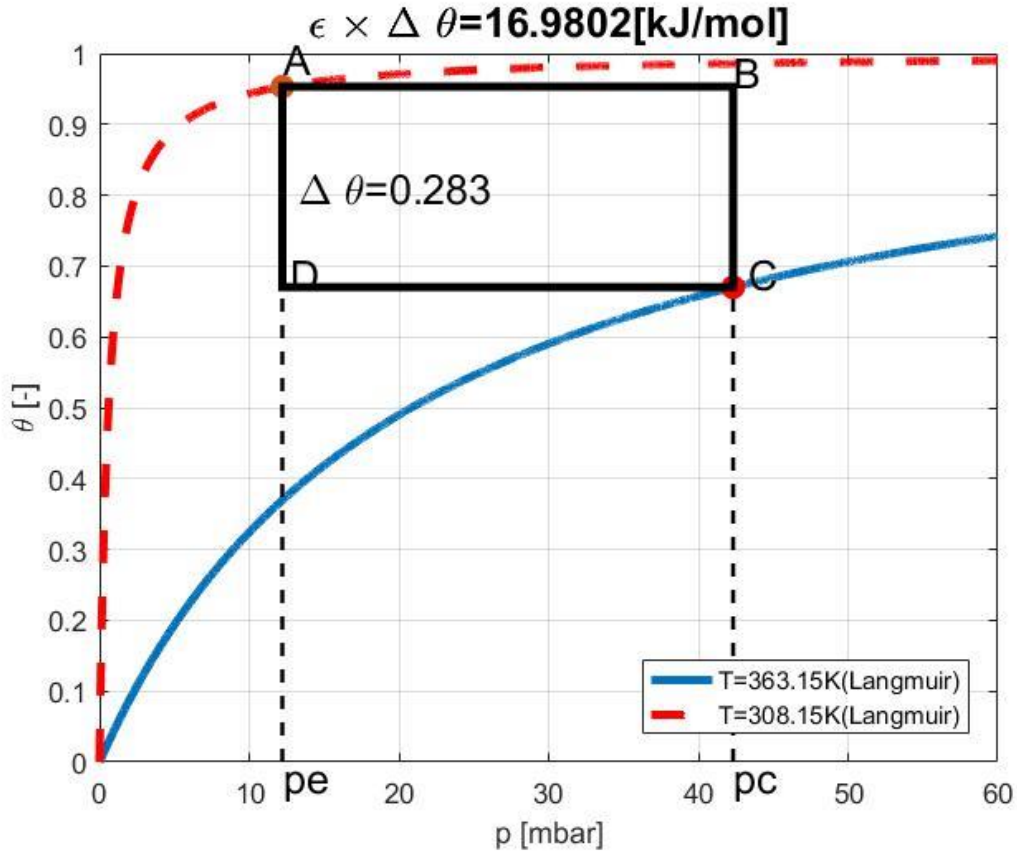
Figure 17 Adsorption ideal cycle in the coverage-pressure chart

The red dashed line represents the Langmuir isotherm at $308.15\ K$ and the blue line is the Langmuir isotherm at $363.15\ K$, both calculated over a pressure range of $0 - 60\ mbar$. The adsorption heat is released during the step D-A at the pressure of $12.2\ mbar$. At point A all the available sites onto the zeolite micropores are occupied, therefore the adsorption process stops.

Table 4 shows the values of the thermodynamic quantities in the 4 cycle points, necessary to represent it on the Clausius-Clapeyron plane.

Table 4 Ideal cycle points

Properties	States			
	A	B	C	D
Pressure [$mbar$]	12.2	42.3	42.3	12.2
Temperature [K]	308.15	325.5	363.15	341.8
Coverage	0.9533	0.9533	0.6703	0.6703
Uptake $\left[\frac{g_{H_2O}}{g_{zeo}}\right]$	0.2860	0.2860	0.2011	0.2011

Figure 18 shows the resulting plot of the Langmuir and the Toth isotherms at $308.15 \, K$ and $363.15 \, K$. The formers are represented by the dashed lines, while the latter are represented by the continuous lines. Eight pressure-uptake couple, indicated by the green dots in Figure 18, were sampled onto the two Toth isotherms.
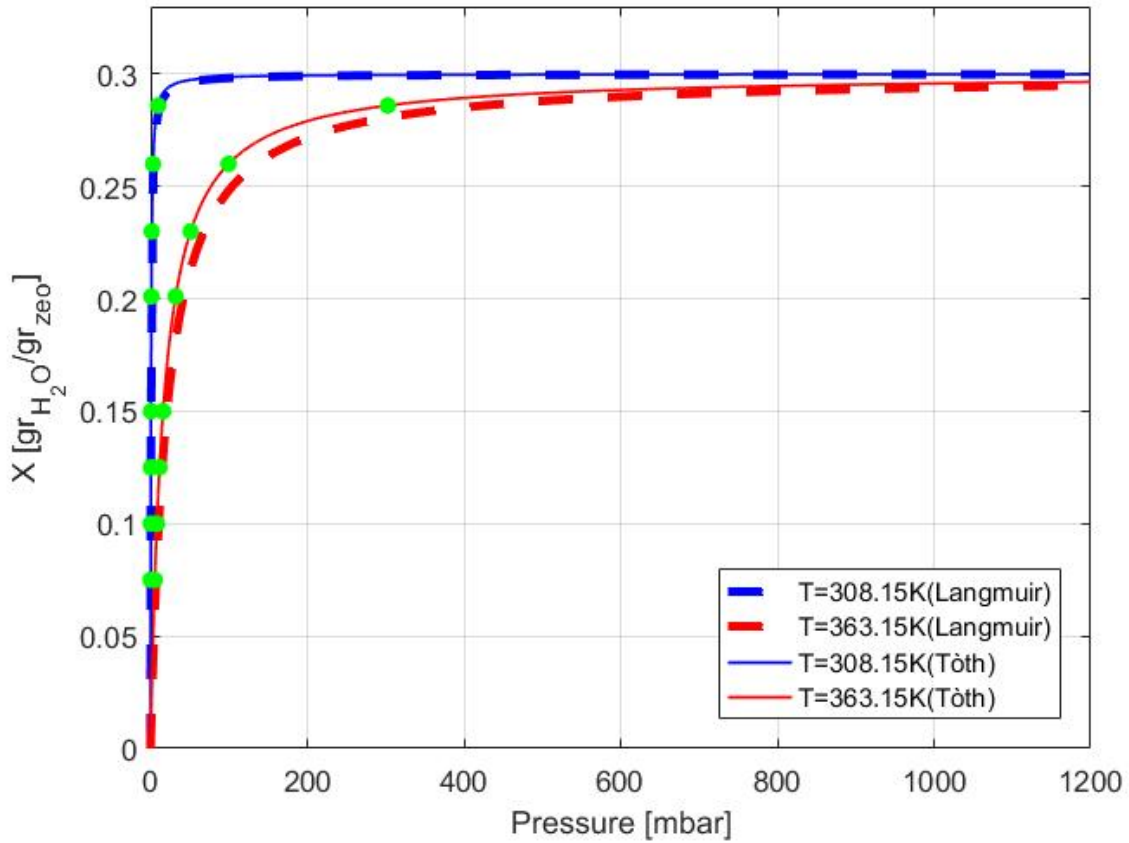
Figure 18 Toth correction to Langmuir and p-Ө sampling

The isosteric heat was then calculated for the sampled couples using the Clausius-Clapeyron equation:

$$q_{st} = -R \left(\frac{\partial \ln p}{\partial 1/T} \right)_{X \to 0} = -R \frac{(\ln p(T = 363.15\ K) - \ln p(T = 308.15\ K))}{\frac{1}{363.15} - \frac{1}{308.15}} \tag{4.1}$$

The values of the isosteric heat sampled from the isosteres are almost constant, as a demonstration that this is true when the sorbate uptake is low. The sampled data were used to represent the isosteres onto the $\left(-\frac{1}{T} \right) \div \ln \left(\frac{p}{p_0} \right)$ plane, where $p_0 = 1\ Pa$ is the reference pressure. The resulting plot is shown in Figure 19.

Figure 19 Adsorption cycle

Table 6 summarizes the results of the first part of the simulation.

Table 5 Adsorption cycle materials to store 100 Wh

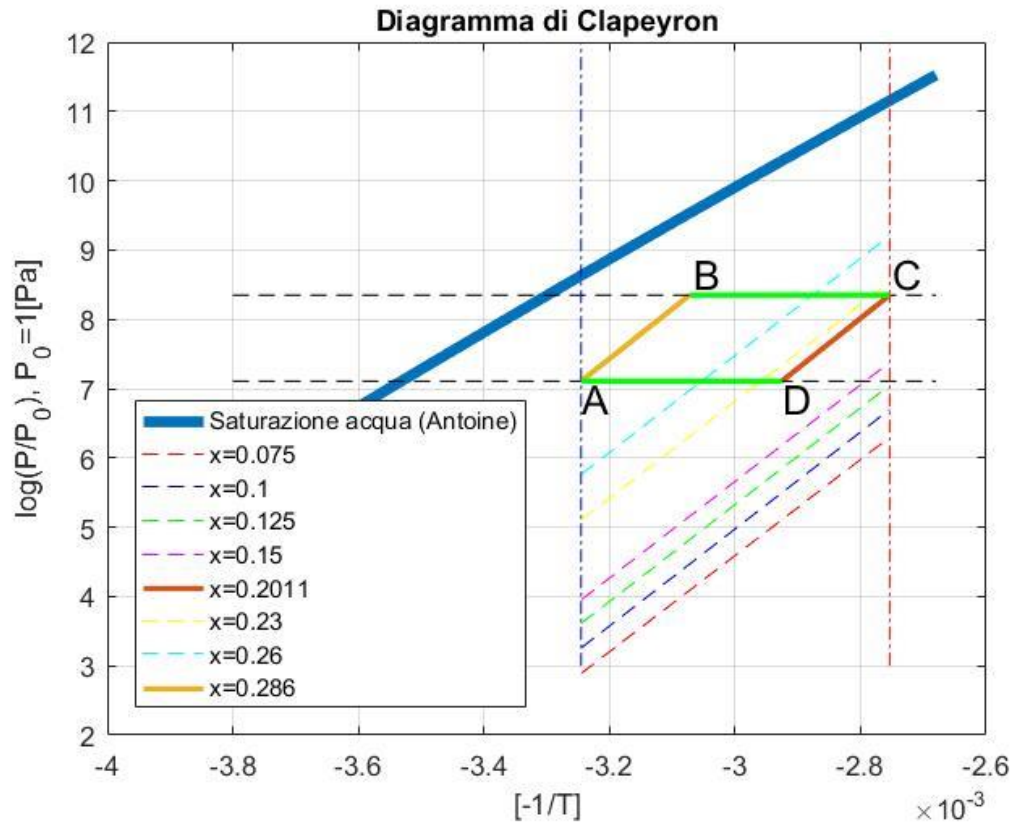|	Unit of measure	Value
Molar thermal energy produced	$\left[\dfrac{kJ}{mol_{H_2O}}\right]$	16.9802
Zeolite necessary	$[g]$	1288
Water to be absorbed	$[g]$	386

4.2 Final considerations

To reach a theoretical energy storage of $100\ Wh$, $386\ g$ of water vapour must be adsorbed into $1288\ g$ of zeolite 13X. This is quite difficult to realize practically, because this model does not consider the difficulty encountered by the water vapour to diffuse towards the further regions of the tank. Furthermore, zeolite 13X has a low thermal conductivity, therefore the heat exchange efficiency should be enhanced by a copper network held in the reactor tank. Another possible solution may be to weld copper fins on the heat exchanger pipe. During the adsorption reaction, a part of the heat released is lost towards the ambient, therefore a thermal isolation of the reactor vessel may be required. The quantities of zeolite and water specified above would require very small tanks. The copper tube that constitutes the heat exchangers has a minimum bending radius, and if not respected, the pipe may collapse or break. Finally, it would be impossible to insert the heat exchangers into a very small tank, due to space limitations. To ensure the target energy storage, a safety coefficient equal to 3 is considered, therefore a mass of zeolite of $3.2\ kg$ has been considered, which requires $0.960\ kg$ of water vapour to be adsorbed to work with the same adsorption cycle modelled. The only difference is that the theoretical energy stored is $256\ Wh$. One more consideration must be done about the quantity of water to be used: the heat exchanger of the evaporator must be always in contact with the liquid water, at least partially, during all the evaporation process, therefore the calculated quantity of water to be placed into the evaporator is multiplied by a factor 1.5, so $1.5\ kg$ of water will be used. The final characteristics of the device, given the last considerations, are summarized in table 7.

Table 6 Reactants and product of the sorption reaction

	Unit of measure	Value
Molar thermal energy stored	$\left[\dfrac{kJ}{mol_{H_2O}}\right]$	16.9802
Energy storage target	$[Wh]$	256
Zeolite necessary	$[g]$	3200
Water to be absorbed	$[g]$	960

5 Geometric design of the components

In this chapter all the steps performed to design the components of the demonstrator are covered. To accomplish this task, the standard of the American Society of Mechanical Engineer (ASME) has been used, which provides the rules to design both the vessels and their lids.

5.1 ASME

The ASME is an American association born in 1880 in response to numerous incidents caused by vessels under pressure. It aims to help engineers worldwide to safely and correctly design, through the publication of codes and standards on multidisciplinary topics. In particular, the ASME code used in this work is the Boiler and Pressure Vessel code (BPVC), which explain the rules and the formulas to be used to correctly design vessels and components subject to pressure loads [1] [2].

5.2 Design requirements

The BPVC does not provide strict rules to design the minimum thickness of vacuum chambers. However, a vessel under vacuum condition can be considered as a shell, where a uniform pressure is applied on the external surface, with an intensity equal to the differential pressure between environmental pressure and the absolute pressure inside the shell. The two vessels must be able to contain $3.2\ kg$ of zeolite and $1.5\ kg$ of water respectively, considering they also have a heat exchanger inside them. One more requisite must be observed to design the vessels thickness: the heat exchanger and the external water circuit necessitate of two fittings being installed into the same threaded hole on the vessels wall. The thickness must be large enough to permit the correct installation of the two fittings in order to guarantee a vacuum tight connection of the heat exchangers, while also allowing their assembly/disassembly.

5.3 Vessels thickness design procedure

According to ASME BPVC-Section VIII-Division 1 [76], the first step to design vessels with external diameter D_0 consists in assuming a plausible value of the thickness t and consequently

calculating the ratios $\frac{L}{D_0}$ and $\frac{D_0}{t}$, where L is the length of the cylinder. Subsequently, a coefficient A must be retrieved from fig. G in ASME BPVC Sec. II-Part 3, shown in Figure 20.

It is possible to apply the linear interpolation:

$$\frac{x - x_b}{x_a - x_b} y_a - \frac{x - x_a}{x_a - x_b} y_b \tag{5.1}$$

in order to find the intermediate values of $\frac{D_0}{t}$ and then calculate the factor A as:

$$A = A_1 + \left[\frac{\frac{D_0}{t} - \left(\frac{D_0}{t}\right)_1}{\left(\frac{D_0}{t}\right)_2 - \left(\frac{D_0}{t}\right)_1} \cdot (A_2 - A_1) \right] \tag{5.2}$$
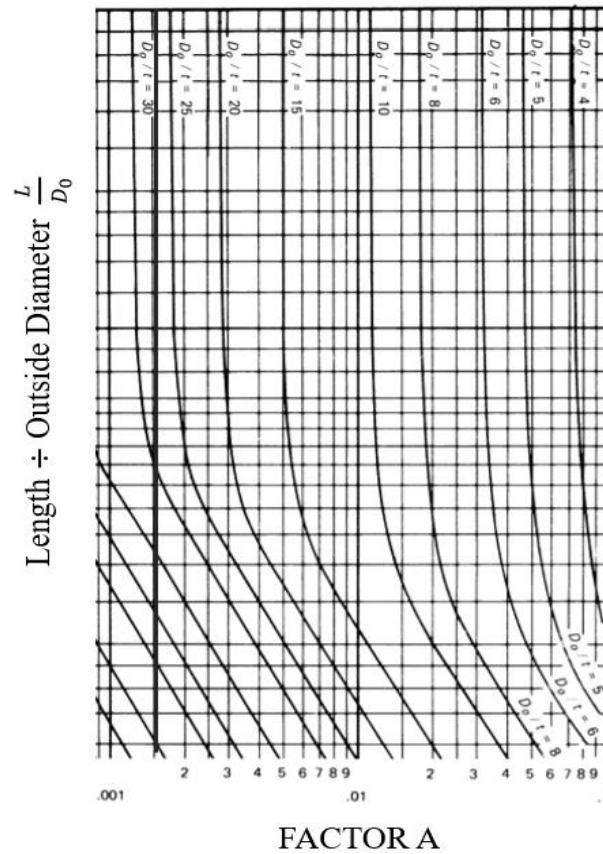

Figure 20 Geometric chart for components under external pressure [77]

With the coefficient A found in the previous step, the coefficient B can be derived from the applicable material chart in Subpart 3 of Section II (shown in Figure 21), which takes into consideration the material of the vessel and the operating temperature. It is possible to interpolate linearly between the temperatures, using the same process specified above, to find the values of B. The permissible pressure P_a is finally calculated from the following equation:

$$P_a = \frac{4B}{3\left(D_0/t\right)} \tag{5.3}$$

The applied pressure P that the vessels must withstand is calculated as:

$$P = P_{atm} - P_{in} \tag{5.4}$$

Where P_{atm} is the standard sea-level pressure and P_{in} is the absolute pressure inside the vessel. If the design pressure is higher than the permissible pressure $(P > P_a)$, the entire procedure must be repeated with an increased value of the thickness t.
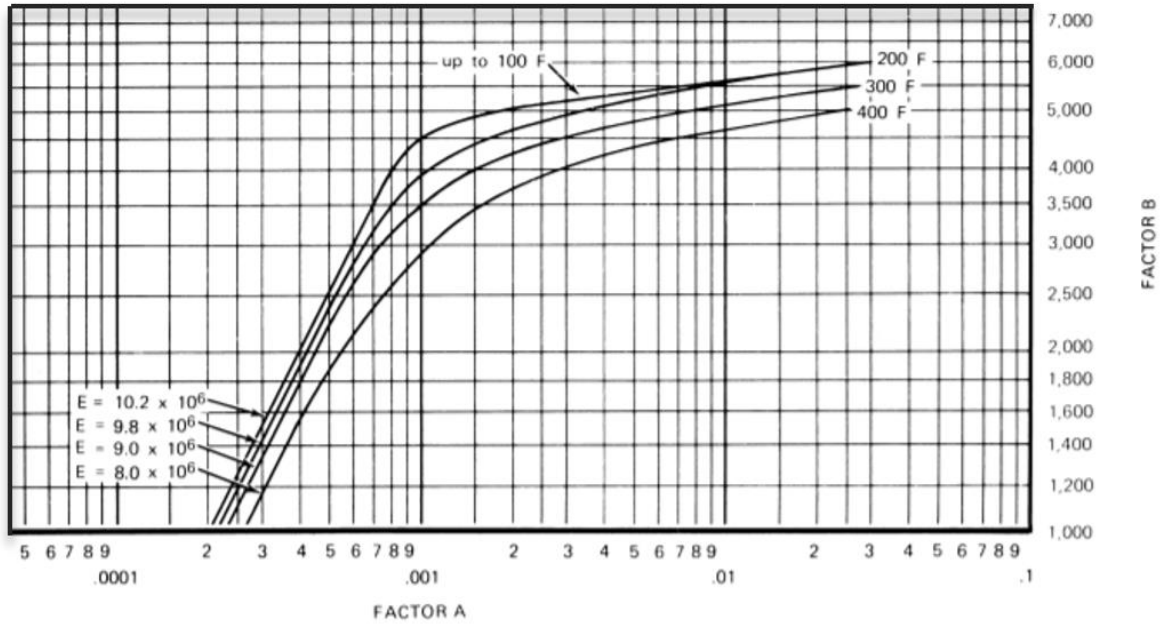

Figure 21 Applicable material chart for coefficient B [77]

44

5.4 Lids structural design

According to the BPVC rules described referring to the configuration shown in Figure 22, the thickness t must be calculated as:

$$t = d \sqrt{\frac{CP}{SE}} \tag{5.5}$$

E is the joint efficiency (also referred to as weld efficiency), P is the differential pressure applied measured in psi and S is the material's maximum allowable stress (under tension). The factor C depends on the method of attachment of the lid and on the shell dimensions. According to the design procedure, the thickness is directly proportional to internal diameter d of the shell, therefore only the design of the reactor's lid has been performed since it has the highest internal diameter of the shell it is attached on.
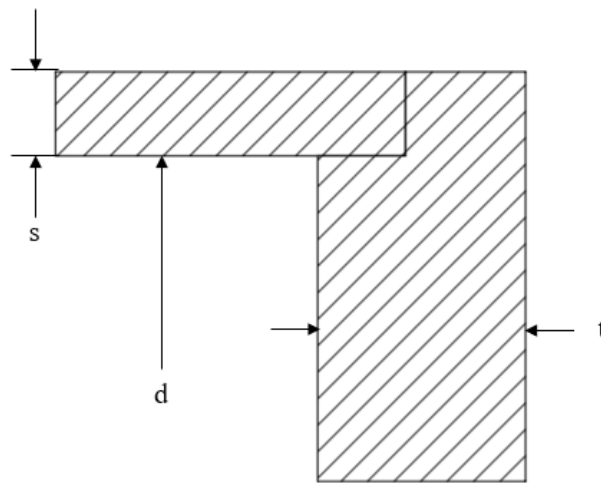
C=0.33

Figure 22 Configuration with C=0.33 [76]

5.5 Design of the flat vessels bottom

The bottom part of the vessels is designed according to the BPVC procedure referred to components such as unstayed flat heads and covers. They present the configuration shown in Figure 23, where also the value of the factor C is displayed. The thickness is then calculated from the previous equation (5.4).
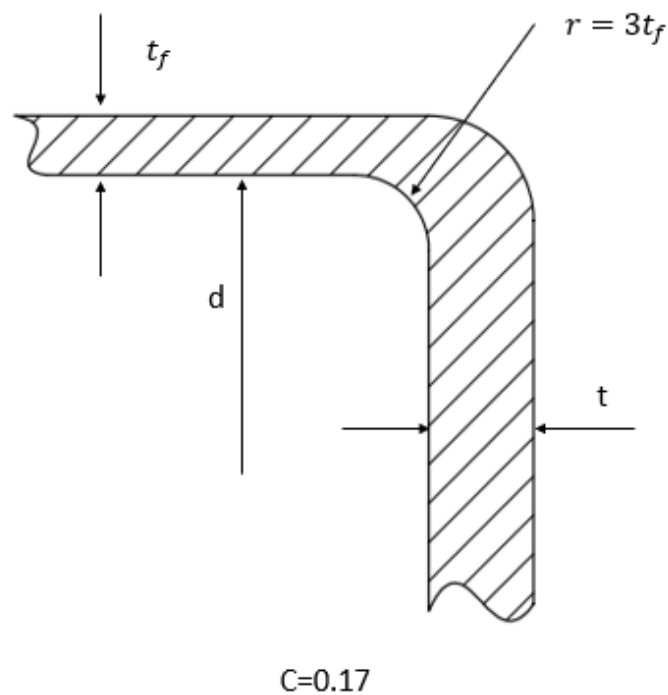

Figure 23 Configuration with C=0.17 [76]

5.6   Results

In this section the results of the structural dimensioning of all the components are presented.

5.6.1   Reactor vessel dimensions

The calculated thickness of the reactor vessel is $30\ mm$ and the material considered in the procedure is the aluminium alloy 5454 in 0 temper. The parameters calculated during the design procedure are summarized in Table 8.

Table 7 Reactor vessel design parameters

Dimensions	ASME coefficients	Permissible pressure
External diameter $D_0 = 235\ mm$	$A = 0.047$	$P_a = 74\ bar$
Thickness $t = 30\ mm$	$B = 6500$	
Height $L = 370\ mm$		

5.6.2   Evaporator/condenser dimensions

The calculated thickness of the evaporator/condenser vessel is $24\ mm$. The parameters considered in the design procedure are summarized in Table 9.

Table 8 Evaporator/condenser design parameters

Dimensions	ASME coefficients	Permissible pressure
External diameter $D_0 = 170\ mm$	$A = 0.038$	$P_a = 79\ bar$
Thickness $t = 24\ mm$	$B = 6000$	
Height $L = 320\ mm$		

5.6.3   Lids and flat bottom heat dimensions

The values of the parameters used during the design procedure of lids and flat unstayed heads are summarized in table 10. The two calculations differ only in the connection factor C. The minimum thicknesses obtained are $3.1\ mm$ and $2.2\ mm$ for lids and flat unstayed heads respectively, but for safety standards they are oversized by a factor 6.5. For the sake of simplicity, the design thickness of all these parts is $20\ mm$.

Table 9 Design parameters of the lids and flat bottom unstayed heads

	Parameters		
	ASME symbols	Values for the lids	Values for the flat unstayed heads
Tank internal diameter	$d\ [mm]$	165	165
Connection factor	C	0.33	0.17
Maximum allowable tensile stress	$S\ [ksi]$	15.7	15.7
Pressure load	$P\ [psi]$	15	15
Minimum thickness	$t\ [mm]$	3.1	2.2
Design thickness	$t_{real}\ [mm]$	20	20

5.7   O-ring gasket seal design

O-ring is an elastomeric ring with circular section, commonly used as sealing gasket for hydraulic and pneumatic applications. They are designed to be allocated in a special housing called groove, which is designed taking into account the typology of sealing attachment and the direction of application of the pressure. The dimensions of the O-ring are regulated by the ISO norm 3601/1, which specifies their internal diameter and thickness. The surface roughness of the groove is a critical parameter for pressurized gases or vacuum applications, because gas can leak through very small paths. Therefore, the surface against which an O-ring is placed should be smooth, and sharp edges should be smoothed to avoid denting the elastomer. A convenient O-ring material to use in the application considered in this work is an IIR-Butyl type because it resists to water and water vapour, and due to its high-density structure it has a very low permeability to gases, which makes it ideal for vacuum tight seals.

For the reactor's seal an O-ring type AISI-264 has been chosen, while the evaporator/condenser is sealed with an O-ring type AISI-248. Since both O-rings have the same section diameter, the groove dimensions are the same for both vessels. Figure 24 shows the groove designed on the two vessels.
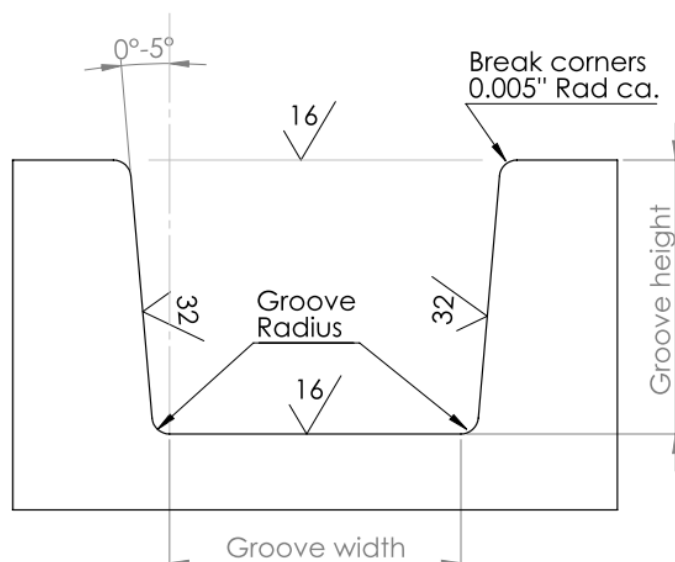

Figure 24 O-ring groove detail

After the O-rings have been placed into the groove, they are squeezed by tightening the bolts which connect the tanks to the lids. The correct dimensioning of the groove and the correct tightening order, shown in figure 25, ensure that the O-ring seals are vacuum tight.
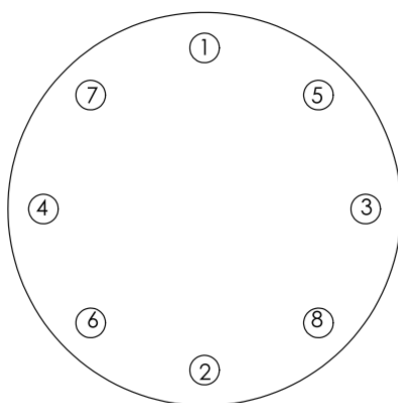

Figure 25 Bolts tightening order

6   Validation of the geometric design

The vessels structural design has been validated by performing a Finite Element Method (FEM) analysis. FEM is a numerical technique used to find the approximated solution of the partial derivative equations over a defined domain. First, the domain is divided into geometrical subdomains, creating the so-called mesh. Then, a generic continuous function can be represented by a linear set of algebraic polynomials, over the defined finite elements. For this reason, the properties of the material can be considered as completely defined over the finite volume of the elements. The solution of the complete system derives from the assembly of all the elements and their properties. In summary, the steps involved in the FEM analysis are the creation of the model, its solution and then the visualization of the results [78]. Figure 26 shows the detailed process involved in the simulation.
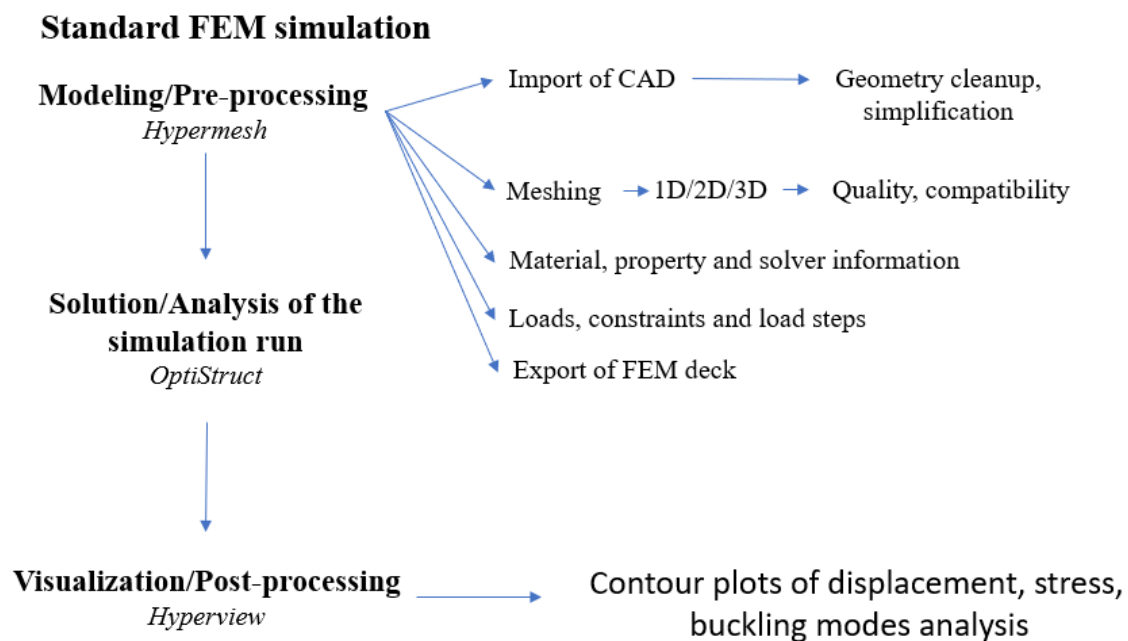

Figure 26 FEM analysis simulation steps

6.1   Geometry simplification and mesh creation

The simplified geometry analysed is a cylindrical tube, closed on the side where there is the flat cover. The critical areas (through holes) are maintained, since it is expected that they are the zones where the higher tensions and deformations arises during the operation of the device.

The component dimensions are similar to each other, therefore the mesh must be composed by 3-D (three-dimensional) finite elements. Since the component is not a rotational solid or obtainable by extrusion of a geometric shape (because there are through holes on the surface), a tetrahedral element type has to be used for the FEM analysis. There are two methods of meshing, one is called "automatic mesh", it is typically fast but does not allow to control the mesh flow and mesh pattern; the other method is called "2-D tria to 3-D tria" and is divided into two parts. In the first part, all the solid surfaces are meshed with two-dimensional elements (2-D quad or tria elements), which can then be adjusted to better represent the surface pattern, for example by increasing the number of elements where a more detailed analysis is requested or where the geometry is more complicated. The second part consists in the creation of the 3-D tetrahedral elements. The element types introduced are shown in figure 27.
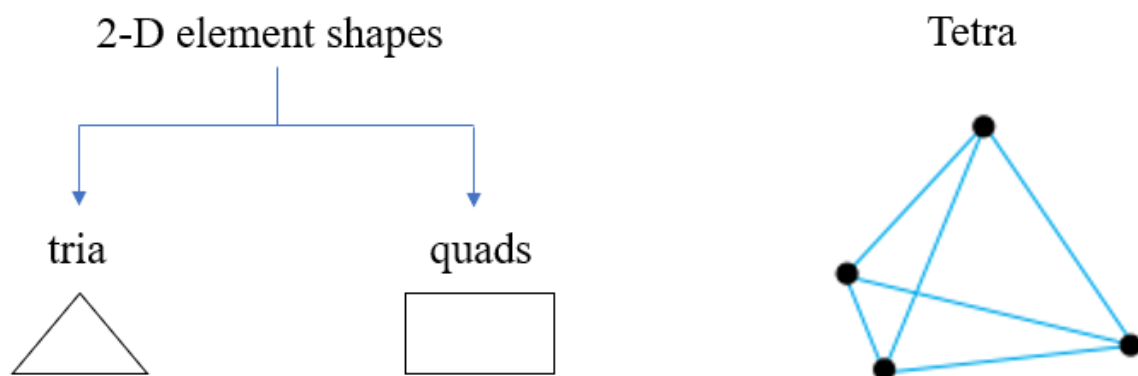

Figure 27 Element types for tetrameshing

In structural analysis, it is better to use small elements size in the critical areas, while the less critical ones should be meshed with a coarse mesh or a bigger elements size. The use of trias creates a smooth transition from a dense mesh to a coarse mesh. In commercial softwares, the default tria mesh produces equilateral triangles, but there is an option to use right-angle triangles called "R-trias". These elements are generated splitting quad elements along their diagonal to form two triangles. Generally, equilateral triangles are better, but in case of contact between two surfaces, the use of R-trias establishes a similar mesh pattern on the two surfaces, resulting in a smoother mesh transition.
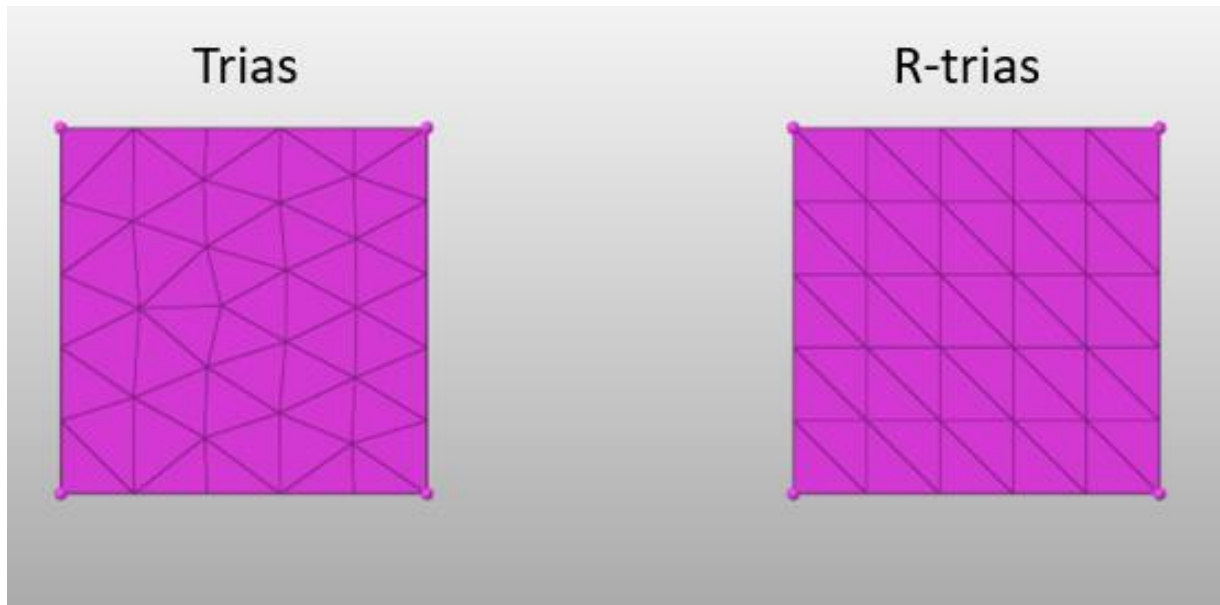
Figure 28 shows the two different trias type.

Figure 28 Types of triangular mesh elements

6.2   Resulting mesh and mesh quality check

For the 2-D mesh, R-tria elements with a side dimension of $0.01\ m$ were used. After all the surfaces were wrapped by the elements, the function "tetramesh" has been used to create the 3-D mesh. This command allows to fill the volume of the vessels with tetrahedral elements. The mesh generated using this function is displayed in figure 29. The mesh shows a regular coarse pattern on the top surface of both vessels while it is finer in the proximity of the critical areas such as through holes.
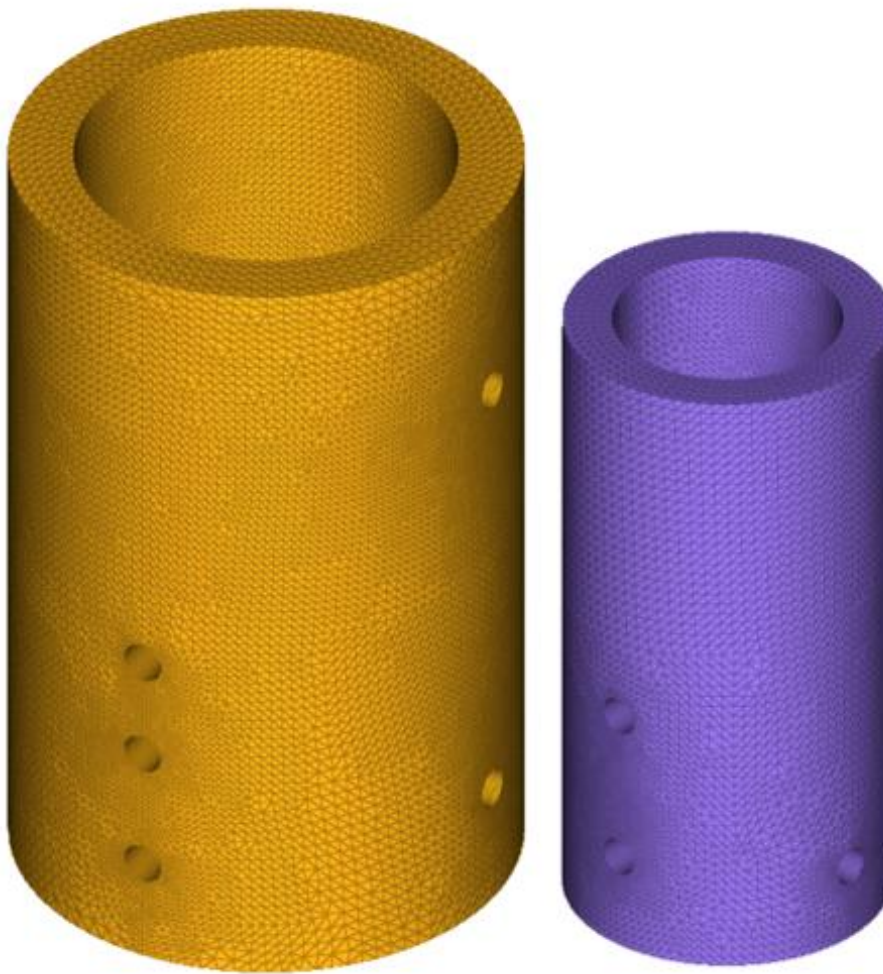

Figure 29 Reactor (on the left) and evaporator (on the right) mesh

The ideal shape of the tetrahedrons is an equilateral tetrahedron. There are several tools that allow to check the quality of the elements of the mesh produced, measuring how far a given element deviates from the ideal shape. The software returns the number of elements that failed the quality check and their percentage over the total number of the mesh elements. Usually, if the elements that failed the quality check are more than 1.5%, a mesh adjustment is necessary in order to improve the quality of the analysis.

6.3   Parameters for the mesh quality check

The first parameter considered is called "Tetra collapse". It is calculated as:

$$Tetra\ collapse = \frac{H_{min}}{1.24\sqrt{A}}$$
(6.1)

where H_{min} is the smaller of the distances measured from each of the four nodes to its opposite surface and A is the opposite surface area. Every element which satisfy the relation $Tetra\ collapse > 0.1$ is considered acceptable. Zero elements of the mesh created failed this test. The second parameter considered is called "Volumetric skew". It is calculated as:

$$Volumetric\ skew = \frac{V_{ideal} - V_{actual}}{V_{ideal}}$$
(6.2)

Considering the sphere passing for the three corners of the tetrahedron, V_{actual} is the volume of the tetrahedron and V_{ideal} is the volume of the equilateral tetrahedron inscribed in the same sphere. The closer it is to zero, the closer the 3-D element is to the ideal equilateral tetrahedron. The acceptable values are at $Volumetric\ skew < 0.7$. Running the quality check, Hypermesh returned that 1.3% of the elements failed the test, which is acceptable. The third parameter considered is called "Jacobian", which is a scale factor arising because the elements are transformed from global coordinates to local coordinates to save computational time. Acceptable values are above 0.5, and the mesh created has zero elements which do not satisfy this condition. After the mesh quality check has been performed, it is necessary to define the material properties and the theoretical model that the software will use to run the FEM analysis.

6.4   Definition of material, properties and solver model

The material characteristics have been specified as shown in figure 30. The "MAT1" label identifies a material which properties are isotropic (true with good approximation for metals), linear and temperature-independent.

Figure 30 Aluminium alloy characteristics

After the material characteristics have been defined, the properties of the elements of the mesh must be specified, as shown in Figure 31. The "PSOLID" label indicates that the elements where the analysis must be performed are 3-D.

Figure 31 Property definition

After materials and properties are defined, a linear static analysis is performed. Linear implies that the material follows a linear elastic behaviour and static implies that the loads applied are

constant over time. The solver keeps following a straight stress-strain line even if the stresses overcome the failure threshold of the material, as shown in figure 32. To control if the component resists to the loads applied, the maximum stress calculated must be compared with the stress at which the material fails.
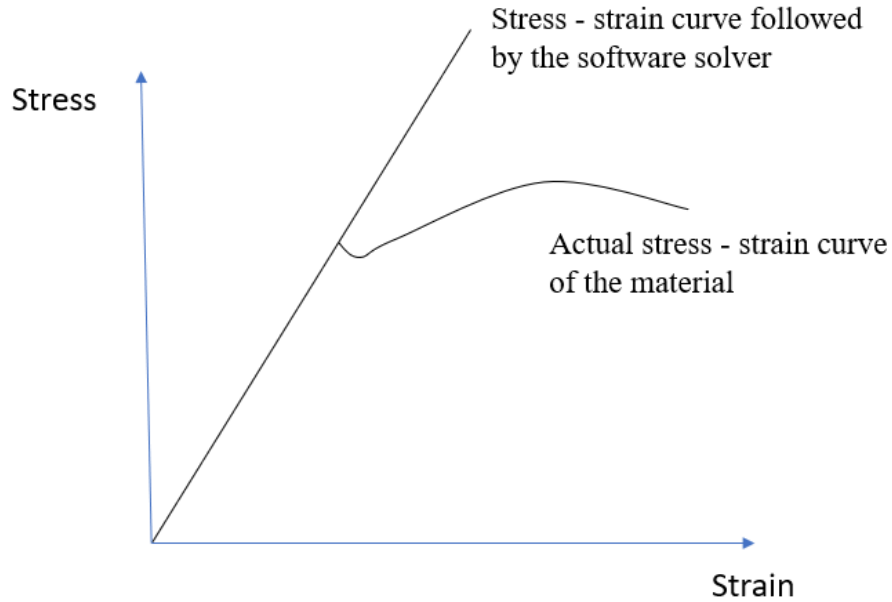
Figure 32 Material law for the solver

The linear static analysis is based on the Hook's law, and the solver uses it to calculate the stress and the displacement that the structure undergoes:

$$\sigma = E\varepsilon \tag{6.3}$$

where σ is the stress, E is the elastic modulus and ε is the strain per unit of length.

6.5 Results

The resulting displacement of the structure is shown in figure 33. The maximum displacement found was $0.50 \ \mu m$ and $0.29 \ \mu m$, located in the middle part of the internal surface of the

cylinders. This is expected, because the top side and the bottom side are restricted from displacement by lids and flat cover respectively.
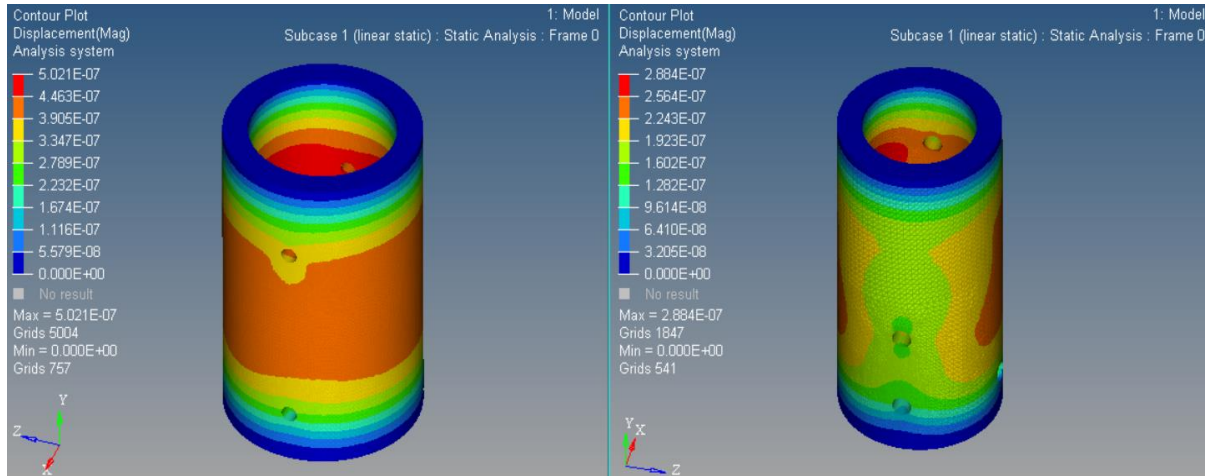
Figure 33 Displacement (in meters) of the reactor tank (to the left) and the evaporator tank (to the right)

Figure 34 shows that the values of the stresses applied to the elements of the mesh. The maximum tensile stress found was 0.91 MPa and 0.76 MPa respectively, located in proximity of the holes of the shells. The minimum stress (failure stress) at which the Aluminium type 5454 in 0 temper starts to show a permanent deformation, measured with a tensile test, is 85 MPa. The designed components can be considered safe for the application predicted. Since the tensile stresses calculated are very small (~1% on the most affected elements) with respect to the failure stress of the material, a more detailed analysis on the critical areas is not required.
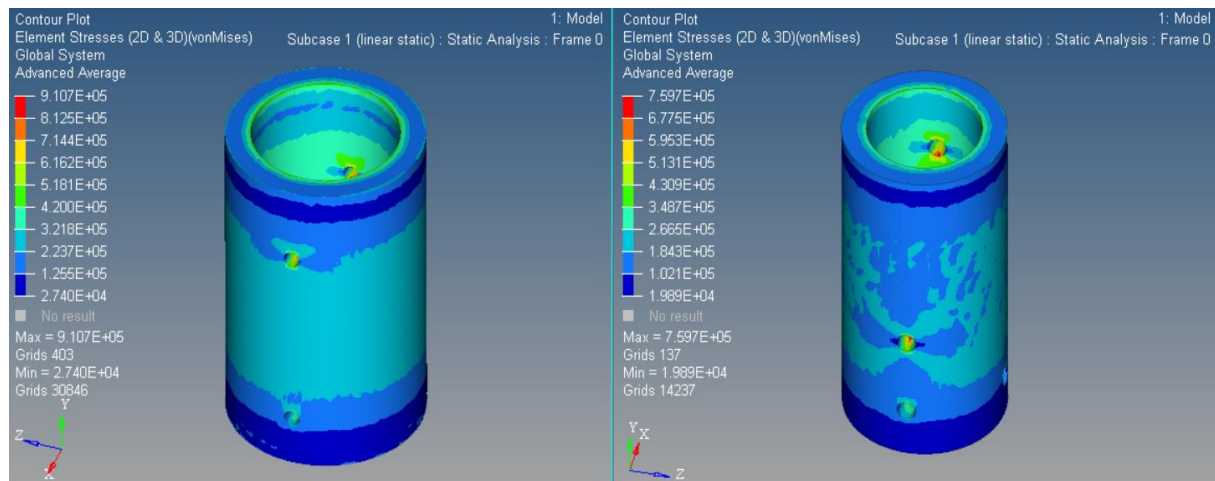
Figure 34 Elements tensile stress (in MPa) of the reactor tank (to the left) and the evaporator/condenser tank (to the right)

7 Design of the heat exchangers and design of heat transfer

Inside the pressure vessels there is a heat exchanger made from a copper tube, inside which water will flow, heating or cooling the substances inside the tanks. Copper is the first material choice for heat exchangers because it is cheap, easy to bend and has a very good thermal conductivity. The type of copper is a CW024A grade and the pipe has the following characteristics:

- thermal conductivity $390 \frac{W}{m^2 K}$
- internal diameter $4.4 \, mm$
- external diameter $6 \, mm$

The heat exchangers for the evaporator/condenser is a conventional helix heat exchanger while three different configurations for the reactor's heat exchanger have been explored.

7.1 Evaporator/condenser heat exchanger

The 3-D model of the helix heat exchanger predicted for the evaporator/condenser is shown in figure 35:

Figure 35 Evaporator heat exchanger design on Solidworks

The evaporator/condenser must contain $1500\ g$ of water and must be able to produce $960\ g$ of water vapour. During all the time required by the evaporation, the heat exchanger must be immersed totally or for the most p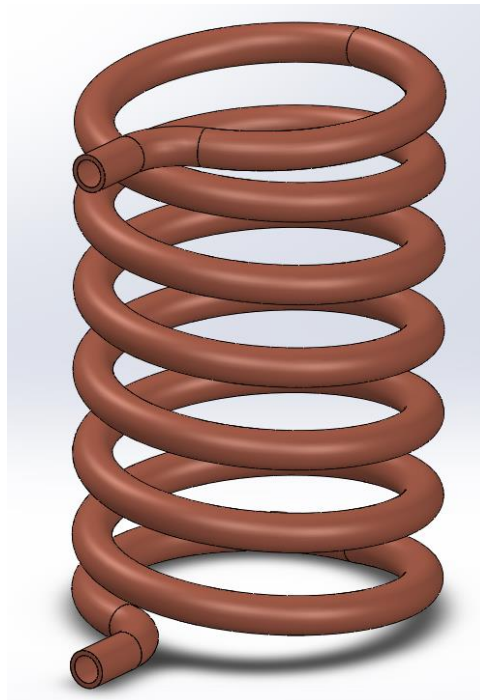art in the liquid water, therefore its dimensions must be designed consequently. The height of the heat exchanger is a little lower than the maximum level of water contained in the evaporator. Since the internal diameter of the evaporator D_i is $112\ mm$ the maximum height H_{max} of water into the tank is calculated as:

$$H_{max} = \frac{m_w}{\rho_w A_{base}} = 153\ mm \tag{7.1}$$

where ρ_w and m_w are the density and the mass of the water inside the tank, while A_{base} is the tank base surface. With the same equation the height of the remaining water H_{min} after the complete evaporation is defined, considering $540\ g$ of water still in the tank. A height $H_{min} = 60\ mm$ has been calculated. Considering these two quantities, the height of the heat exchanger has been chosen at 80 mm, in order to keep an efficient heat exchange during all the evaporation process. The helix has 7 revolutions and a base circumference of $50\ mm$. This ensures that there is enough space clearance to allow the assembly of the heat exchanger onto the compression fittings. The software Solidworks has a feature that allows to measure the total length of the heat exchanger, which is $1134\ mm$.

7.2   Evaporation heat transfer design

The design of the heat transfer allows to find the time necessary for the evaporation of the amount of water needed for the adsorption reaction. This analysis is carried out using the ε-NTU method, considering that the heat flux is transmitted from the water flowing in the copper pipe towards the water inside the tank. At first, the maximum heat flow achievable is calculated from the equation:

$$\varphi_{max} = \dot{m}_w c_{p,w} \Delta T \tag{7.2}$$

where $\dot{m}_w$ and $c_{p,w}$ are the mass flow and the specific heat of the water inside the heat exchanger, and ΔT is the temperature difference between the water to be evaporated and the water flowing into the heat exchanger.

The inlet mass flow $\dot{m}_w$ of the water is estimated considering a flow speed v_w of $5\ m/s$ inside the copper pipe with internal diameter D_i equal to $4.4\ mm$:

$$\dot{m}_w = \rho_w \frac{\pi D_i^2}{4} v_w \qquad (7.3)$$

The actual mass flow $\dot{m}_w$ is measured directly by a piston flow-meter mounted on the inlet water pipe. The water flowing into the heat exchanger is delivering heat to the water to be evaporated, and to describe this phenomenon the pipe thermal resistance is considered, as shown in figure 36.
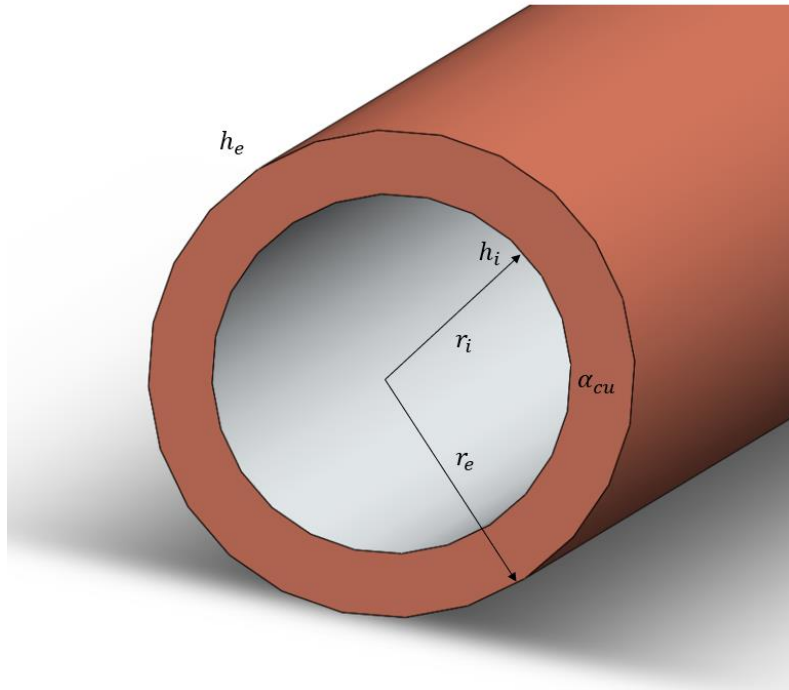
Figure 36 Geometry and heat exchange coefficients

From the Fourier equation, the thermal resistance of the pipe can be found as:

$$R_t = \frac{1}{2\pi r_i h_i L} \qquad (7.4)$$

Since the water inside the tank is undergoing a phase change, the coefficient h_e is significantly higher than the coefficient h_i, therefore the external thermal resistance of the pipe may be considered negligible [16]. The same consideration can be made about the conductive resistance of the pipe, since copper is characterized by high thermal conductivity (about $390\frac{W}{mK}$ [79]).

The convective heat exchange coefficient h_i is found considering the Dittus-Boelter relation:

$$Nu = 0.023Re^{0.8}Pr^{0.3} \qquad (7.5)$$

where Nu, Re and Pr are the dimensionless Nusselt, Reynolds and Prandtl numbers respectively and α_w is the thermal conductivity of water. The Reynold number is given by the following equation:

$$Re = \frac{\rho_w v_w d_i}{\mu} \qquad (7.6)$$

where μ is the dynamic viscosity of the water flowing inside the copper pipe. The Prandtl number has this expression:

$$Pr = \frac{c_p \mu}{k_w} \qquad (7.7)$$

where c_p is the water specific heat at constant pressure and k is the thermal conductivity. Finally, the convective heat transfer coefficients h_i is calculated from the following equation:

$$h = \frac{Nu * k_w}{d_i} \qquad (7.8)$$

The water characteristics values used for the calculations are summarized in table 11.

Table 10 Water thermal properties

	Symbol	Unit of measurement	Value
Density	ρ_w	$\dfrac{kg}{m^3}$	1000
Specific heat	c_p	$\dfrac{J}{kgK}$	4186,8
Thermal conductivity	k	$\dfrac{W}{mK}$	0,6
Speed	v_w	$\dfrac{m}{s}$	5
Dynamic viscosity	μ	$Pa \cdot s$	$8,94 \cdot 10^{-4}$

The ε-NTU coefficients are then found using the following equations:

$$NTU = \frac{U \cdot A}{(\dot{m}_w \cdot c_p)} \tag{7.9}$$

$$\varepsilon = 1 - e^{-NTU} \tag{7.10}$$

where $U \cdot A$ is the product between the copper tube external area A and the global heat exchange coefficient U. The term ε is the ratio between actual and maximum heat exchanged.

$$\varepsilon = \frac{\varphi}{\varphi_{max}} \tag{7.11}$$

$$\varphi = \varepsilon * \varphi_{max} \tag{7.12}$$

This way, the thermal power φ to be supplied during the evaporation can be found. Finally, the time t needed for the complete evaporation process has been calculated comparing φ to the enthalpy of evaporation of water ($2260 \frac{kJ}{kg}$). With the thermal energy generated the mass flow of vapour $\dot{m}_{vap}$ that is produced can be calculated as:

$$\dot{m}_{vap} = \frac{\varphi}{\Delta H_{vap}} \tag{7.13}$$

The time needed for the whole evaporation of the water mass Q_{vap} ($960\ g$) process is:

$$t = \frac{Q_{vap}}{\dot{m}_{vap}} \tag{7.14}$$

7.3 Results

The calculations have been carried out considering that the water flowing inside the heat exchanger is coming from the water mains at a temperature of 20°C. A temperature range of the water inside the tank going from 5°C to 15°C is applied, considering that the vacuum inside the evaporator tank brings down the temperature to 10°C, but in winter the temperature can be lower. Figure 37 shows the time needed for the full evaporation, depending on the temperature of the water inside the tank.
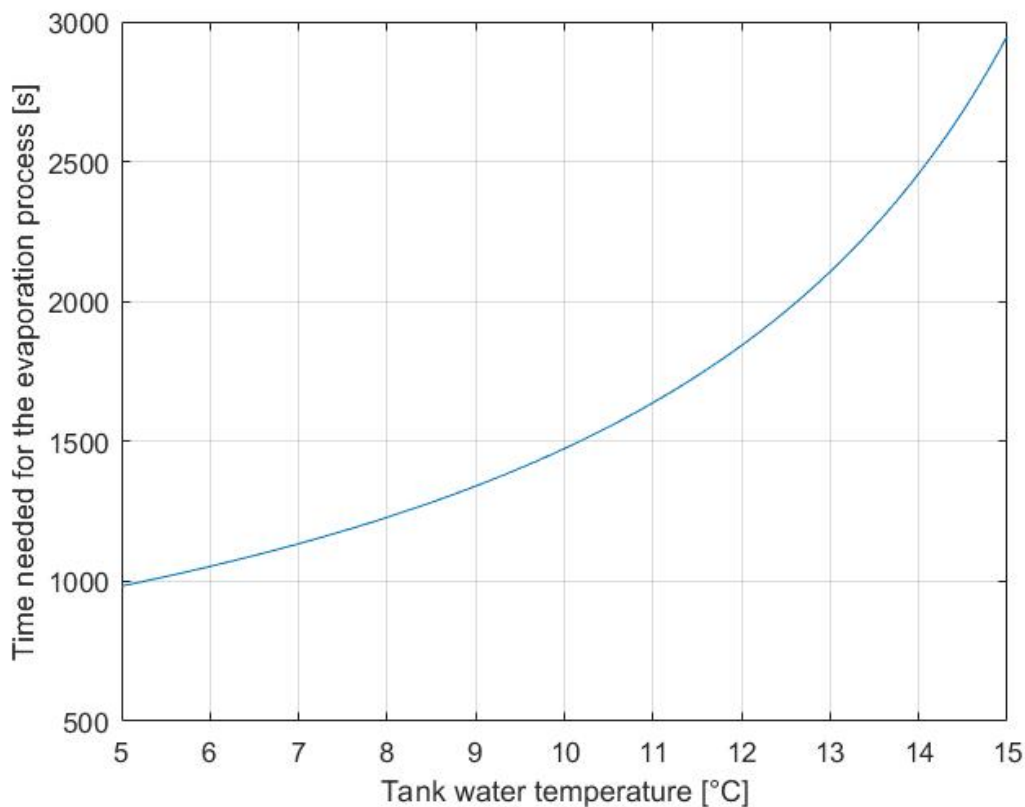
Figure 37 Evaporation process duration

The best situation occurs during winter, when the temperature of the water is considered equal to $5°C$ and the evaporation takes 983 seconds to complete. On the other side of the temperature range, this time is much higher because the temperature inside the water reaches $10°C$ after the vacuum pump has brought the atmosphere inside the tank at $12.2\ mbar$. In this situation the evaporation takes 1475 seconds to complete. Figure 38 shows the magnitude of the water vapour mass flow during evaporation, and it makes clear that the winter operation of the device is faster due to the greater temperature difference between the two exchange fluids.

64
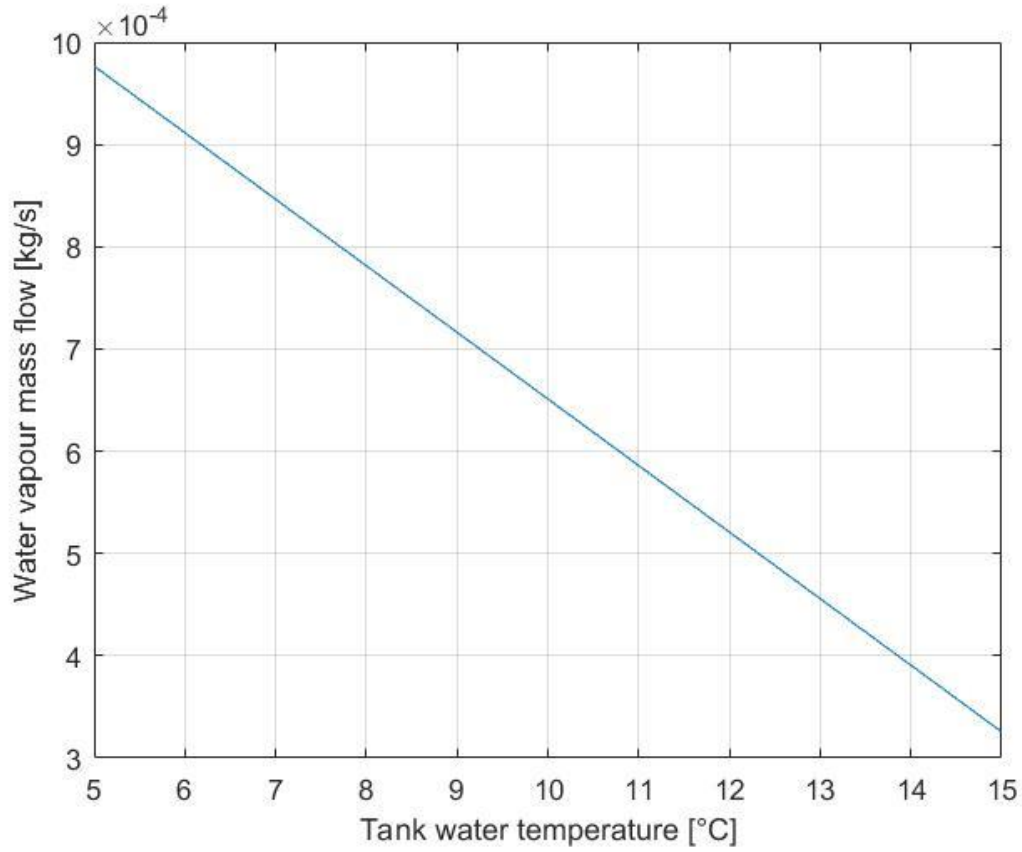
Figure 38 Mass flow rate of water vapour

During winter, when temperatures are lower ($5°C$), it has been calculated that the mass flow of water vapour is $0,98 \frac{g}{s}$. During summer, the slower evaporation rate reflects the lower mass flow of vapour produced, which is $0,33 \frac{g}{s}$ (at 15°C).

7.4   Reactor heat exchanger design

The heat exchanger reactor is placed, with direct contact and completely covered, in a granular bed of zeolites. His height must be lower than the zeolite bed, which is calculated as:

$$H_{bed} = \frac{m_{bed}}{\rho_{bed} A_{base}}$$

(7.15)

where m_{bed} is the total mass of the zeolite, ρ_{bed} is the density and A_{base} is the internal base area of the tank.

The first concept of heat exchanger reactor design is shown in figure 39:

Figure 39 First concept of the reactor's heat exchanger configuration

This heat exchanger is formed by three spirals jointed by welded copper tube. The spirals outer ring has been dimensioned with enough clearance to allow the assembly/disassembly of the component into the reactor vessels by means of two compression fittings. During the charge phase, the water flow inside the heat exchanger works as heat source for the desorption reaction. During discharge, the heat released from the adsorption reaction increases the water flow temperature.

8 Analogy between sorption and phase change

In this chapter, the behaviour of a PCM (from solid to liquid and from solid to liquid) is described by an analytical model, making the assumption that the heat is exchanged perpendicularly to the surface of a PCM slab. The model is then adapted to describe the behaviour of the sorbate-sorbent pair during the adsorption and desorption reactions.

8.1 PCM analytical model

The model aims to calculate the time needed by a semi-infinite slab (PCM) to complete the phase change process and to describe the position of the solid/liquid interface over time. Figure 40 shows the PCM during the solidification and melting process.
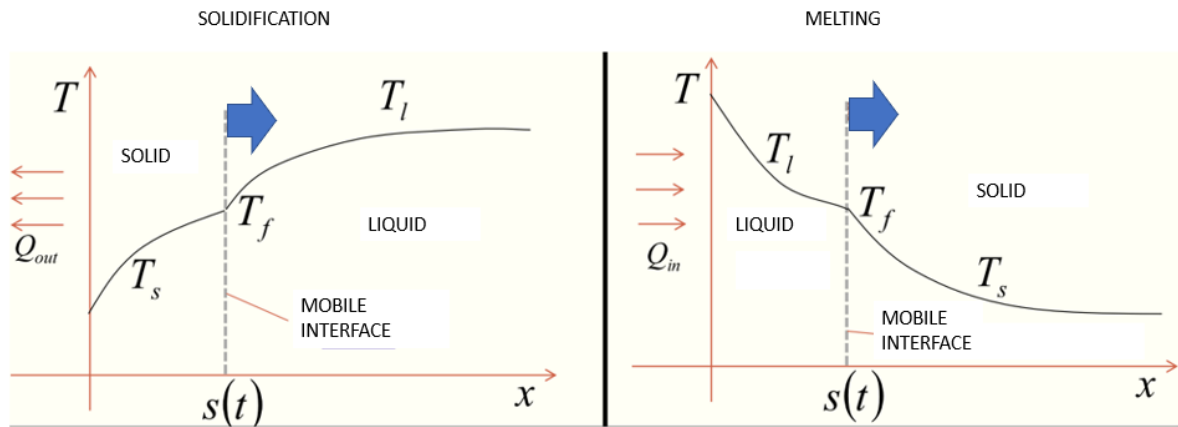

Figure 40 PCM solidification and melting process [70]

To describe the solid phase temperature T_s, the Fourier equation can be applied:

$$\begin{cases} \dfrac{\vartheta^2 T_s}{\vartheta x^2} = \dfrac{1}{\alpha_s} \dfrac{\vartheta T_s}{\vartheta t} \\ T_s = T_l \qquad x = 0; t > 0 \end{cases} \tag{8.1}$$

The model assumes that in the liquid phase, heat exchange occurs predominantly by conduction, therefore the Fourier equation can be applied as well:

$$\begin{cases} \dfrac{\vartheta^2 T_l}{\vartheta x^2} = \dfrac{1}{\alpha_l} \dfrac{\vartheta T_l}{\vartheta t} \\ \dfrac{\vartheta T_l}{\vartheta x} = 0 \quad x \to \infty; t > 0 \\ T_l = T_i \quad x > 0; t = 0 \end{cases}$$

(8.2)

Figure 41 shows the heat fluxes involved in the process of solidification (discharge). Heat flux Q_s is being released during the PCM cooling. During the phase change, the liquid portion exchanges the heat flux Q_l with the solid part, due to the temperature gradient between them. The term $\bar{S}$ is referred to a heat flux arising in the volume of the PCM due to the phase change. The thermal balance of the heat fluxes at the interface between solid and liquid can be formulated as:

$$|Q_l| + \bar{S} = |Q_s|$$

(8.3)

The density ρ is assumed to be equal and constant for the solid and the liquid phases. Making all the terms of equation (8.3) explicit, the interface condition becomes:

$$\lambda_s \frac{\partial T_s}{\partial x} - \lambda_l \frac{\partial T_l}{\partial x} = \rho L \frac{ds}{dt}$$

(8.4)

Where λ is the thermal conductivity and L is the latent heat of solidification.
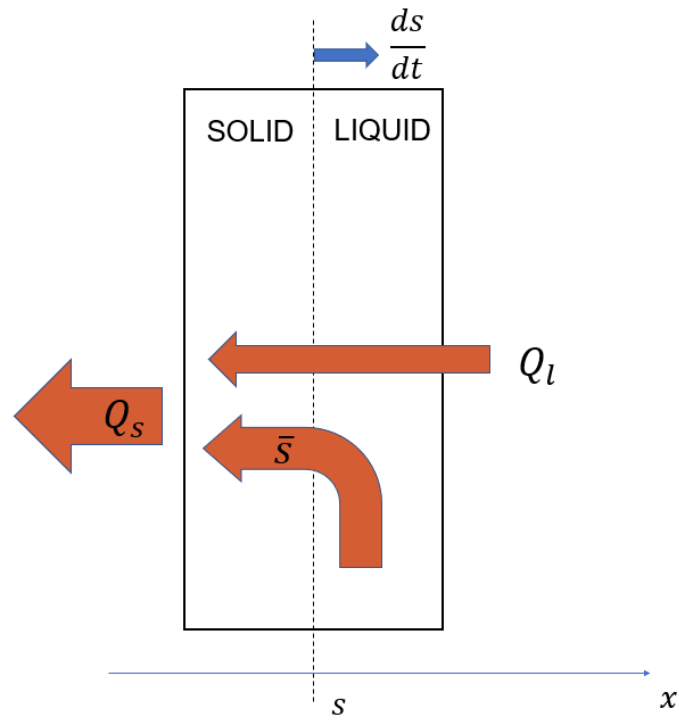
Figure 41 PCM discharge phase [80]

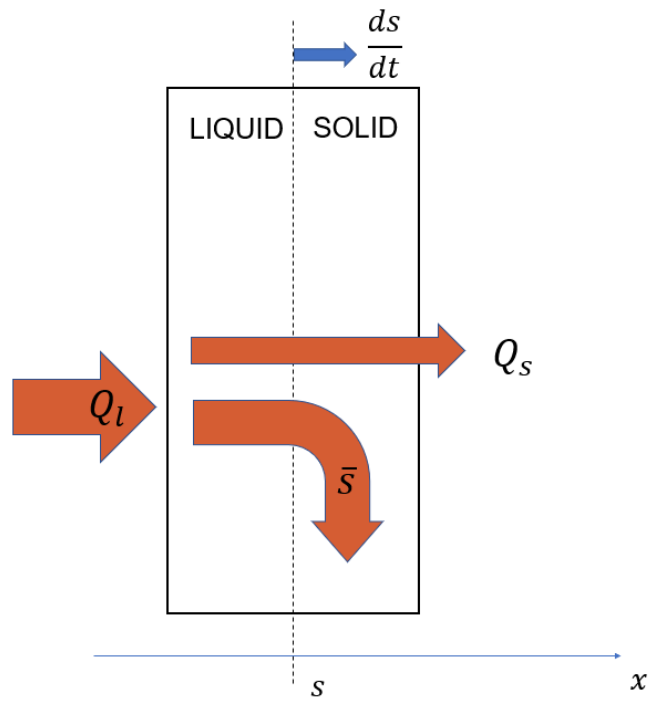During fusion (charge), the heat exchanged by the PCM is shown in Figure 42.

Figure 42 PCM charge phase [80]

In this configuration, the heat balance at the interface position $s(t)$ is:

$$|Q_l| = |Q_s| + \bar{S} \tag{8.5}$$

The interface condition can then be written as:

$$\lambda_s \frac{\partial T_s}{\partial x} - \lambda_l \frac{\partial T_l}{\partial x} = \rho L \frac{ds}{dt} \tag{8.6}$$

This demonstrates that the interface condition is equal during charge (equation 8.6) and discharge (equation 8.4). This method was first formulated by Stefan [81]. Stefan's solution with constant thermophysical properties shows that the rate of melting or solidification in a semi-infinite region is governed by a dimensionless number, known as the Stefan number St:

$$St = \frac{c_s(T_f - T_l)}{L} \tag{8.7}$$

where T_f is the temperature on the interface between solid and liquid phase. The final exact analytical solution of the problem was obtained by Neumann as a function of a constant k [82]:

$$s(t) = 2k\sqrt{\alpha_s t} \tag{8.8}$$

The thermal profiles of the solid and the liquid portions can be consequently described by the following system:

$$\begin{cases} \dfrac{T_s - T_i}{T_f - T_i} = \dfrac{\mathrm{erf}\left(\dfrac{x}{2\sqrt{\alpha_s t}}\right)}{\mathrm{erf}(k)} \\[4ex] \dfrac{T_s - T_i}{T_f - T_i} = \dfrac{\mathrm{erfc}\left(\dfrac{x}{2\sqrt{\alpha_l t}}\right)}{\mathrm{erfc}\left(k\sqrt{\dfrac{\alpha_s}{\alpha_l}}\right)} \end{cases} \tag{8.9}$$

Combining the system (8.9) with the interface condition (8.6), it is possible to obtain an equation to recover the parameter k:

$$\frac{e^{-k^2}}{\text{erf}(k)} + \frac{\lambda_l}{\lambda_s} \frac{e^{-k^2 \alpha_s/\alpha_l}}{\text{erfc}\left(k\sqrt{\frac{\alpha_s}{\alpha_l}}\right)} \frac{T_f - T_i}{T_f - T_l} = \frac{kL\sqrt{\pi}}{c_s(T_f - T_i)} \tag{8.10}$$

Where α is the thermal diffusivity and c_s is the specific heat. Assuming that the melting temperature T_f of the PCM is equal to its initial temperature T_i, equation (8.10) can be written as:

$$ke^{k^2}\,\text{erf}(k) = \frac{c_s(T_f - T_l)}{2L} \tag{8.11}$$

If $St < 0.1$, the Neumann formulation reduces to a one-phase problem, where only one phase (solid) is changing its temperature, while the other (liquid) remains at constant temperature (T_f) [83]. Consequently, the interface condition reduces as:

$$\lambda_s \frac{\partial T_s}{\partial x} = \rho L \frac{ds}{dt} \tag{8.12}$$

Separating the variables s and t and integrating, equation (8.12) can be rewritten as:

$$\frac{s^2}{2} = \lambda_s \frac{T_f - T_l}{\rho L} t \tag{8.13}$$

Combining equation (8.13) with equation (8.8), the parameter k can be written as a function of the Stefan's number:

$$k = \sqrt{\frac{St}{2}} \tag{8.14}$$

8.2   Analogy between water vapour and PCM

In the first instance, a physical model of the reactor heat exchanger was developed, assuming the three spirals as three plates constituted by the water flowing into the heat exchanger. Between the plates is situated the zeolite, and the heat is exchanged in the direction perpendicular to the plates. The physical model is shown in figure 43:
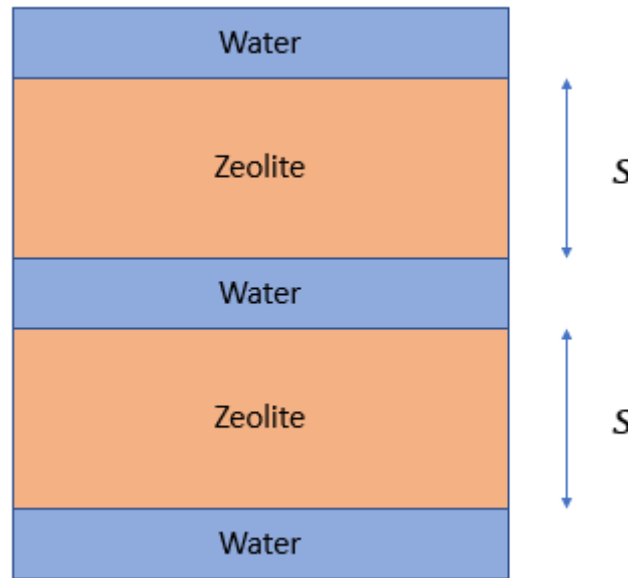

Figure 43 2-D configuration for the adsorption reactor

During the adsorption (and desorption) reaction, the water vapour is changing phase from gas to a condensed state inside the zeolite micropores (and vice-versa). Hence, the analogy between PCM and water vapour has been used to develop a numerical model that tries to estimate (approximatively) the time spent by the two reactions and therefore roughly estimates the thermal power cycled by the storage system. The parameters used to calculate the Stefan number must be addressed. Equation (8.7) is used considering that the term L (the latent heat of solidification for the PCM) is the isosteric heat of the zeolite and c is its specific heat. During charge, T_f is considered as the inversion temperature of the adsorption reaction, estimated as the mean between the maximum and minimum temperature of the process ($363.15K$ and $325.5K$ respectively). During discharge, T_f has the same definition, being $341.8K$ the maximum temperature and $308.15K$ the minimum temperature. T_l is assumed to be the temperature of the sorbate. During charge, T_l is the temperature of the water vapour after the desorption process has been completed ($325.5K$), while during the discharge phase it is the

temperature of the water vapour coming from the evaporator ($308.15K$). Equation (8.8) above represents the correlation between the thickness of zeolite s affected by the adsorption/desorption reaction over time (t). The term α_s is the thermal diffusivity of zeolites, calculated as:

$$\alpha_s = \frac{\lambda_s}{\rho c_s}$$

(8.15)

Where λ_s and ρ are the thermal conductivity and the density of zeolite respectively. The thermal power released/stored can then be calculated. The former is the ratio between the released thermal energy and the time required by the process, while the latter is the ratio between the thermal energy stored during charge and the charging time.

8.3   Results

The Stefan's number for adsorption and desorption was calculated, using the quantities shown in table 12.

Table 11 Zeolite thermal characteristics for the calculation of the Stefan number

	Symbol	Unit of measurement	Value
Specific heat	c_s	$\dfrac{kJ}{kgK}$	0,9
Adsorption heat	L	$\dfrac{kJ}{kg_{zeo}}$	283
Density	ρ	$\dfrac{kg}{m^3}$	700
Thermal conductivity	λ_s	$\dfrac{W}{mK}$	0,58
$\left(T_f - T_l\right)_{adsorption}$		K	16,825
$\left(T_f - T_l\right)_{desorption}$		K	18,825

The Stefan numbers found were 0.0535 (adsorption) and 0.0599 (desorption), and then the value of k was calculated with equation (8.14). Different values of thickness s was considered (between 20 mm and 90 mm) for the next steps. It is assumed that the water plates exchange heat only with half of the zeolite bed ($s/_2$) for symmetry reasons.

8.3.1   Charge phase results

The estimation of the time required for the charge phase is showed in Figure 44. As expected, the desorption time increases for larger thicknesses since a larger quantity of water has to be desorbed, while the heat flux remains the same. The charge phase can take from 907 seconds (if $s = 20$ mm) to 18370 seconds (if $s = 90$ mm) to complete.
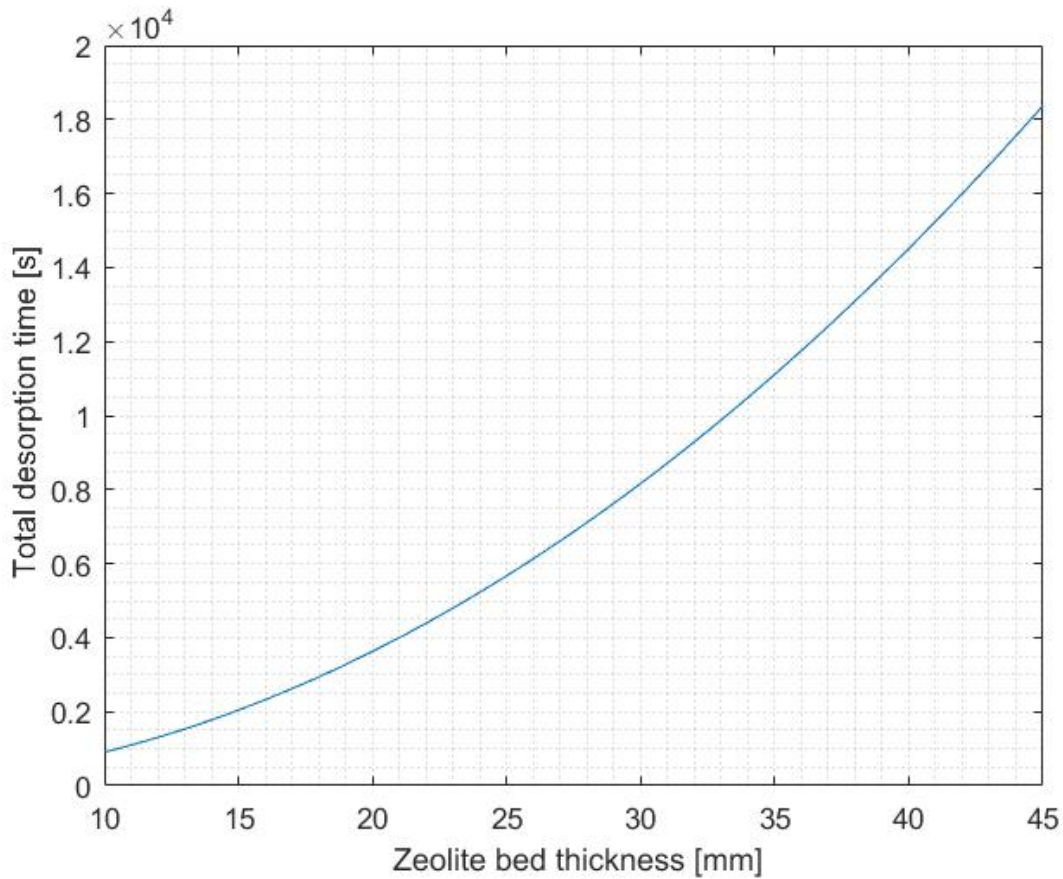

Figure 44 Time spent by the charging process

The estimation of the thermal power stored is showed in Figure 45. The power is inversely proportional to the time t (with constant energy stored), thus if the distance between the plates of the heat exchanger is lower, the power stored will be higher. The maximum power stored is $998\ W$, if $s = 20\ mm$.
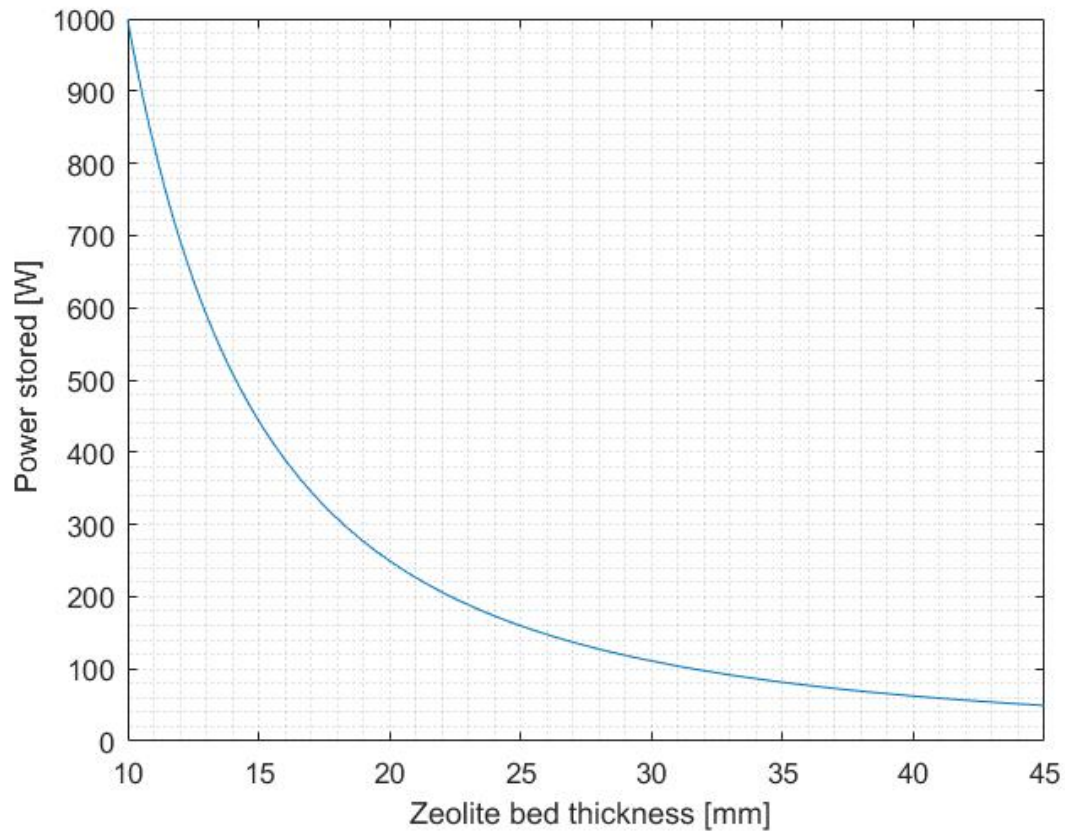

Figure 45 Estimated thermal power stored

8.3.2   Discharge phase results

The estimation of the time required for the discharge phase is showed in Figure 46. The charge phase can take from 1015 seconds (if $s = 20\ mm$) to 20554 seconds (if $s = 90\ mm$) to complete.
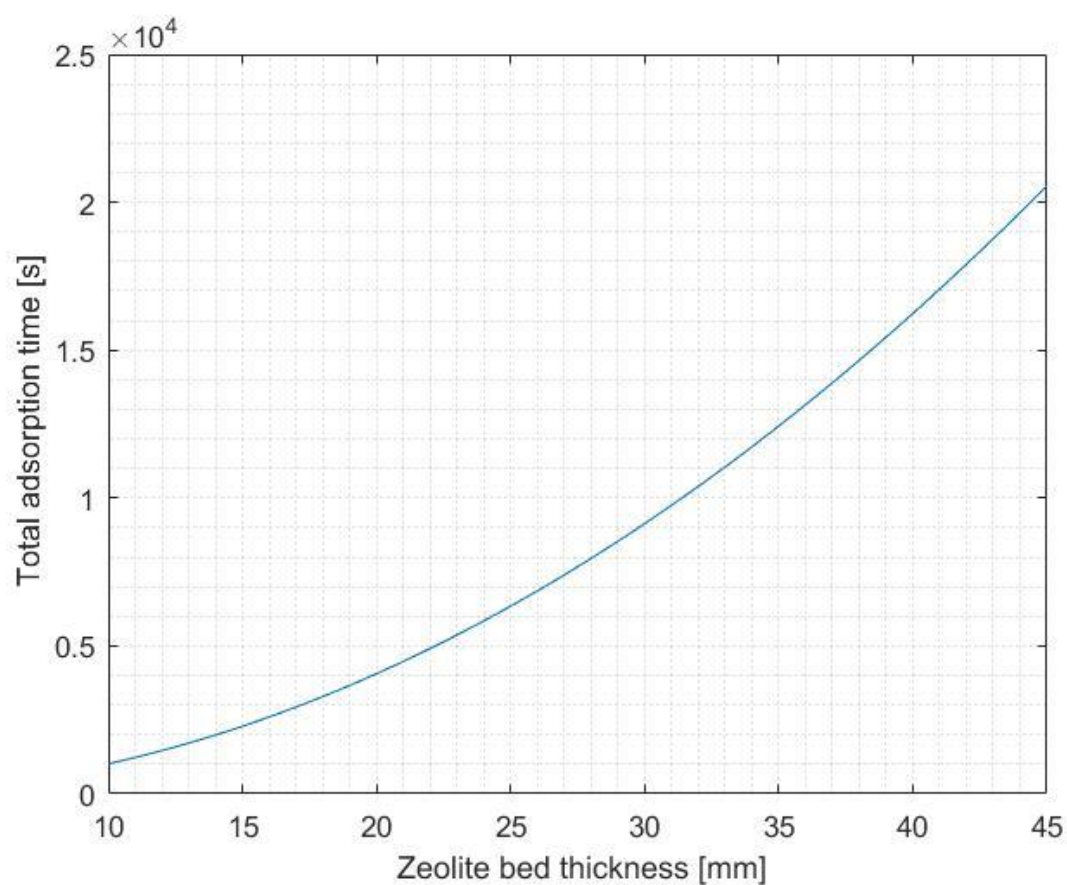

Figure 46 Time spent by the discharging process

Figure 47 shows the estimated power released during the adsorption reaction, which is lower than the power stored during charge. Indeed, the maximum value found was $982.2\ W$ obtained for a thickness $s = 20\ mm$, while the minimum was $44.1\ W$ (at $s = 90\ mm$).This is due to the fact that the temperature variation during the adsorption ($16.825°C$) is $2°C$ smaller than desorption ($18.825°C$), therefore the former takes more time to complete than the latter.
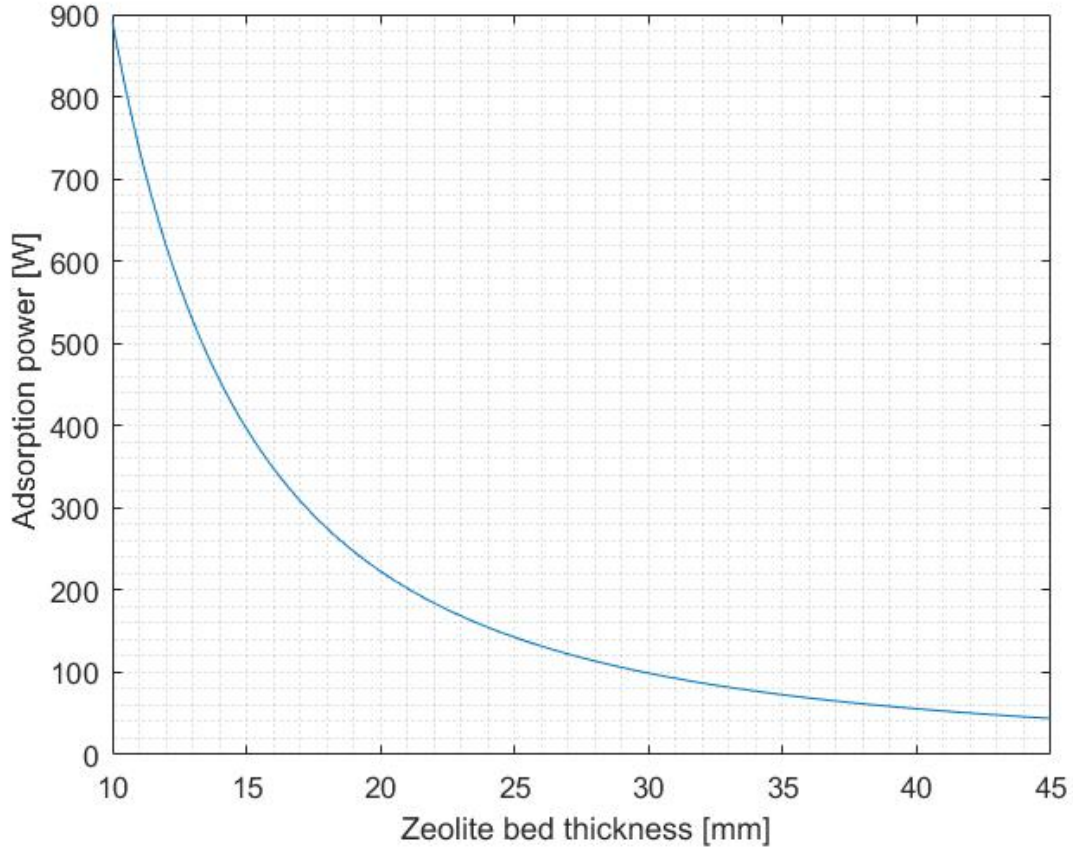
Figure 47 Estimated thermal power released

The values obtained were estimated by a new approach: the Stefan model designed to perform numerical analyses on PCMs were adjusted exploiting the fact that the sorbate changes phase during the sorption reaction. The thermal power P released/stored during the reactions increases if the thickness s (and consequently t) is reduced, since P is defined as:

$$P = \frac{E}{t} \tag{8.16}$$

9 Conclusions

Thermal energy storage is one of the key technologies that are studied and employed in all the applications requiring energy production with high efficiency and low emissions. The current work has analysed all the phases concerning the design of a thermochemical heat storage which exploits the adsorption reaction of water vapour into an adsorbent material (zeolite 13X). A theoretical model employing the Langmuir formulation has been used to calculate all the characteristic of the thermodynamic cycle needed to obtain a cycled heat of at least $100\ Wh$. This specific cycle has been analysed in order to build a small-scale thermochemical heat storage at the Energy Department of -Politecnico di Torino. This system is composed by a few main components, namely one reactor vessel, one evaporator/condenser, the lids sealing them, and two heat exchangers. The structural design of these components has been covered in detail and then the design of the vessels was verified through a FEM analysis using the software Hypermesh. It was found that the tensile stresses on the two vessels (about $1\ Mpa$) are significantly lower than the failure tensile stress of the material ($87\ Mpa$). Since the objective is to build a system that works with a heat source at ambient temperature, a vacuum pump is needed to decrease the absolute pressure inside the tanks and to allow the evaporation of the water at 10°C. From the Antoine's equation, it has been found that in order to evaporate the water at such a low temperature, a minimum absolute pressure of $12.2\ mbar$ must be reached inside the tanks. Later on, all the complementary components necessary to connect the designed components were searched on the E-market of the Public Administration (MEPA), considering that they must work in a depressurized ambient. These includes pipes, fittings, vacuum pump, thermo-wells and a vacuum control unit. The MEPA allows to shorten the transaction time and reduce the costs of those components. Finally, two models have been developed in order to calculate the theoretical performances of the device. One was developed to find the time needed for the evaporation of the quantity of water necessary for the complete adsorption reaction, using the $\varepsilon - NTU$ method. The other model uses the analogy between a PCM and the water vapour and finds the power produced by the adsorption reaction if the heat exchanger is formed by interconnected spirals. As the PCM changes phase when it exchanges heat, the water being adsorbed is changing phase from water vapour to a condensed state inside the zeolite micropores. All the components CAD drawings produced in Solidworks are showed, with all the drawing quotas necessary for the construction. All the drawings were showed to the mechanical workshop manager, who indicated there would be no problems to produce the required components except the spiral heat exchanger, which would require special equipment.

Therefore, a simpler helix configuration will be adopted for the reactor heat exchanger. Future efforts should be directed to the research of more complicated heat exchanger configurations, in order to improve the efficiency of the device. Moreover, this work can be a starting point for other studies on this type of plant, starting from the design of all the components needed and arriving to the design of the operating applications, using other adsorbent/adsorbate pairs to achieve different results.

10 Appendix

10.1 3-D CAD drawings

In this section the drawings of the device designed in Solidworks are attached.
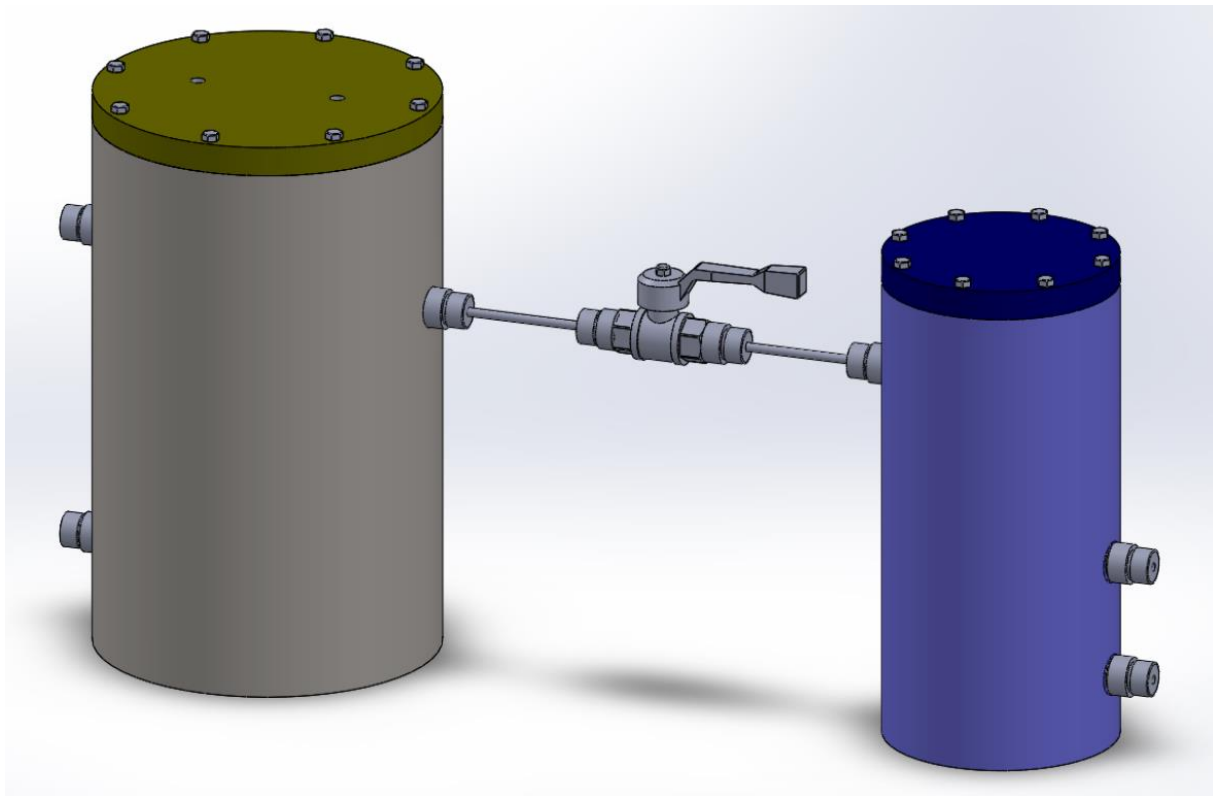

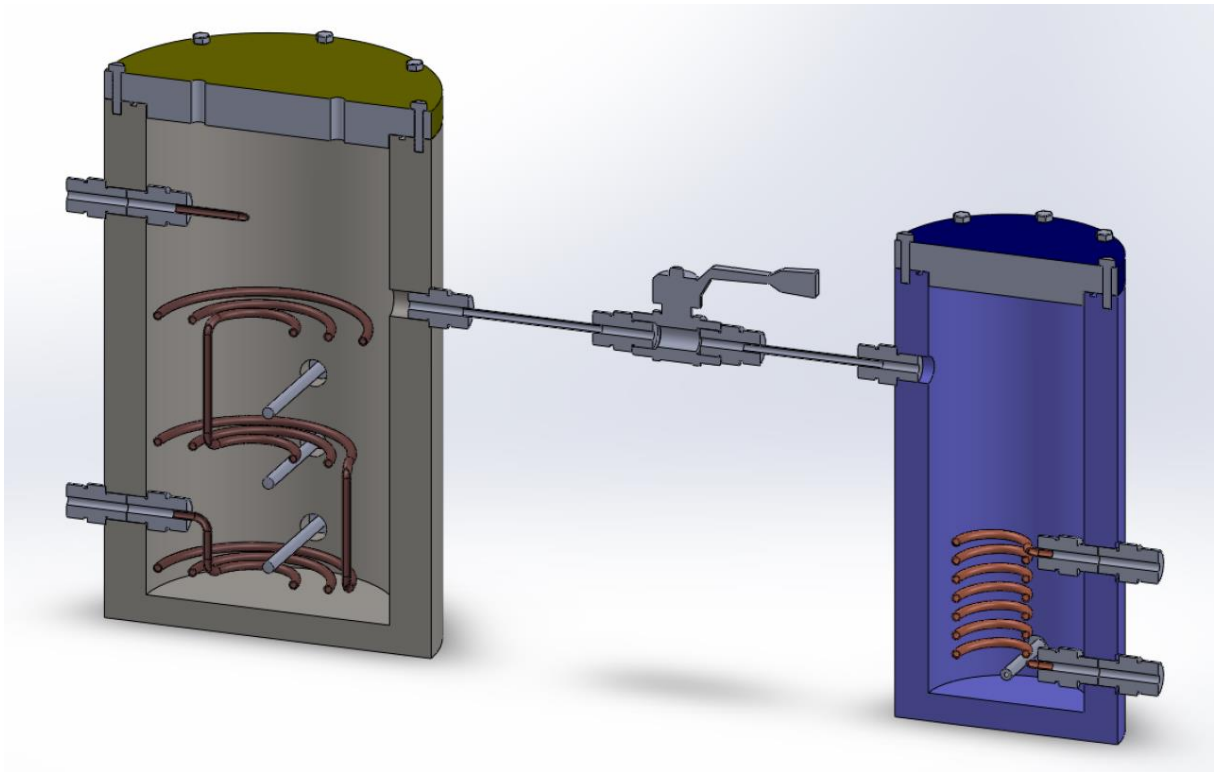*Figure 48 3-D view of the device*

Figure 49 3-D frontal section of the device configuration with spirals heat exchanger

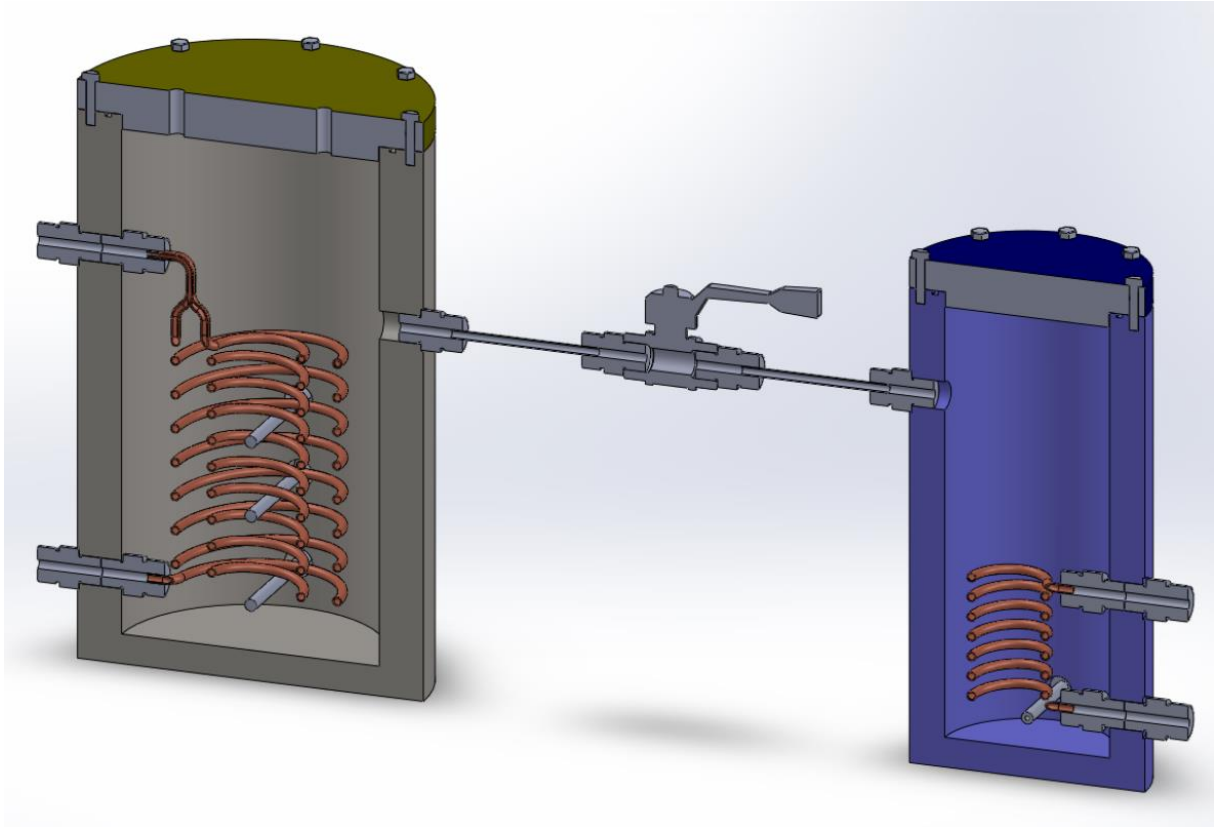*Figure 50 3-D frontal section of the device configuration with double-helix heat exchanger*
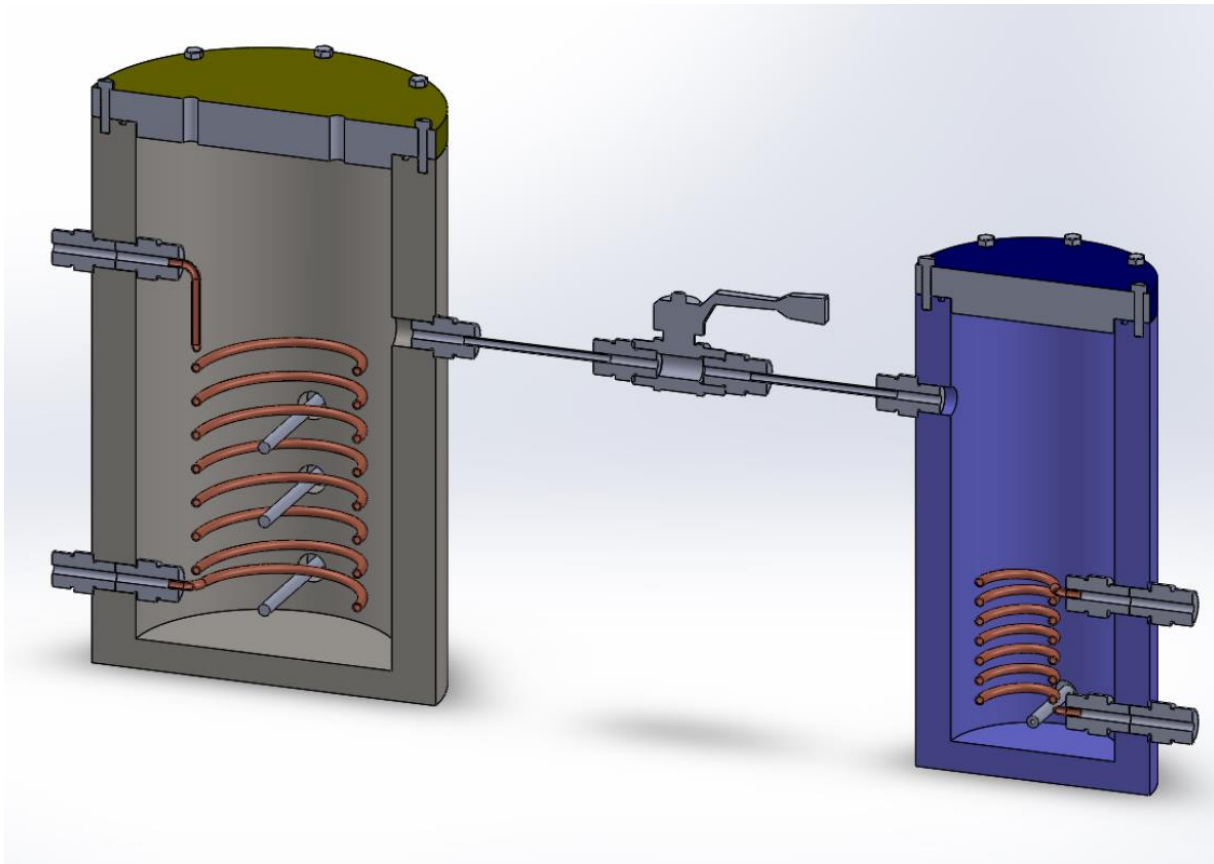
Figure 51 3-D frontal section of the device configuration with simple-helix heat exchanger

10.2 Components CAD engineering drawings

In this section the engineering drawings of the single components created in Solidworks are attached.
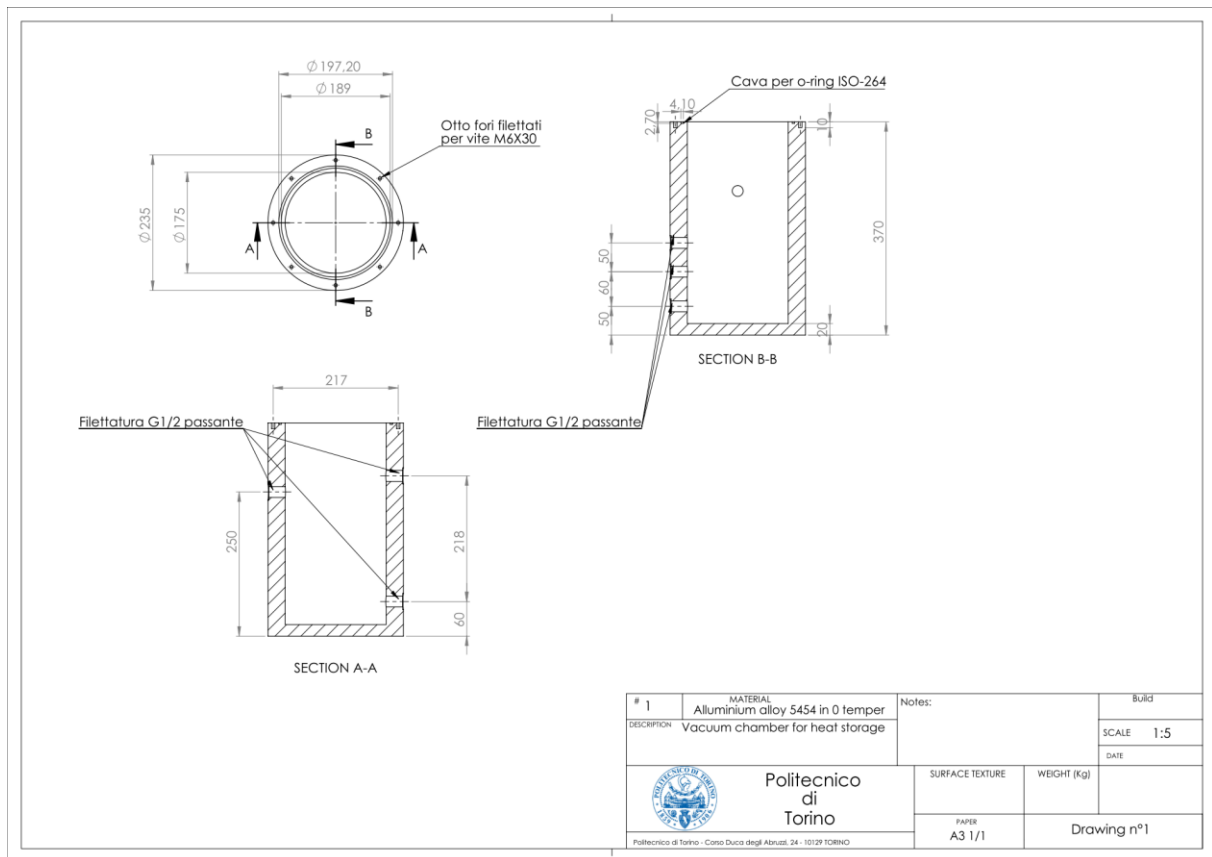
Figure 52 Engineering design of the vessel containing the zeolite
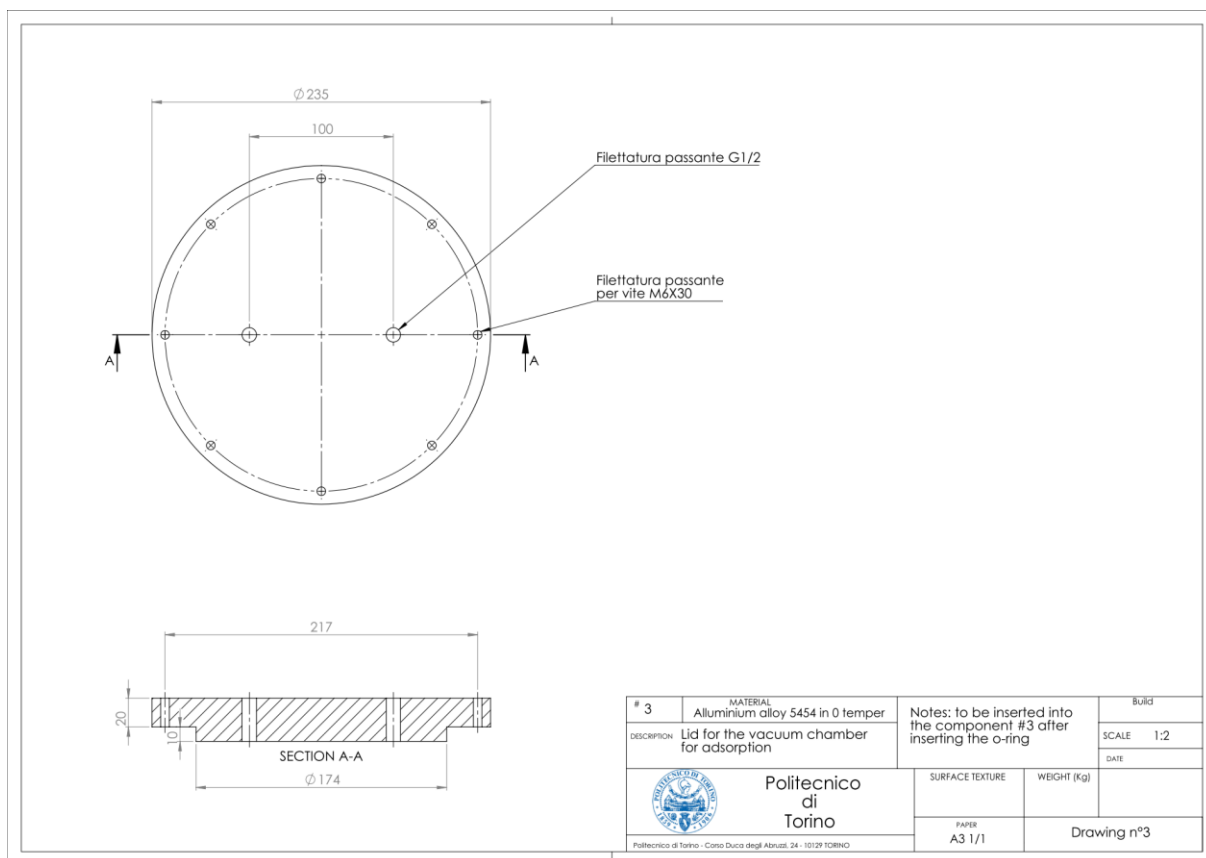
Figure 53 Lid of the vessel containing the zeolite

Figure 54 Engineering design of the evaporator/condenser vessel

Figure 55 Engineering design of the lid of the evaporator/condenser vessel

Figure 56 Engineering design of the heat exchanger held in the reactor vessel

Figure 57 Engineering design of the heat exchanger held in evaporator/condenser vessel

Figure 58 Engineering design of the connections between the components

Bibliography

[1] OECD, «OECD green growth study: energy,» 2011.

[2] UNCC, «Climate action and support trends,» 2019.

[3] IEA, «Energy efficiency – Analysis and outlooks to 2040,» 2018.
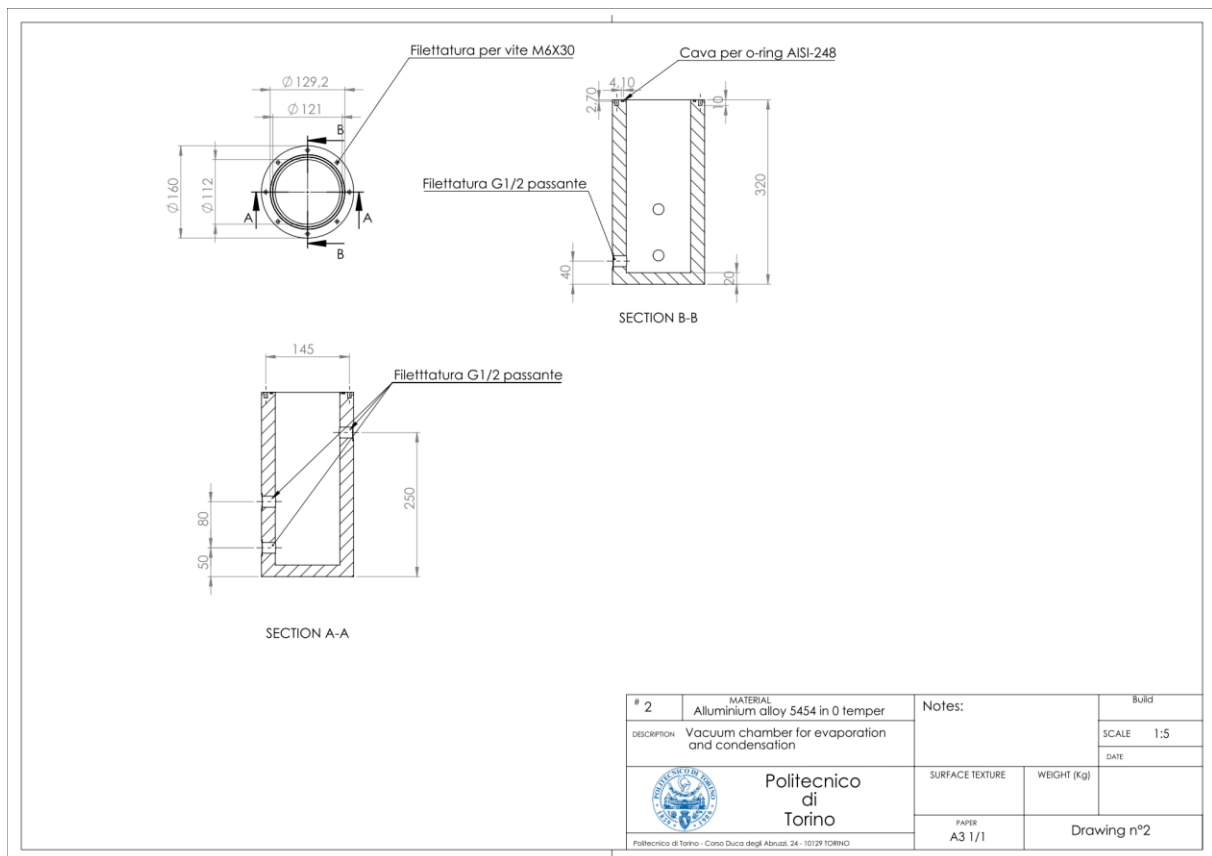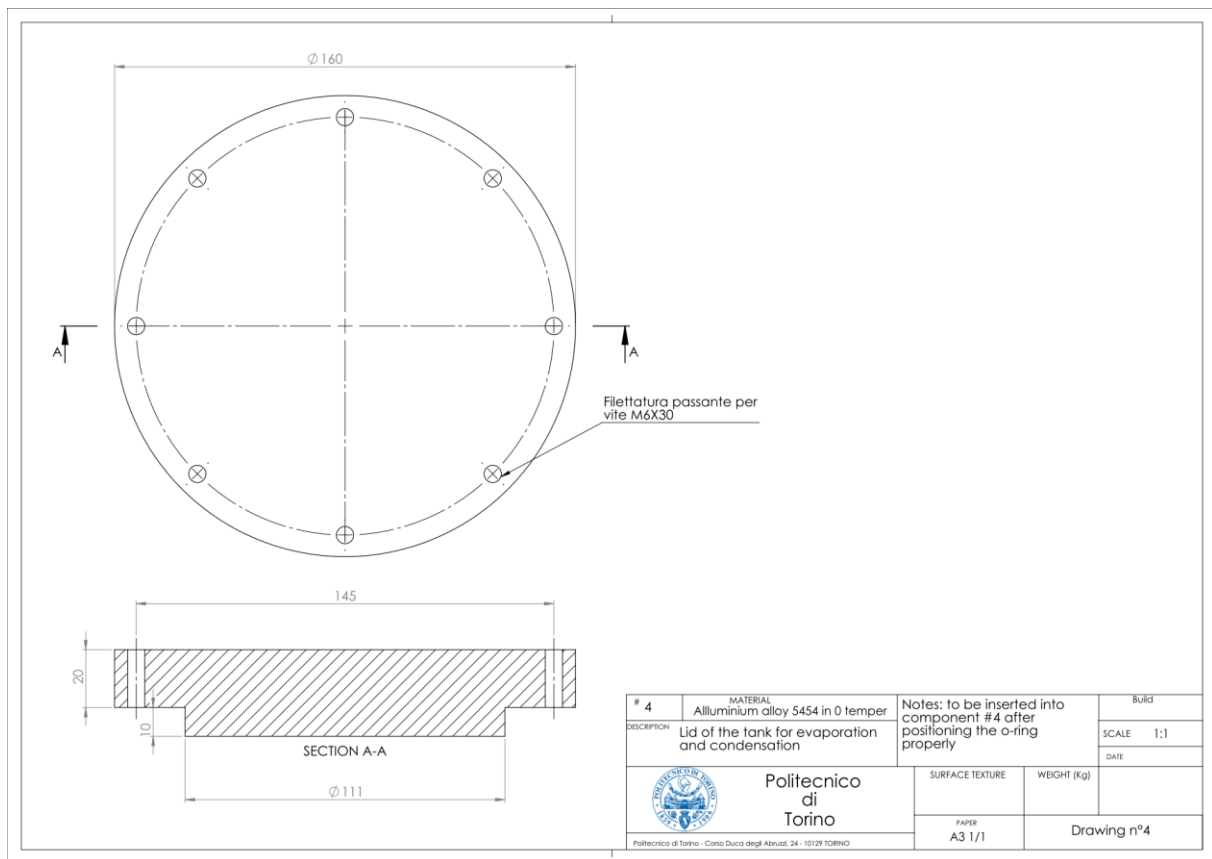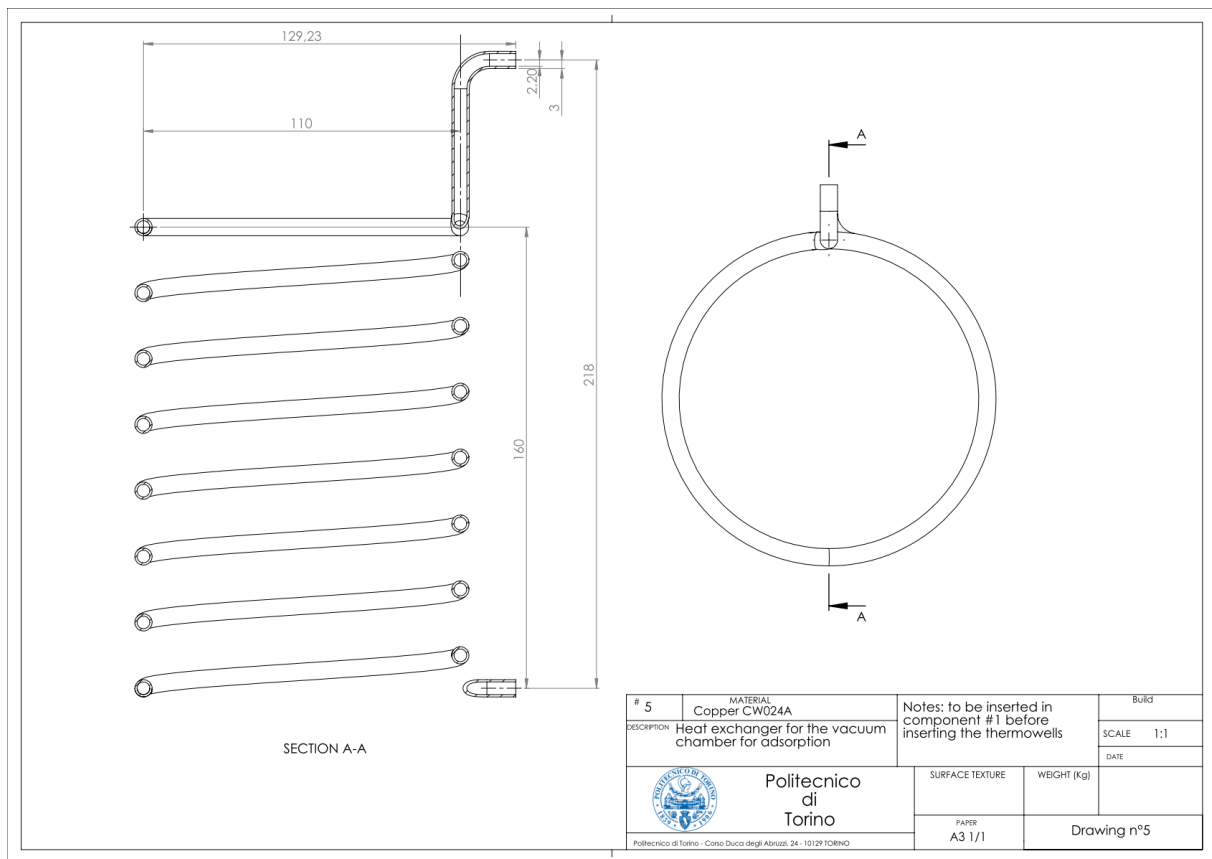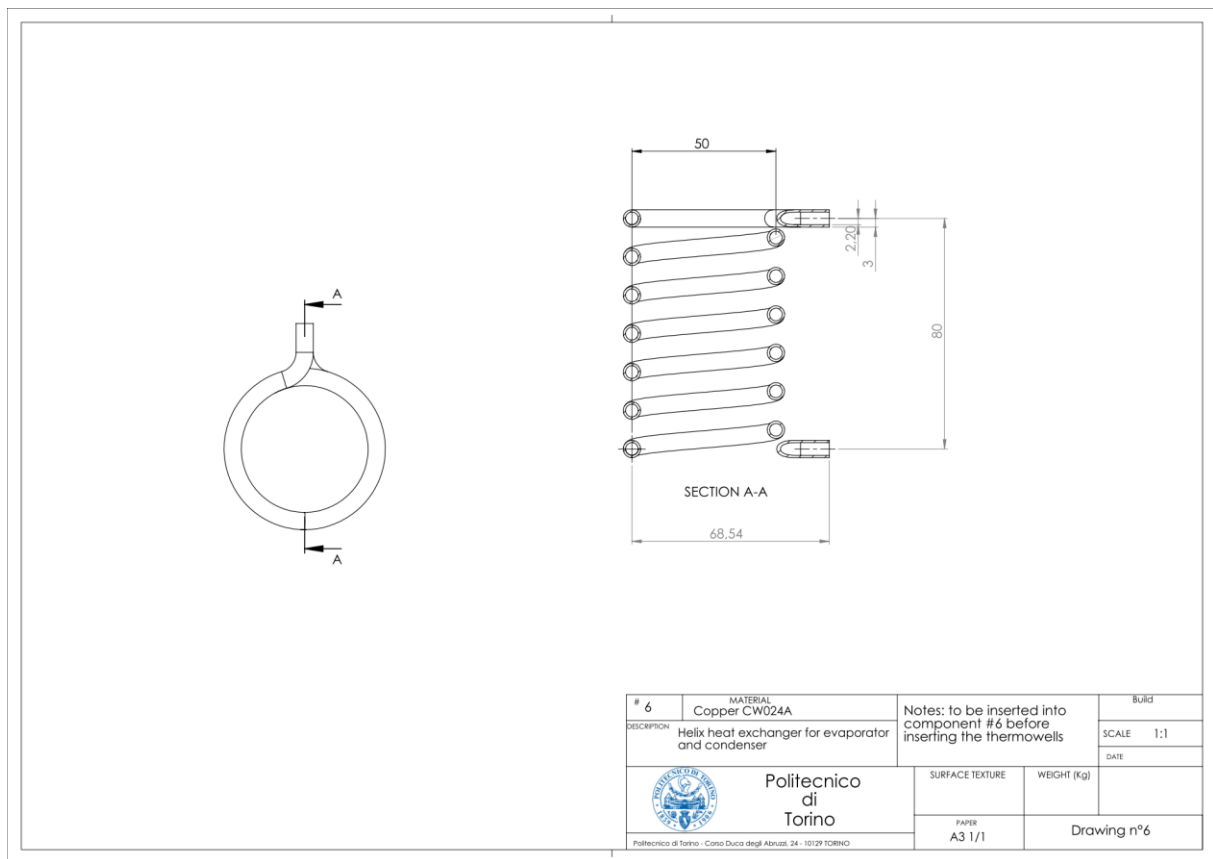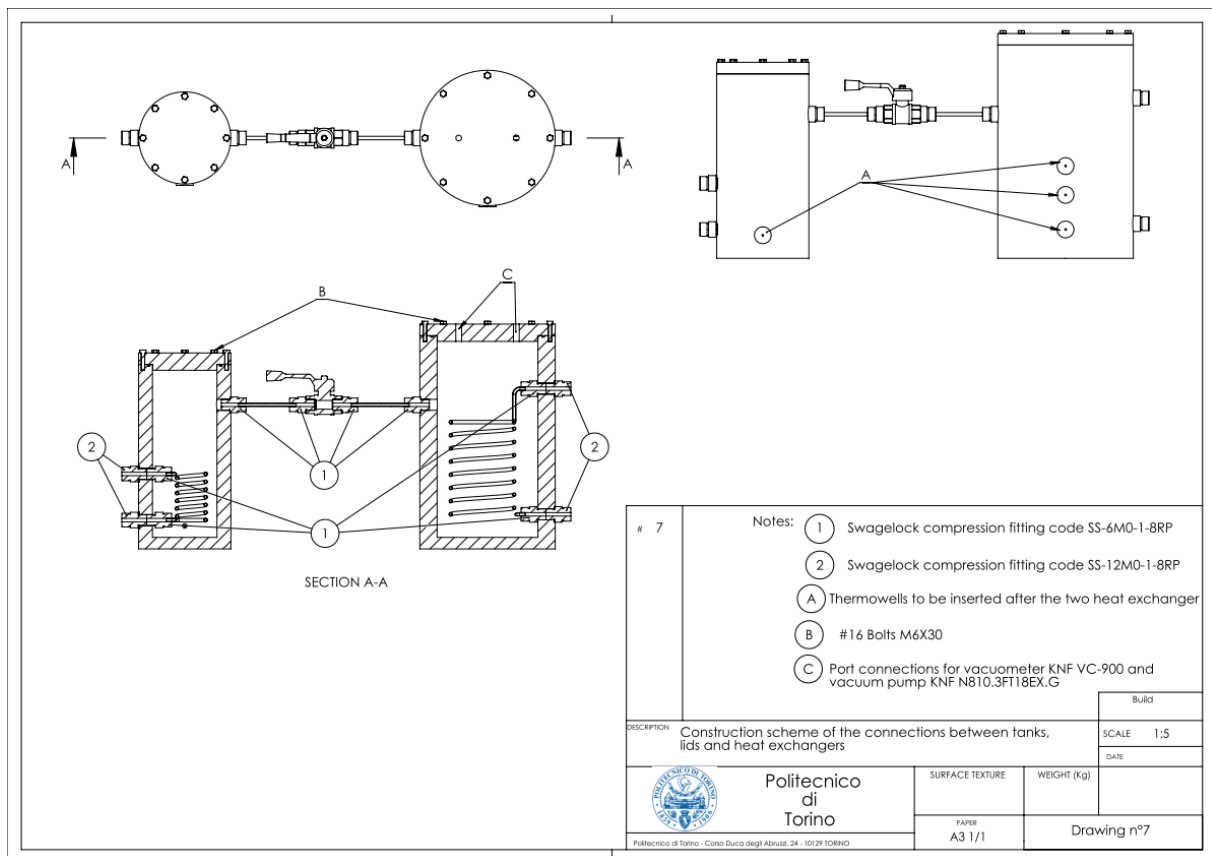
[4] IEA, «Renewables information: Overview,» 2018.

[5] B. Bolund, H. Bernhoff and M. Leijon, "Flywheel energy and power storage systems," *Renewables and sustainable energy reviews,* vol. 11, pp. 235-258, 2007.

[6] M. Amiryar and K. Pullen, "A review of flywheel energy storage system technologies and their applications," *Applied Energy,* vol. 7, 2017.

[7] J. Bai, X. Zhang and L. Wang, "A Flywheel Energy Storage System with Active Magnetic Bearings," *Energy Procedia,* vol. 16, pp. 1124-1128, 2012.

[8] C. Yang, «Pumped hydroelectric storage,» *Storing energy,* pp. 25-38, 2016.

[9] S. Rehman, L. M. Al-Hadhrami and M. M. Alam, "Pumped hydro energy storage system: A technological review," *Renewable and Sustainable Energy Reviews,* vol. 44, pp. 586-598, 2015.

[10] H. Lund, G. Salgi, B. Elmegaard and A. N. Andersen, "Optimal Operation Strategies of Compressed Air Energy Storage (CAES) on Electricity Spot Markets with Fluctuating Prices," *Applied Thermal Engineering,* vol. 29, p. 799, 2010.

[11] M. Winter and R. Brodd, "What are batteries, fuel cell and supercapacitors?," *Chem. Rev.,* vol. 104, pp. 4245-4270.

[12] P. Leung, X. Li, C. P. d. Leon, L. Berlouis, C. Low and F. Walsh, "Progress in redox flow batteries, remaining challenges and their applications in energy storage," *RSD Adv.,* vol. 2, pp. 10125-10156, 2012.

[13] P. Simon, Y. Gogotsi and B. Dunn, "Where Do Batteries End and Supercapacitors Begin?," *Science Magazine,* vol. 343, pp. 1210-1211, 2014.

[14] Q. Ke and J. Wang, "Graphene-based materials for supercapacitors electrodes – A review," *Journal of Materiomics,* vol. 2, pp. 37-54, 2016.

[15] P. Simon and Y. Gogotsi, "Materials for electrochemical capacitors," *Nature Materials,* vol. 7, pp. 845-854, 2008.

[16] I. Dincer and M. A. Rosen, Thermal energy storage systems and applications, 2011.

[17] P. Taylor, L. Johnson, K. Reichart, P. DiPietro, J. Philip and P. Butler, "A Summary of the State of the Art of SMES, FES and CAES," *Electrical Engineering,* vol. 3, 1999.

[18] S. Hasnain, "Review on sustainable thermal energy storage technologies, Part 1: heat storage materials and techniques," *Energy conversion and management,* vol. 39, pp. 1127-1138, 1998.

[19] A. Abedin and M. Rosen, "A Critical Review of Thermochemical Energy Storage Systems," *The Open Renewable Energy Journal,* vol. 4, pp. 42-46, 2011.

[20] D. Lefebvre and T. F. H., "A review of energy storage technologies with a focus on adsorption thermal energy storage processes for heating applications," *Renewable and Sustainable Energy Reviews,* vol. 67, pp. 15-16, 2017.

[21] H. Zhang, J. Baejens, G. Caceres, J. Degrève and Y. Lv, "Thermal energy storage: Recent developements and practical aspects," *Progress in energy and combustion science,* vol. 53, pp. 1-40, 2016.

[22] D. Groulx and W. Ogoh, "Solid-Liquid Phase Change Simulation Applied to a Cylindrical Latent Heat Energy Storage System," *Excerpt from the Proceedings of the COMSOL Conference,* 2009.

[23] R. Singh, S. Sadeghi and B. Shabani, "Thermal conductivity enhancement of phase change materials for low temperature thermal energy storage applications," *Energies,* vol. 12, 2019.

[24] A. Bland, M. Khzouz, T. Statheros and E. Gkanas, "PCMs for Residential Building Applications: A Short Review Focused on Disadvantages and Proposals for Future Development," *Buildings,* vol. 7, 2017.

[25] A. J. Carrillo, D. Sastre, D. P. Serrano, P. Pizarro and J. M. Coronado, "Revisiting the BaO2/BaO redox cycle for solar thermochemical energy storage," *Phys. Chem. Chem. Phys.,* vol. 18, pp. 8038-8048, 2016.

[26] A. J. Carrillo, J. Moya, A. Bayón, P. Jana, V. A. d. l. P. O'Shea, M. Romero, J. Gonzalez-Aguilar, D. P. Serrano, P. Pizarro and J. M. Coronado, "Thermochemical energy storage at high temperature via redox cycles of Mn and Co oxides: Pure oxides versus mixed ones," *Solar Energy Materials and Solar Cells,* vol. 123, pp. 47-57, 2014.

[27] A. J. Carrillo, D. P. Serrano, P. Pizarro and J. M. Coronado, "Thermochemical heat storage based on the Mn2O3/ Mn3O4 redox couple: influence of the initial particle size on the morphological evolution and cyclability," *J. Mater. Chem. A,* vol. 2, pp. 19435-19443, 2014.

[28] S. K. Henninger, F. Jeremias, H. Kummer, P. Schossig and H. Henning, "Novel sorption materials for solar heating and cooling," *Energy Procedia,* vol. 30, pp. 279-288.

[29] G. Gartler, D. Jähnig, G. Purkarthofer and W. Wagner, "Developement of a high energy density sorption storage system," AEE-INTEC, 2003.

[30] J. R. Camargo, E. Godoy and C. D. Ebinuma, "An evaporative and desiccant cooling system for air conditioning in humid climates," *J. Braz. Soc. Mech. Sci. & Eng.,* vol. 27, pp. 243-247, 2005.

[31] L. Scapino, H. Zondag, J. Bael, J. Diriken and C. Rindt, "Sorption heat storage for long-term low-temperature applications: A review on advancements at material and prototype scale," *Applied Energy,* vol. 190, pp. 920-948, 2017.

[32] H. Z. Hassan, A. Mohamad and a. R. Bennacer, "Simulation of an adsorption solar cooling system," *Energy,* vol. 36, pp. 530-537, 2011.

[33] M. Khamooshi, K. Parham e U. Atikol, «Overview of Ionic Liquids Used as Working Fluids in Absorption Cycles,» *Advances in Mechanical Engineering,* 2013.

[34] G. Florides, S. Kalogirou, S. Tassou and L. Wrobel, "Design and construction of a LiBr–water absorption machine," *Energy Conversion and Management,* vol. 44, pp. 2483-2508, 2003.

[35] N. L. Pierrès, F. Huaylla, B. Stutz and J. Perraud, "Long-term solar heat storage process by absorption with the KCOOH/H2O couple: Experimental investigation," *Energy,* vol. 141, pp. 1313-1323, 2017.

[36] M. Fasano, T. Humplik, A. Bevilacqua, M. Tsapatsis, E. Chiavazzo, E. N. Wang and P. Asinari, "Interplay between hydrophilicity and surface barriers on water transport in zeolite membranes," *Nature Communications,* vol. 7, 2016.

[37] N. Srivastava and I. Eames, "A review of adsorbents and adsorbates in solid-vapour adsorption heat pump systems," *Applied thermal engineering,* vol. 18, pp. 707-714, 1998.

[38] P. Zhang, *Adsorption and desorption isotherms,* 2016.

[39] Y. I. Aristov, "Novel materials for adsorptive heat pumping and storage: Screening and nanotailoring of sorption properties (review)," *Journal of chemical engineering of Japan,* vol. 40, pp. 1241-1251, 2008.

[40] M. Fasano, G. Falciani, V. Brancato, V. Palomba, P. Asinari, E. Chiavazzo and A. Frazzica, "Atomistic modelling of water transport and adsorption mechanisms insilicoaluminophosphate for thermal energy storage," *Applied Thermal Engineering,* vol. 160, 2019.

[41] M. Fasano, D. Borri, E. Chiavazzo and P. Asinari, "Protocols for atomistic modeling of water uptake into zeolite crystalsfor thermal storage and other applications," *Applied Thermal Engineering,* vol. 101, pp. 762-769, 2016.

[42] H. Demira, M. Mobedib and S. Ülkü, "A review on adsorption heat pump: Problems and solutions," *Renewable and Sustainable Energy Reviews,* vol. 12, pp. 2381-2403, 2008.

[43] F. Kuznika, K. Johannes and C. Obrecht, "Chemisorption heat storage in buildings: State-of-the-art and outlook," *Energy and Buildings,* vol. 106, pp. 183-191, 2015.

[44] R. Oliveira, R. Wang, J. Kiplagat and C. Wang, "Novel composite sorbent for resorption systems and for chemisorption air conditioners driven by low generation temperature," *Renewable Energy,* vol. 34, pp. 2757-2764, 2009.

[45] F. Kuznik and K. Johannes, "A review on chemisorption heat storage in low-energy buildings," *Energy Procedia,* vol. 57, pp. 2333-2341, 2014.

[46] G. Krese, R. Koželj, V. Butala and U. Stritih, "Thermochemical seasonal solar energy storage for heating and cooling of buildings," *Energy and Buildings,* vol. 164, pp. 239-253, 2018.

[47] N. Yu, R. Z. Wang and L. W. Wang, "Sorption thermal storage for solar energy," *Progress in Energy and Combustion Science,* vol. 39, pp. 489-514, 2013.

[48] T. J. Barton, L. M. Bull, W. G. Klemperer, D. A. Loy, B. McEnaney, M. Misono, P. A. Monson, G. Pez, G. W. Scherer, J. C. Vartuli e O. M. Yaghi, «Tailored porous material,» *Chem. Mater.,* vol. 11, pp. 2663-2656, 1999.

[49] Y. Pang, M. Y. Soliman, H. Deng and H. Emadi, Effect of Methane Adsorption on Stress-Dependent Porosity and Permeability in Shale Gas Reservoirs, 2016.

[50] K. S. W. Sing, D. H. Everett, R. A. W. Haul, L. Moscou, R. A. Pierotti, J. Rouquerol and T. Simieniewska, "Reporting physisorption data for gas/solid systems with special reference to the determination of surface area and porosity (Recommendations 1984)," *Pure and Applied Chemistry,* vol. 57, pp. 603-619, 2009.

[51] M. D. Donohue and G. L. Aranovich, "A new classification of isotherms for Gibbs adsorption of gases on solids," *Fluid Phase Equilibria,* vol. 158, pp. 557-563, 1999.

[52] M. Muttakin, S. Mitra, K. Thu, K. Ito and B. B. Saha, "Theoretical framework to evaluate minimum desorption temeperature for IUPAC classified adsorption isotherms," *International Journal of Heat and Mass Transfer,* vol. 122, pp. 795-805, 2018.

[53] K. Ariga, A. Vinu, Y. Yamauchi, Q. Ji and J. P. Hill, "Nanoarchitectonics for Mesoporous Material," *Bullettin of the Chemical Society of Japan,* vol. 85, pp. 1-32, 2012.

[54] G. Leofanti, M. Padovan, G. Tozzola and B. Venturelli, "Surface area and pore texture of catalysts," *Catalysis Today,* vol. 41, pp. 207-219, 1998.

[55] K. C. Ng, H. T. Chua, C. Y. Chung, C. H. Loke, T. Kashiwagi, A. Akisawa and B. B. Saha, "Experimental investigation of the silica gel-water adsorption isotherm characteristics," *Applied Thermal Engineering,* vol. 21, pp. 1631-1642, 2001.

[56] D. Wang, J. Zhang, X. Tian and K. S. D. Liu, "Progress in silica gel–water adsorption refrigeration technology," *Renewable and Sustainable Energy Reviews,* vol. 30, pp. 85-104, 2014.

[57] J. Bauer, R. Herrmann, W. Mittelbach and W. Schwieger, "Zeolite/aluminum composite adsorbents for application in adsorption refrigeration," *Int. J. Energy Res.,* vol. 33, pp. 1233-1249, 2009.

[58] S. Vasta, V. Brancato, D. L. Rosa, V. Palomba, G. Restuccia, A. Sapienza and A. Frazzica, "Adsorption Heat Storage: State-of-the-Art and Future Perspectives," *Nanomaterials,* vol. 8, 2018.

[59] L. Scapino, H. A. Zondag, J. V. Bael, J. Diriken and R. C, "Sorption heat storage for long-term low-temperature applications: A review on the advancements at material and prototype scale," *Applied Energy,* vol. 190, pp. 920-948, 2017.

[60] V. Marakatti, "Design of solid acid catalysts for prins reaction and toluene methylation," 2015.

[61] S. K. Henninger, F. P. Schmidt and H. M. Henning, "Water adsorption characteristics of novel materials for heat transformation applications," *Applied Thermal Engineering,* vol. 30, pp. 1692-1702, 2010.

[62] A. Freni, G. Maggio, A. Sapienza, A. Frazzica, G. Restuccia and S. Vasta, "Comparative analysis of promising adsorbent/adsorbate pairsfor adsorptive heat pumping, air conditioning and refrigeration," *Applied Thermal Engineering,* vol. 104, pp. 85-96, 2016.

[63] H. Furukawa, K. E. Cordova, M. O'Keeffe and O. M. Yaghi, "The chemistry and Application of Metal-Organic Frameworks," *Science,* vol. 341, 2013.

[64] H. Jarimi, D. Aydin, Z. Yanan, G. Ozankaya, X. Chen and S. Riffat, "Review on the recent progress of thermochemical materials and processes for solar thermal energy storage and industrial waste heat recovery," *International Journal of Low-carbon Technologies,* vol. 14, pp. 44-69, 2019.

[65] F. Meunier, "Adsorption heat powered heat pumps," *Applied Thermal Engineering,* vol. 61, pp. 830-836, 2013.

[66] K. Thu, S. Mitra and B. B. Saha, "Theoretical development on the isosteric heat of adsorption and experimental confirmation," 2017. [Online]. Available: https://arxiv.org/ftp/arxiv/papers/1709/1709.01723.pdf.

[67] M. D. LeVan and T. Vermeulen, "Binary Langmuir and Freundlich Isotherms for Ideal Adsorbed Solutions," *J. Phys. Chem.,* vol. 85, pp. 3247-3250, 1981.

[68] A. P. Terzyk, J. Chatłas, P. A. Gauden, G. Rychlicki and P. Kowalczyk, "Developing the solution analogue of the Toth adsorption isotherm equation," *Journal of Colloid and Interface Science,* vol. 266, pp. 473-476, 2003.

[69] K. Kim, H. Oh, S. Lim, K. Ho, Y. Park and C. Lee, "Adsorption Equilibria of Water Vapor on Zeolite 3A, Zeolite 13X, and Dealuminated Y zeolite," *J. Chem. Eng. Data,* vol. 61, pp. 1547-1554, 2016.

[70] E. Chiavazzo and M. Fasano, "Accumulo e trasporto di energia," *Slides of the course - Politecnico di Torino,* 2019.

[71] F. Cortès, F. Janna, F. Marin and C. Castilla, "Water adsorption on zeolite 13X: Comparison of the two methods based on mass spectrometry and thermogravimetryy," *Adsorption,* vol. 16, pp. 141-146, 2010.

[72] N. I. o. S. a. Technology, "NIST Chemistry WebBook," 2018. [Online]. Available: https://webbook.nist.gov/cgi/cbook.cgi?ID=C7732185&Units=SI&Mask=7. [Accessed 8 10 2019].

[73] D. d. bank, "Saturated vapor pressure - Calculation by Antoine Equation," [Online]. Available: http://ddbonline.ddbst.de/AntoineCalculation/AntoineCalculationCGI.exe?component=Water. [Accessed 8 10 2019].

[74] K. S. ORGANIZATION, "KNF Datasheet E 260," [Online]. Available: https://www.knf.it/it/prodotti/pompe-oem/product/products/pompe-a-membrana-per-gas/pompe-da-vuoto-e-compressori/. [Accessed 14 10 2019].

[75] K. S. DEPARTMENT, "KNF DATA SHEET E 320," [Online]. Available: https://www.knf.it/it/prodotti/strumenti-da-laboratorio/product/products/controllore-di-vuoto/controllore-di-vuoto-vc-900/. [Accessed 14 10 2019].

[76] ASME, "Boiler Pressure and Vessel Code-Sec VIII-Div.1," pp. 21-49, 2011.

[77] ASME, "Boiler and Pressure Vessel code-Sec.2 Part D," 2015.

[78] A. University, Practical Aspects of Finite Element Simulation, 2019.

[79] E. Toolbox, "Thermal conductivity of common metals, metallic elements and Alloys," [Online]. Available: https://www.engineeringtoolbox.com/thermal-conductivity-metals-d_858.html. [Accessed 14 10 2019].

[80] T. Ling and C. Poon, "Use of phase change materials for thermal energy storage in concrete: An overview," *Construction and Building Materials,* vol. 46, pp. 55-62, 2013.

[81] J. Stefan, *S B Wien Akad. Mat. Natur. ,* vol. 98, pp. 473-484, 965-983, 1889.

[82] F. Neumann, "Die Partiellen Differentialgleichungen der Mathematischen Physik," p. 162, 1912.

[83] H. Hu and S. Argyropoulos, "Mathematical modelling of solidification and melting: a review," *Modelling Simul. Mater. Sci. Eng.,* vol. 4, pp. 371-396, 1996.

[84] H. Chen, T. N. Cong, W. Yang, C. Tan, Y. Li and Y. Ding, "Progress in electrical energy storage system: A critical review," *Progress in Natural Science,* vol. 19, pp. 291-312, 2009.

[85] X. Luo, J. Wang, M. Dooner and J. Clarke, "Overview of current development in electrical energy storage technologies and the application potential in power system operation," *Applied Energy,* vol. 137, pp. 511-536, 2015.

[86] J. Ibarra-Bahena and R. J. Romero, "Performance of Different Experimental Absorber Designs in Absorption Heat Pump Cycle Technologies: A Review," *Energies,* vol. 7, pp. 751-766, 2014.

[87] J. Jänchen and H. Stach, "Adsorption properties of porous materials for solar thermal energy storage and heat pump applications," *Energy Procedia,* vol. 30, pp. 289-293, 2012.

[88] C. Bonacina, A. Cavallini and L. Mattarolo, Trasmissione del calore, CLEUP, 1989.